BIO-HYDROTREATED FUEL PRODUCTION FROM NON-EDIBLE OIL USING
SUPPORTED NI-BASED CATALYST

By

MISS Kanokthip PONGSIRIYAKUL

A Thesis Submitted in Partial Fulfillment of the Requirements
for Doctor of Engineering (CHEMICAL ENGINEERING)
Department of CHEMICAL ENGINEERING
Graduate School, Silpakorn University
Academic Year 2020
Copyright of Graduate School, Silpakorn University

# การผลิตเชื้อเพลิงไฮโดรทรีตจากน้ำมันที่ไม่ใช่อาหารด้วยตัวเร่งปฏิกิริยานิกเกิล

โดย
นางสาวกนกทิพย์ พงษ์ศิริยะกุล

วิทยานิพนธ์นี้เป็นส่วนหนึ่งของการศึกษาตามหลักสูตรวิศวกรรมศาสตรดุษฎีบัณฑิต
สาขาวิชาวิศวกรรมเคมี แบบ 2.2 ระดับปริญญาดุษฎีบัณฑิต
ภาควิชาวิศวกรรมเคมี
บัณฑิตวิทยาลัย มหาวิทยาลัยศิลปากร
ปีการศึกษา 2563
ลิขสิทธิ์ของบัณฑิตวิทยาลัย มหาวิทยาลัยศิลปากร

# BIO-HYDROTREATED FUEL PRODUCTION FROM NON-EDIBLE OIL USING SUPPORTED NI-BASED CATALYST

By

MISS Kanokthip PONGSIRIYAKUL

Title  Bio-hydrotreated fuel production from non-edible oil using supported Ni-based catalyst
By  Kanokthip PONGSIRIYAKUL
Field of Study  (CHEMICAL ENGINEERING)
Advisor  Assistant Professor Dr. Worapon Kiatkitipong

Graduate School Silpakorn University in Partial Fulfillment of the Requirements for the Doctor of Engineering

............................................................................ Dean of graduate school
(Associate Professor Jurairat Nunthanid, Ph.D.)

Approved by

............................................................................ Chair person
(Assistant Professor Dr. Tarawipa Puangpetch )

............................................................................ Advisor
(Assistant Professor Dr. Worapon Kiatkitipong )

............................................................................ Co advisor
(Professor Dr. Suttichai Assabumrungrat )

............................................................................ Co advisor
(Dr. Kajornsak Faungnawakij )

............................................................................ External Examiner
(Professor Dr. Navadol Laosiripojana )
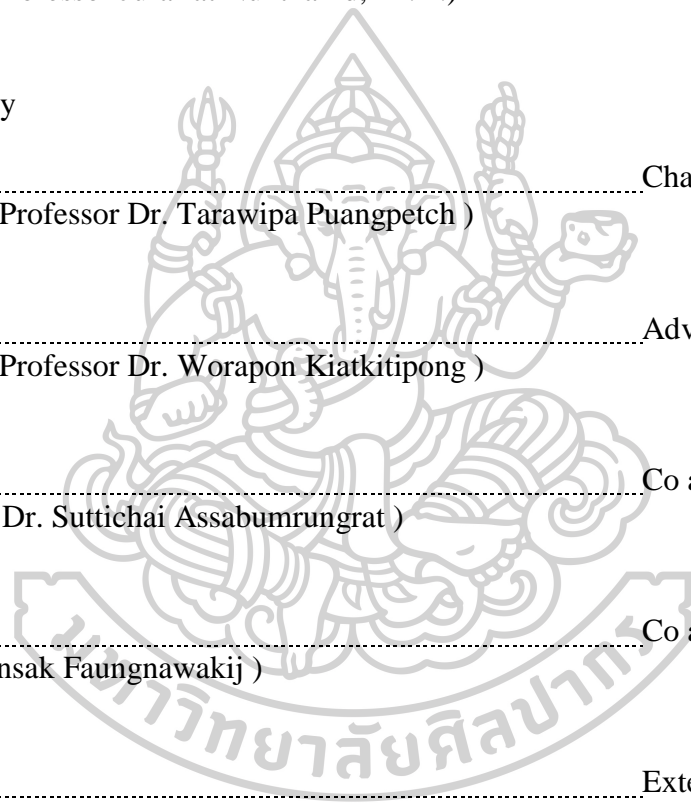
55404805 : Major (CHEMICAL ENGINEERING)
Keyword : Ni-based catalysts; Biofuels; Algae ; Catalytic upgrading; Catalyst deactivation.

MISS KANOKTHIP PONGSIRIYAKUL : BIO-HYDROTREATED FUEL PRODUCTION FROM NON-EDIBLE OIL USING SUPPORTED NI-BASED CATALYST THESIS ADVISOR : ASSISTANT PROFESSOR DR. WORAPON KIATKITIPONG

This thesis is dedicated to the investigation, and development of catalysts for catalytic hydrotreating of biomass-based oil with the aim of producing high quality liquid fuel from non-edible biomass.
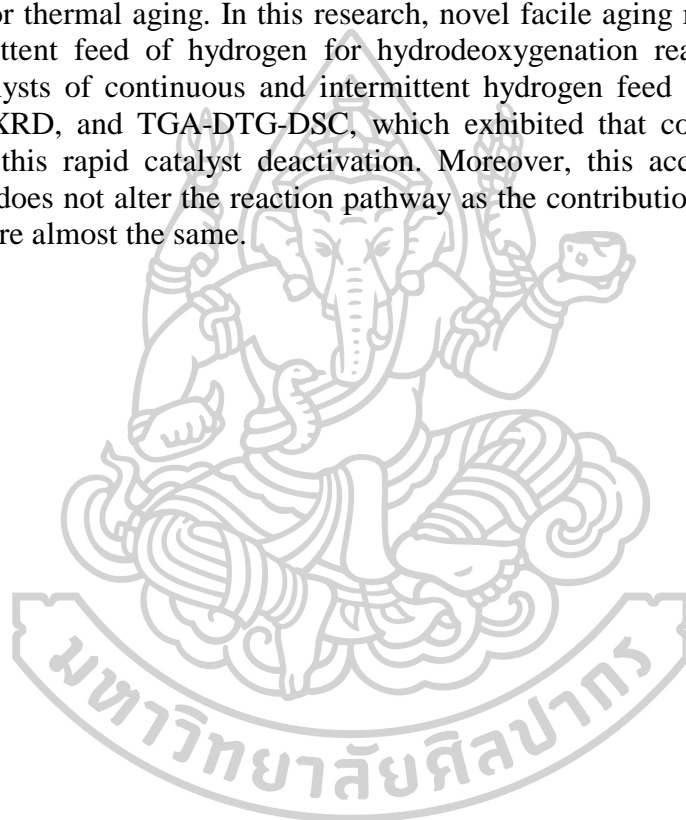
Ni metal supported on alumina (Ni/$\gamma$-Al$_2$O$_3$) catalysts were prepared and tested for hydrotreating activity of algae bio-crude oil produced from hydrothermal liquefaction of *Nannochloropsis* sp. In addition, the effect of Cu and Re addition on $\gamma$-Al$_2$O$_3$ supported Ni catalyst were investigated for the same purpose. The reaction was performed in high pressure batch reactor setup at 350 °C, 75 bar H$_2$, and reaction time of 4 h, using the different Ni-based catalysts including Ni/$\gamma$-Al$_2$O$_3$, Ni-Cu/$\gamma$-Al$_2$O$_3$, Ni-Re/$\gamma$-Al$_2$O$_3$ and Ni-Cu-Re/$\gamma$-Al$_2$O$_3$, (10%Ni, 5%Cu, 2.5%Re) were used in upgrading of the bio-crude oil. Several characterization techniques including N$_2$-physisorption, temperature program reduction (H$_2$-TPR), X-ray diffraction (XRD), scanning electron microscope equipped with energy dispersion X-ray spectroscopy (SEM-EDS), and transmission electron microscopy (TEM) were employed to unravel the composition, morphology, and properties of the prepared catalysts. Upgraded bio-oil yield, elemental content (CHNS/O), and oil properties were here used to point out the activity of the catalysts. In addition, the chemical compositions of upgraded bio-oil were identified using GC-MS to address the effect of Cu and Re promotion on the catalytic activity and also selectivity.

Most catalytic systems could effectively eliminate S and decrease the N and O contents, and enhance more than 20% improvement in the higher heating value (HHV) of the bio-oil (34 to 41-45 MJ/kg). Ni-Cu-Re/$\gamma$-Al$_2$O$_3$ ternary alloy offered the best results on the overall performance, achieving the highest upgraded bio-oil yield of 58 wt. %. Moreover, the carbon efficiency and overall energy recovery (ER$_{overall}$) including ER from biomass algae to bio-crude oil (ER$_{HTL}$) and ER from bio-crude oil to upgraded bio-oil (ER$_{upgrade}$) are calculated. Finally, the reaction pathways for the formation of different hydrotreated products catalyzed by mono-, bi-, and tri metallic Ni-Cu-Re have been proposed.

The behavior of the prepared catalysts during the hydrotreating reaction was studied by performing in continuous down-flow packed-bed reactor. In this part, *Pongamia pinnata (P. pinnata)* oil was used, representing the non-edible triglyceride-based oil. All the catalysts revealed good deoxygenation and hydrogenation activity, which enabled liquid fuel yield of 65-77 % which are mainly in diesel boiling range product. The constantly 100% conversion of *Pongamia pinnata* oil along 15 h time on stream under 330 °C, LHSV 1 h$^{-1}$, 50 bar H$_2$ and continuously flow of hydrogen,

demonstrating the high potential of prepared supported Ni catalysts in hydrodeoxygenation (HDO). The carbonaceous deposition occurred during the HDO, which could be a majority cause for loss of catalyst surface and active site toward catalyst deactivation. The addition of Cu and Re could inhibit the coke formation with their synergistic effect.

However, the process for testing and screening of numerous catalysts can be costly and time-consuming due to highly energy-intensive and required significant amount of feedstock and catalyst. Coking has been reported as the most prevalence cause of catalyst deactivation in other hydrodeoxygenation studies, and it was also evident in this work. Typically, the accelerated coking deactivation was performed via chemical or thermal aging. In this research, novel facile aging method was proposed by intermittent feed of hydrogen for hydrodeoxygenation reaction. The fresh and spent catalysts of continuous and intermittent hydrogen feed were analyzed by $N_2$ sorption, XRD, and TGA-DTG-DSC, which exhibited that coke formation were a reason of this rapid catalyst deactivation. Moreover, this accelerated deactivation technique does not alter the reaction pathway as the contribution of DCOx and HDO reactions are almost the same.

# ACKNOWLEDGEMENTS

Dr.Worapon Kiatkittipong (SU), my advisor who has guided me throughout this work in a dedicated manner, allowed me to plan or do everything with my own way if sometime it doesn't work. He give me the valuable suggestion and feedback both in the work and my future. He always provide me the great opportunity to improve myself e.g. funds, and corporation with talented people. I couldn't thank you enough for his patience and believe in me.

Dr. Sushil Adhikari who gave me the opportunity to cooperate with his team at Bioenergy and Bioproducts research laboratory, Auburn University. He provided me the valuable mentor-ship, insights into Hydrothermal liquefaction technique and enabled biomass and bio-oil characterization. Apart from knowledge suggestion, he also gave support for my housing necessity, finance and opportunity for work presentation at AiChE 2018.

Dr. Kajornsak Faungnawakij (Research unit director of Nanocatalysis and Molecular Simulation Research Group, National Nanotechnology center), who allowed me accesses to the laboratory at National Nanotechnology Center. I have gained new skills, knowledge and joined seminars. His team research, too, gave me technical support, especially Rungnapa Kaewameesri.

I would thankful for the useful suggestion and valuable support from Dr. Suttichai Assabumrungrat and Dr. Navadol Laosiripojana, and also Dr. Tarawipa Puangpetch for being the head of thesis defense committee.

l would like to thank Dr. Saravanan R. Shanmugam, Dr. Rajdeep Shakya,

# TABLE OF CONTENTS

**Page**

# LIST OF FIGURES

# LIST OF TABLES

# CHAPTER 1

# INTRODUCTION

## 1.1 Statement and Significance of the Problems

Recently, the world's energy consumption continuously increases, especially for non-OECD countries which increase nearly 70% between 2018 and 2050. Petroleum has been the largest source of fossil-based energy for the world and the primary transportation fuel for several decades. At this consumption rate and the limit of petroleum source causes fluctuating oil prices and insecurity. Moreover, the high level of fossil fuel using can lead to environmental issues such as air pollution, acid rain, and global warming problem, as well as effect on human health [1,2]. As a result of these problem, human are driving to seek out the alternative fuel or renewable energy sources in order to attempts to decrease dependence on fossil-based energy and to reduce the environmental problem result in increasing the use of biofuels which is expected to provide 27% of the global transportation energy use in 2050 [3,4].

As mentioned above, liquid biofuels (such as ethanol [5,6], ethanol-derived fuel [7,8], biodiesel [9,10], glycerol-derived fuel [11,12], and bio-hydrotreated fuel [13]) are currently the promising choice to use with existing infrastructure and vehicles. Biomass, is generally classified into agricultural-, forage-, energy crops, and their residues, forest (wood) residues, animal and municipal organic wastes, has been investigated and undoubtedly considered as a high potential feedstock for production of biofuels, chemicals and other value-added products.

Over the past decade, the production of first generation biofuel has been studies and further developed into commercialize, producing bioethanol and biodiesel mainly from edible biomass such as starch, sugar, vegetable oil (e.g. palm oil, soybean oil, etc), and animal fat [14]. However, these feedstock cause a negative impact on a human-food supply chain in long term by increasing food price and competitive demand for arable land between energy and food sector [2]. Hence, Non-edible resources including the biofuels produced from agriculture residues, forestry and waste materials such as woody crops and lignocellulosic biomass, are gaining

attention to use as transportation fuel; however, most of them are still being developed [15,16].

Algae is considered as a potential feedstock for the third generation biofuel due to its great productivity, high growing rate, and high lipid content [17,18]. The oil content in algae has been reported of approximately 20-50 wt.% by dry weight of the algae, while the highest oil observed in some microalgae can reach up to 60 wt.% [19]. Also, the cultivation of algae does not require arable land because it grows in saline, fresh water, even waste water, severally reducing the competitive issue of food production and environmental impact [20]. To convert the algae biomass into bio-crude oil, hydrothermal liquefaction (HTL) is considered as an attractive method because it can convert high moisture-content (> 90%) algae into bio-crude oil with needless drying process, which saves more input energy [21]. Unfortunately, the bio-crude oil is not proper for direct use in vehicle engines due to its negative properties such as high acidity, high viscosity, low heating value, and instability, by the high level of heteroatoms (N, O, and S) and water content in the bio-crude oil [20]. Consequently, the treatment of bio-crude oil is essential for the quality improvement before applying the bio-oil as transportation fuel [22,23].

Catalytic hydroprocessing has been demonstrated to be an effective way for bio-oil upgrading due to its excellent activity for heteroatoms removal leading to improving properties of bio-oil comparable to that of petroleum fuel. Furthermore, the commercialization was done by Neste oil (Finland) and UOP which produce commercially trademark as NExBTL and Eni Ecofining, respectively. However, it requires large amount of hydrogen which leads to high operation cost arisen from hydrogen generation and purification[24]. Hence, the challenges of catalytic hydrodeoxygenation process is catalyst development for high oxygen removal activity with minimum hydrogen consumption, including eliminating the side reaction, and high desired products selectivity. So far various catalyst types for bio-oil upgrading have been investigated such as NiMo and CoMo sulfide catalysts [25–28], Pt [17,29], Pd [17,29], and Ru [17,30]. Although these catalysts have shown high activity in deoxygenation reaction, the addition of sulfur source is generally required for NiMo and CoMo-based catalysts to activate and preserve their activity, causing increase of S content in

final product [19], whereas the use of noble metal catalysts (i.e. Pd, Pt, Rh, Ru, etc.) was limited by their high cost.

Ni-based catalyst is one of the most attractive catalysts for the bio-oil upgrading because its high activity in hydrotreating, abundance, and inexpensive cost [31]. Supported Ni-based catalyst on deoxygenation of fatty acid was firstly proposed by Snare and co-worker (2006) [32] and showed good activity for oxygen removal of triglycerides-based and biomass-based (e.g. guaiacol, phenol etc.). As reported by Shakya *et al,* the upgrading of HTL algae bio-crude oil was conducted at 300 and 350°C for 10 h using various catalysts. The results showed that the highest upgraded bio-oil yield of 61 wt. % was obtained from Ni/C at 350°C with high higher heating value (HHV) of 42 MJ/kg [33]. Though supported Ni-based catalyst has been reported as a potentially effective catalyst in hydrodeoxygenation of oxygen containing compounds and a high quality bio-oil was obtained, solid residue was also formed, causing the reduction of bio-oil yield and catalyst deactivation by deposition on the catalyst surface [34].

The addition of other metals into Ni catalyst to form Ni-metal bimetallic catalysts has been reported to enhance conversion, yield, and stability of catalyst. Bimetallic Ni-Cu is widely investigated for hydrotreating of pyrolysis oil [35,36] and its model compounds (such as anisole [37], guaiacol [38], and vanillin [39]), which showed a superior catalytic performance compared to the corresponding Ni monometallic, viz., higher oil yield, and better inhibition of the catalyst deactivation by reducing agglomeration of the catalysts. Even though Ni-Cu presents the great ability for hydrogenation of bio-oil which mostly produced from lignocellulosic biomass, investigation of Ni-Cu performance has been limited in hydrotreating of algae bio-crude oil from HTL. The Ni based catalyst modification with Re was motivated by its performance from many studies [40–42]. Addition of Re in sulfided Ni-Mo/γ-Al$_2$O$_3$ greatly improve deoxygenation activity of palm oil toward green diesel production. It was reported that the addition of Re as a second metal results in reduced metal particle sizes, leading to enhancing the metal dispersion [41].

## 1.2 Objectives and scope of research

The aim of this work was to produce high quality fuel from non-edible biomass-based oil via hydrotreating reaction using supported Ni-based catalysts. The algae biomass and *Pongamia pinnata* seeds were selected to study, representing the potential alternative non-edible bio-feedstock for biofuel productions. The experiment was performed following the scope of research:

- Supported Ni catalyst development for hydrotreating of bio-crude oil to optimize liquid yields and to eliminate heteroatoms (O, S, N) from bio-crude oil: Modification single metal Ni catalyst via addition Cu and Re to form bi- and tri-metallic, namely Ni-Cu, Ni-Re, and Ni-Cu-Re supported alumina

- Investigation the effect of Cu and Re on physicochemical properties of the catalysts and the hydrotreating activity. Upgraded bio-oil yield, elemental content, and oil properties were here used to point out the activity of the catalysts.

- Better understanding of the reaction mechanism occurring during the hydrotreating of the bio-crude oil, including influence of modified Cu and Re catalysts on other side reactions, which affect the selectivity towards deoxygenation activity.

- Investigation of catalyst stability and deactivation.

# CHAPTER 2

# METHODOLOGY

The materials and experimental setup used in this work are describes in this chapter. These includes the method of catalyst preparation, bio-crude oil preparation, and hydrotreating process, as well as the characterization techniques. Typical operating conditions and calculations employed for activity assessment are included.

## 2.1 Catalyst preparation

Ni-supported catalysts were prepared by incipient wetness impregnation method. $\gamma$-Al$_2$O$_3$ was purchased from Alfa Aesar in a form of pellets. It was crushed and sieved to obtain the catalyst particle with size of $\leq$ 0.25 mm prior to impregnation with metal salt solution. The metal salt solutions were prepared from Ni (NO$_3$)$_2$·6H$_2$O (Alfa Aesar, 98%), Cu (NO$_3$)$_2$·3H$_2$O (Acros, 99%) and NH$_4$ReO$_4$ (BTC, 99%). These aqueous solutions were then loaded into the $\gamma$-Al$_2$O$_3$ support to produce the supported catalysts at 10%Ni, 10%Ni-5%Cu, 10%Ni-2.5%Re and 10%Ni-5%Cu-2.5%Re (thereafter as called Ni/$\gamma$-Al$_2$O$_3$, Ni-Cu/$\gamma$-Al$_2$O$_3$, Ni-Re/$\gamma$-Al$_2$O$_3$, and Ni-Cu-Re/$\gamma$-Al$_2$O$_3$, respectively). Subsequently, these catalysts were dried at 105°C overnight and calcined in atmospheric air at 500°C (5 °C/min) for 4 h.

The size of catalyst employed in packed-bed reactor is 0.425-1 mm which slightly larger than that using in batch reactor (Chapter 4) in order to lessen the pressure drop. Prior to impregnation step, the $\gamma$-Al$_2$O$_3$ support (Sasol, Germany) was crushed and sieved to 0.425-1 mm. Then, aqueous solution of precursors (Ni 10%, Cu 2% and Re 2%) was loaded into the support, following calcination and reduction before hydrotreating step.

## 2.2 Catalysts characterization

The physisorption of the catalysts were analyzed using Quantachrome Autosorb-iQ. The physisorption analysis was conducted by nitrogen adsorption, including Brunauer-Emmett-Teller (BET) surface area, pore size diameter, and pore volume. The catalysts were outgassed at 300 °C for 3 h before analysis.

Temperature program experiments were carried out in Micromeritics AutoChem 2910. The reducibility of the catalysts was determined by hydrogen temperature program reduction ($H_2$-TPR). Prior to analysis, the sample was pretreated at 100 °C under nitrogen atmosphere for 1 h. Then it was heated from 40 to 800 °C with a ramping rate of 5 °C/min under 5% $H_2/N_2$ gas.

The X-ray diffraction (XRD) patterns of the catalysts were analyzed using Bruker D2 phaser equipped with Cu-Kα radiation, operated at 30 kV and 10 mA in 2θ range of 10-80° with step size of 0.02° and step time of 1 s.

Transmission electron microscope (TEM) images were also taken via Jeol (JEM 2010). The samples were dispersed in ethanol by a sonicator before dropping on a carbon-coated gold grid. Also, the elemental composition were analyzed by Energy Dispersive X-Ray Spectroscopy (EDS).

In addition, the morphology and elemental composition of the catalysts were examined via Zeiss EVO 50VP scanning electron microscope equipped with energy dispersion X-ray spectroscopy (SEM-EDS). Amount of coke deposit on spent catalyst was detected by thermo gravimetric analysis (TGA).

## 2.3 Feed preparation

### 2.3.1 Hydrothermal liquefaction (HTL) of algae

The bio-crude oil was produced via hydrothermal liquefaction (HTL) of *Nannochloropsis* sp. (Reed Mariculture Inc., CA) using a 1000 mL Parr reactor. The operating condition and the experimental procedure of HTL were conducted according to the previous work reported by Shakya *et al* [33,43]. A 300 g of

*Nannochloropsis* sp. microalgae paste and 300 mL of deionized water were loaded into the reactor to make a 15 wt. % of solid content. Prior to the reaction, the reactor was purged with nitrogen gas for 10 min to remove air inside. The reactor was then pressurized with 5 bar nitrogen (initial pressure) and heated to 320 °C for the reaction. After holding for 30 min, the reactor was quenched to stop the reaction, in an ice-water bath. When the reactor was cooled to room temperature, the pressure was released, and the products (oil, aqueous, and solid) were collected. Bio-crude oil's yield of 50 wt. % with dry basis was obtained with an elemental composition of C 64.1%, H 9.6%, N 5.1%, S 0.8%, and O 20.4%.

The reactor was rinsed with dichloromethane (DCM, $\geq$ 200 mL) to recover the remaining product. The DCM-mixed product was then vacuum filtered and decanted into a separatory funnel to separate the solid residue and aqueous phase, respectively. The DCM in the extracted was separated using a rotary evaporator (IKA RV 10 control). The remaining material was the algae bio-crude oil.

### 2.3.2 Liquid extraction of *Pongamia Pinnata* seeds

*Pongamia Pinnata* seeds were kept from Chanthaburi, Thailand. Prior to extraction step, the seed kernel is dried at 110 °C until the weight is constant, then dry seed kernel was ground in a grinder. Crude *P.pinnata* oil was extracted using hexane as solvent by soxhlet extractor as shown in **Figure 1**. 400 g of ground kernels was packed in thimble, and the oil was extracted with 3 L of hexane for 12 hr. Subsequently, the oil was separated from hexane by high vacuum rotary evaporator (IKA, RV 10 digital)**.** *Pongamia Pinnata* oil is pretreated by degumming with water and phosphoric acid at 70 °C. After degumming, gums is separated by filtration.
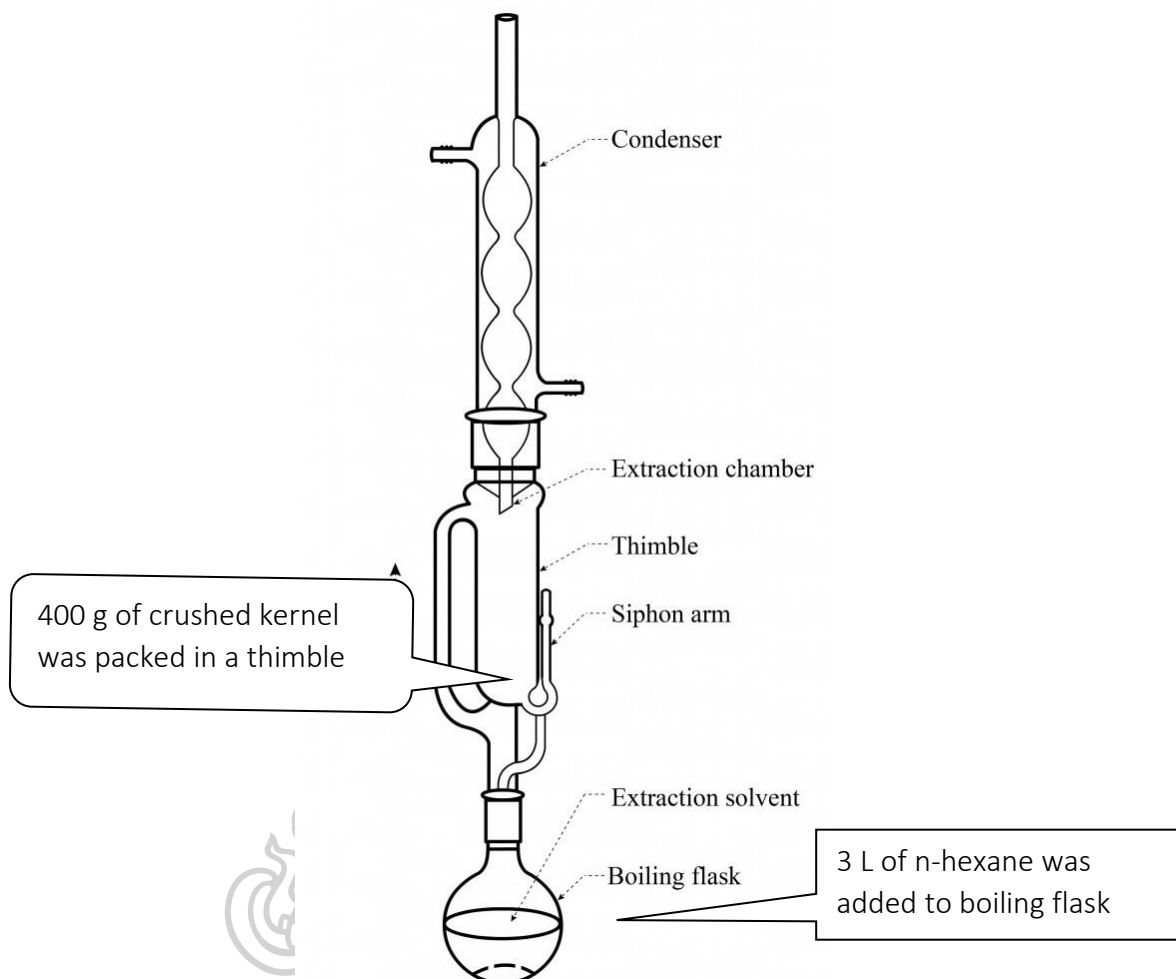
**Figure 1.** Oil extraction by soxhlet extractor

## 2.4 Hydrotreating experiment

### 2.4.1 Upgrading of algae bio-crude oil

The upgrading of algae bio-crude oil (for chapter 4) was conducted in a 100 mL Parr reactor. In a typical run, 15 g of bio-crude oil with 5 wt. % of catalyst relative to bio-crude oil were loaded into the reactor. Before the upgrading experiment, the catalyst was pretreated by reduction with $H_2$ gas at 500 °C for 3 h. After that, the reactor was flushed for 3 times and purged for 5 min with hydrogen gas

to remove air inside the reactor. Then, it was charged to 75 bar with pure hydrogen and heated to 350 °C for 4 h with stirring at a speed of 600 rpm.

After a desired reaction period, the reactor was immersed in an ice-water bath to stop the reaction. The pressure profiles in the reactor during the reaction until final pressure at room temperature was recorded, and the uncondensed gaseous products were collected in a gas cylinder for the analysis. The amount of gaseous products was calculated by the difference in overall mass before and after the reaction. The upgraded bio-oil was collected with the same procedure of bio-crude oil production as described in section 2.3. The solid residue was rinsed once more with DCM to recover the remaining oil phase product, then dried and weighted. All experiments were performed in duplicates. The product yields of each phase was calculated using Eg. (1) according to [33]. In addition, the mass balance of the experiment was calculated by the relative amount of different products in each phase.

$$\text{Product yield (\%)} = \frac{\text{mass of product (g)}}{\text{mass of initial algae bio−crude oil (g)}} \times 100 \tag{1}$$

Energy recovery for the algae bio-crude ($ER_{HTL}$) and upgraded bio-oil ($ER_{upgrading}$) was evaluated as following:

$$ER_{HTL}(\%) = \frac{\text{HHV of bio−crude} \times \text{Mass of bio−crude}}{(\text{HHV of algae biomass} \times \text{Mass of algae biomass})} \times 100 \tag{2}$$

$$ER_{upgrade}(\%) =$$
$$\frac{\text{HHV of upgraded bio−oil} \times \text{Mass of upgraded bio−oil}}{(\text{HHV of bio−crude} \times \text{Mass of bio−crude}) + (\text{HHV of } H_2 \times \text{Mass of } H_2 \text{ consumption})} \times 100 \tag{3}$$

## 2.4.2 Hydrotreating in packed-bed reactor
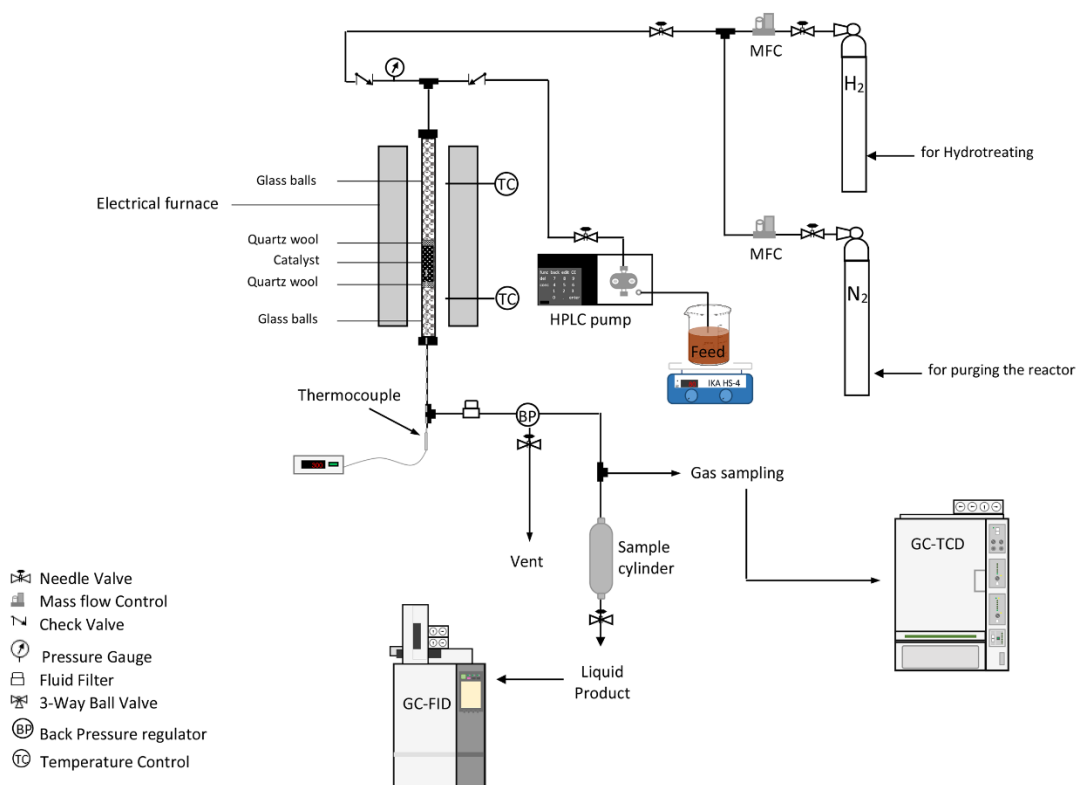


**Figure 2.** Schematic diagram of the experimental apparatus

The hydrotreating catalytic activity and long-term stability test of supported Ni-based catalyst were carried out in down-flow, packed-bed reactor with an inner diameter of 10 mm, length of 50 cm. The setup reactor was equipped with a back-pressure regulator, gas-liquid separator and GC-TCD. The experimental apparatus is shown in **Figure 2**. The catalysts were loaded into the reactor with glass beads (diameter 3 mm) at the bottom and the top of the reactor for distributing gas and liquid phase substance, whereas the 3 g of catalyst was packed at the center with quartz wool to prevent the catalyst flutter down. Prior to reaction testing, the catalyst was reduced in-situ under 10 bar of $H_2$ with flow rate of 60 ml/min at temperature of 500 °C for 3 h. Then the system was heated to temperature of 330 °C and pressurized with $H_2$ of 50 bar controlled by back pressure regulator (BPR). Subsequently, the oil and $H_2$ were introduced into the reactor by $H_2$/oil ratio of 1000 $Ncm^3/cm^3$ and liquid hourly space velocity (LHSV) of 1 $h^{-1}$, which controlled by HPLC pump and mass

flow controller, respectively. The oil was preheated at 180 °C before feed into the reactor.

The conversion, product selectivity and yield are calculated using the area of chromatogram as follows: Eq. (4)-(8), respectively.

Conversion (%) = (4)
$$\frac{\text{Weight percent of TG and FFA in feed} - \text{Weight percent of TG and FFA in product}}{\text{Weight percent of TG and FFA in feed}} \times 100$$

Gasoline selectivity (%) = (5)
$$\frac{\text{Weight percent of C6-C12 product}}{\text{Weight percent of TG and FFA in feed} - \text{Weight percent of TG and FFA in product}} \times 100$$

Diesel selectivity (%) = (6)
$$\frac{\text{Weight percent of C13-C22 product}}{\text{Weight percent of TG and FFA in feed} - \text{Weight percent of TG and FFA in product}} \times 100$$

Product yield (%) = $\frac{\text{Weight of liquid product}}{\text{Weight of feed}} \times$ conversion $\times$ product selectivity (7)

Yield of liquid fuel = diesel yield + gasoline yield (8)

As hydrodeoxygenation (HDO and decarboxylation/decarbonylation (DCO$_x$) are predominant reaction pathways for hydrotreating of biomass-based oil. The percent contribution of these two reaction HDO and DCO$_x$ are calculated based on mass balance of hydrocarbon containing C$_n$ and C$_{n-1}$, representing by C$_{16}$ and C$_{18,}$ and C$_{15}$ and C$_{17}$, respectively; as following equations:

HDO (%) = $\frac{\text{Weight percent of C16 and C18 in product}}{\text{Total weight percent of C15-C18 in product}} \times 100$ (9)

DCOx (%) = $\frac{\text{Weight percent of C15 and C17 in product}}{\text{Total weight percent of C15-C18 in product}} \times 100$ (10)

## 2.5 Feed and hydrotreated products analysis

### 2.5.1 Algae experiment

The algae bio-crude and upgrading oil were analyzed by gas chromatography coupled with mass spectrometric detector (GC-MS) to determine the chemical composition. The GC-MS was carried out on an Agilent 7890A GC-MS equipped with DB-1701 column (30 m × 0.25 mm × 25 μm). The samples were diluted with dichloromethane to a concentration of 5wt. %. 4 μL of diluted sample was injected. The inlet temperature was set at 250 °C with split ratio of 10:1. The column temperature was programed as follow: held at 50 °C for 2 min, then heated to 250 °C with ramping rate of 5 °C/min and held for 10 min. Helium was served as carrier gas. The National Institute of Standards and Technology (NIST) mass spectral library was used to identify the compound. The gas product composition was analyzed using an Agilent 3000 micro GC equipped with a thermal conductivity detector (TCD) and 4 different columns containing a Mol Sieve 5A PLOT (10 m × 0.32 mm × 12 μm), a PLOTU (8 m × 0.32 mm × 30 μm), an Alumina PLOT (10 m × 0.32 mm × 8 μm), and an OV1 column (14 m × 0.15 mm × 2 μm).

### 2.5.2 For *Pongamia pinnata* oil

The liquid reaction products were analyzed by an off-line gas chromatograph equipped with capillary column DB-1HT (30 m× 0.32 mm × 0.1 µm) and a flame ionization detector (FID). Prior to injection, 50 mg of sample was diluted with 1 ml of chloroform, and 1 μL of diluted sample was injected into GC with split ratio of 100. The injector and detector temperature were maintained at 340 and 370°C, respectively. The column temperature was controlled by a temperature program which increased from 40 to 270°C with ramping rate of 8°C/min, and held for 11 min, followed by an increase of 15°C/min to 370°C, and held for 15 min. The composition of gaseous product was analyzed using online a gas chromatography (GC-14B, Shimadzu.) equipped with a molecular sieve 5A, Porapak Q columns and a thermal conductivity detector (TCD).

### 2.5.3 Other properties of feedstock and liquid product analysis

The water content in samples was detected by Karl-Fischer titration using a Mettler Toledo V20. Total acid number (TAN) value was determined using a Mettler Toledo T50 titrator (ASTM D664). The higher heating value (HHV) was obtained using an IKA C2000 bomb calorimeter. The elemental analysis (CHNS/O) was determined using Vario MICRO Elementar.

To determine the functional groups in liquid samples, FT-IR analysis was performed using Nicolet iS10 (Thermo Fisher Scientific). The samples were analyzed for 34 scans in the range of 500-4000 $cm^{-1}$ at a resolution of 4 $cm^{-1}$.

Moreover, the boiling point range of the upgraded oil was evaluated using Simulated distillation (Sim-dist) following ASTM D2887. The Sim-dist was performed using an Agilent 7890A GC equipped with flame ionization detector (FID) and an Agilent DB-2887 column (10 m × 0.53 mm × 3 μm).
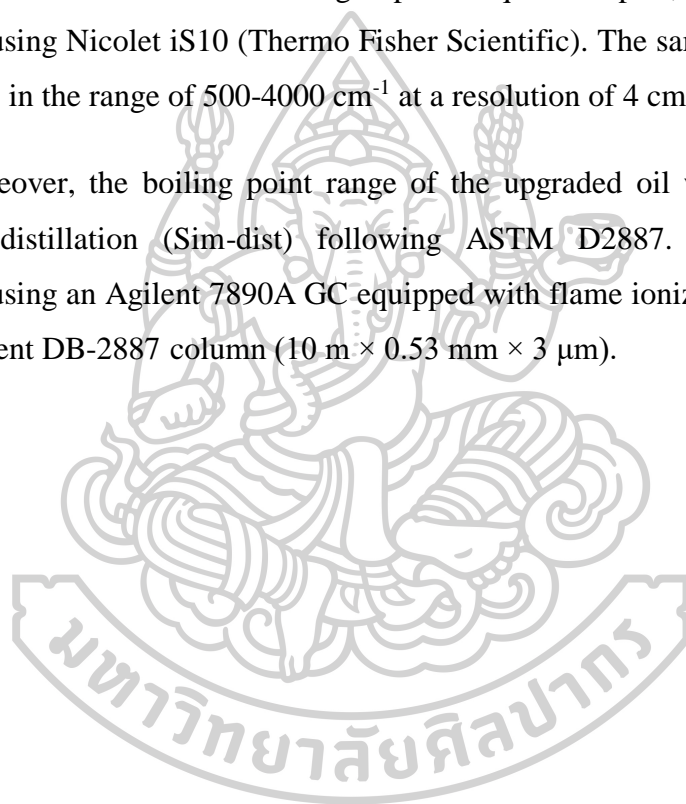
# CHAPTER 3

# LITERATURE REVIEW

## 3.1 Hydrothermal liquefaction

Hydrothermal liquefaction (HTL) or direct liquefaction, involves a thermal decomposition of biomass in the presence of water, and a catalyst is used occasionally. The products produced from this process consist of bio-oil or bio-crude oil which is a main product, gas, solid residue (char), and water-soluble product. HTL has more advantages due to relatively lower operating temperature and heating rate, and no need of biomass drying process, higher quality of bio-oil product with high heating value and low oxygen content [44–46].

Typical HTL, biomass-water slurry is carried out at moderate temperature between 200-400 °C and pressure of approximately 5-25 MPa which sufficient to maintain water in liquid stare, and residence time of up to 90 min [47]. At near critical point of water (374 °C, 22.1 MPa), the properties of water are changed opposite to those at normal condition (25 °C, atmospheric pressure) [44]. At elevate temperature, density and dielectric constant of water are decreased, resulting increased diffusivity and decreased in polarity of water, respectively. Also, at high pressure, an ionization of hot water is increased and highly dissociated. For these substantial changes in properties, water becomes a compressible non-polar solvent which can efficiently penetrate into biomass structure and extract its organic compounds that are typically water-insoluble to form bio-oil or other value product, and can acts as a reactant and accelerator for ionic reaction of organic matter by its acid-base behavior at high temperature [48,49]. Besides these, using water as medium in HTL exhibits several advantages due to its simplicity, low cost, and environmental-friendly.

**Table 1** Some properties of water at normal, subcritical and supercritical condition [49,50]

| Properties | 25 °C, 101. kPa | Subcritical | Supercritical |
|---|---|---|---|
| Dielectric constant | 78.5 | 14-27 | 6-10 |
| Density (g.cm$^3$) | 1 | 0.6-0.8 | 0.17-0.58 |
| Ionic product (pK$_w$) | 14.0 | 11-12 | 12-19 |
| Solubility of organic compounds | Very low | high | Very high |
| Solubility of inorganic compounds | Highly soluble | - | ≈0 |

**HTL Mechanism**

In HTL of lignocellulosic biomass, many complex reaction both physical and chemical take place simultaneously. Basically, the HTL mechanism involves three main pathways, depolymerization, decomposition, and rearrangement/recombination [45,51]. Firstly, the macromolecules in biomass is depolymerized into monomers. At elevate temperature, the dissociation of water facilitates disintegration of the lignocellulosic biomass into cellulose, hemicellulose, and lignin, which are subsequently depolymerized into oligomer and monomer compound by hydrolysis.

Degradation step involves several reaction, including cleavage, dehydration, decarboxylation, and deamination. During this step, the oligomers and monomers from the first step are degraded, forming relatively smaller compounds, and removed oxygen molecule through dehydration and decarboxylation, forming water ($H_2O$) and carbon dioxide ($CO_2$), respectively. The main products from this step are carboxylic acids, phenolic compounds, alcohols and aldehydes which are mostly unstable and active compound, and water-soluble [45,51,52].

The unstable and active small compounds can further undergo rearrangement (e.g. isomerization, cyclization) and recombination or repolymerization (aldol condensation), to form high-molecular-weight compound and solid residue (char) [52].

Moreover, there are other reaction occurred such as hydrogenation, deoxygenation to form organic hydrocarbon compound, as well as steam reforming and cracking to generate gas product such as CO, $CO_2$, $H_2$, and light hydrocarbon (C1-C4) [51,53].

**Table 2.** Physiochemical of pyrolysis bio-oil, HTL bio-crude, hydrotreating bio-oil and petroleum-based oil.

| Properties | Heavy fuel petroleum oil [54,55] | Diesel [54–56] | Hydrotreated bio-oil [55,57] | HTL bio-crude [45,51,58] |
|---|---|---|---|---|
| Moisture (wt. %) | <0.1 | <0.05 | <0.001 | 0.8-9.3 |
| pH | - | - | - | - |
| HHV (MJ/kg) | 40 | 43 | 41-46 | 15.8-38.6 |
| Density (15°C, kg·m$^{-3}$) | 0.95 | 0.82-0.86 | 0.83-0.93 | 0.96-0.99 |
| Viscosity (40-50 °C, cP) | 180 | 2.5 | 1 – 4.6 (at 23 °C) | 495 – 15,000 |
| Ash (wt. %) | 0.1 | - | - | 0.2- 1.43 |
| C (wt. %) | 85 | 84-87 | 76-87 | 44-81.4 |
| H (wt. %) | 11 | 13 | 9.7-13 | 5.2-9.76 |
| N (wt. %) | 0.3 | <0.1 | <0.6 | 0.095-4.47 |
| S (wt. %) | 15-2.5 | <0.001 | 0.005 | 0.01-0.18 |
| O (wt. %) | 1 | <0.1 | 0.02-14.2 | 9.8-16, 47.13 |
| Flash point (°C, min) | 65-100 | ≥ 52 | - | 29 |
| Pour point (°C, max) | 15-21 | -20 | - | 24 |

## 3.2 Hydroprocessing of biomass-based oil

Hydroprocessing of vegetable oil involves many catalytic reactions at moderate temperature (300-500°C) with high hydrogen pressure [57], including hydrotreating which eliminate the oxygen atom (hydrodeoxygenation, HDO), and also hydrocracking, hydrogenation, hydro-isomerization. Generally, the catalysts employed in hydroprocessing of triglyceride-based material and bio-oil upgrading can be categorized into two types: (1) sulfided metal catalysts e.g. conventional hydroprocessing molybdenum (Mo) based catalyst [59,60] and (2) noble metals such as Pd, Ni, and Pt [32,61].

Sulfidation forms is the most common of Mo supported on alumina. CoMo and NiMo sulfide catalysts are commercially used in hydroprocessing of triglycerides because this catalyst is well established as hydrodesulfurization (HDS) catalysts for sulfur removal from crude oil streams for many decade. High activity of sulfided catalysts revealed the complete conversion over hydrodeoxygenation of triglycerides[60,62]. The liquid product over NiMo and CoMo sulfided catalyst was produced through hydrodeoxygenation and decarboxylation/decarbonylation pathway but hydrodeoxygenation more favor than decarboxylation/decarbonylation pathway [63]. However, the sulfided catalysts could be deactivated by water poisoning [59] and leaching of sulfur from surface of catalyst [64]. It is necessary to blend triglyceride feedstock with sulfiding agent in order to maintain catalyst in sulfided form, but the end-product could be impurified with sulfur [65]. This is the reason that non-sulfided catalysts both of precious metal such as Pt [66], Pd [67–70], Ru [32], Rh [71] and non-precious metal such as Ni [72] and Co [73,74] have been developed for deoxygenation of triglyceride.

The investigation of non-sulfided catalysts has been shown to convert triglycerides, fatty acids and their ester into *n*-alkane by decarboxylation/decarbonylation reaction[75,76]. Thus, as compared with hydrodeoxygenation pathway (favor pathway over sulfide metal catalyst), supported metals catalyst promoting decarboxylation/decarbonylation pathway offers the advantage of lower hydrogen consumption [60]. Among these catalyst, palladium supported on activated carbon has been studied extensively and revealed that it is the most selective and active catalysts for deoxygenation of fatty acids and their ester [32,77,78]. However, the applicability of noble metal catalyst was limited in large scale of deoxygenated biofuel production due to their extremely high cost and low availability [79,80]. In contrast, transition metal catalysts such as Ni and Co, especially supported Ni-based catalyst, have been revealed an attractive catalyst for hydroprocessing because their less expensive and highly abundance.

### 3.2.1 Deoxygenation mechanism

Deoxygenation is known as a catalytic reaction for removal of oxygen from oxygenated molecules, which is one of the most promising mechanisms for biofuels production from biomass-based oil and animal fat. Biomass-based materials contain highly amount of oxygenated compound which has some adverse effects to their conversion to liquid fuels (bio-oil) such as low heating value, thermal instability, and corrosive. Hence, the efficient elimination of oxygen from both bio-oil and triglycerides-based (e.g. vegetable oil) molecules are necessary to overcome the disadvantages and improve the physiochemical properties of bio-oil.

The deoxygenation of triglycerides have been studies for several years. There are many reports about the reaction pathways consist of liquid and gas phase reaction. Veriansyah et al [81] proposed the possible reaction pathways of deoxygenation of soybean oil over hydrotreating catalysts, as shown in *Figure 3*. Firstly, triglycerides is hydrogenated and decomposed into various intermediates, including monoglycerides, diglycerides and free fatty acid.
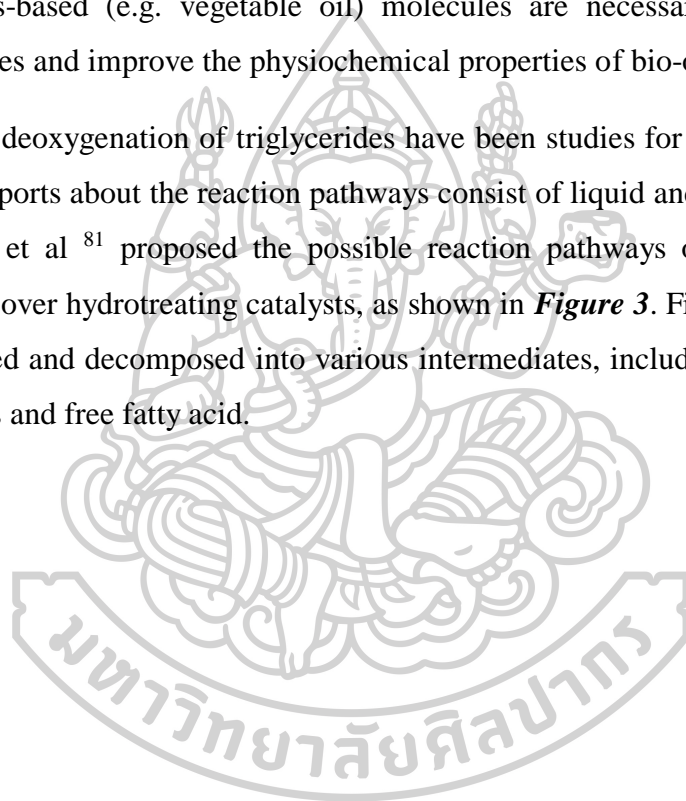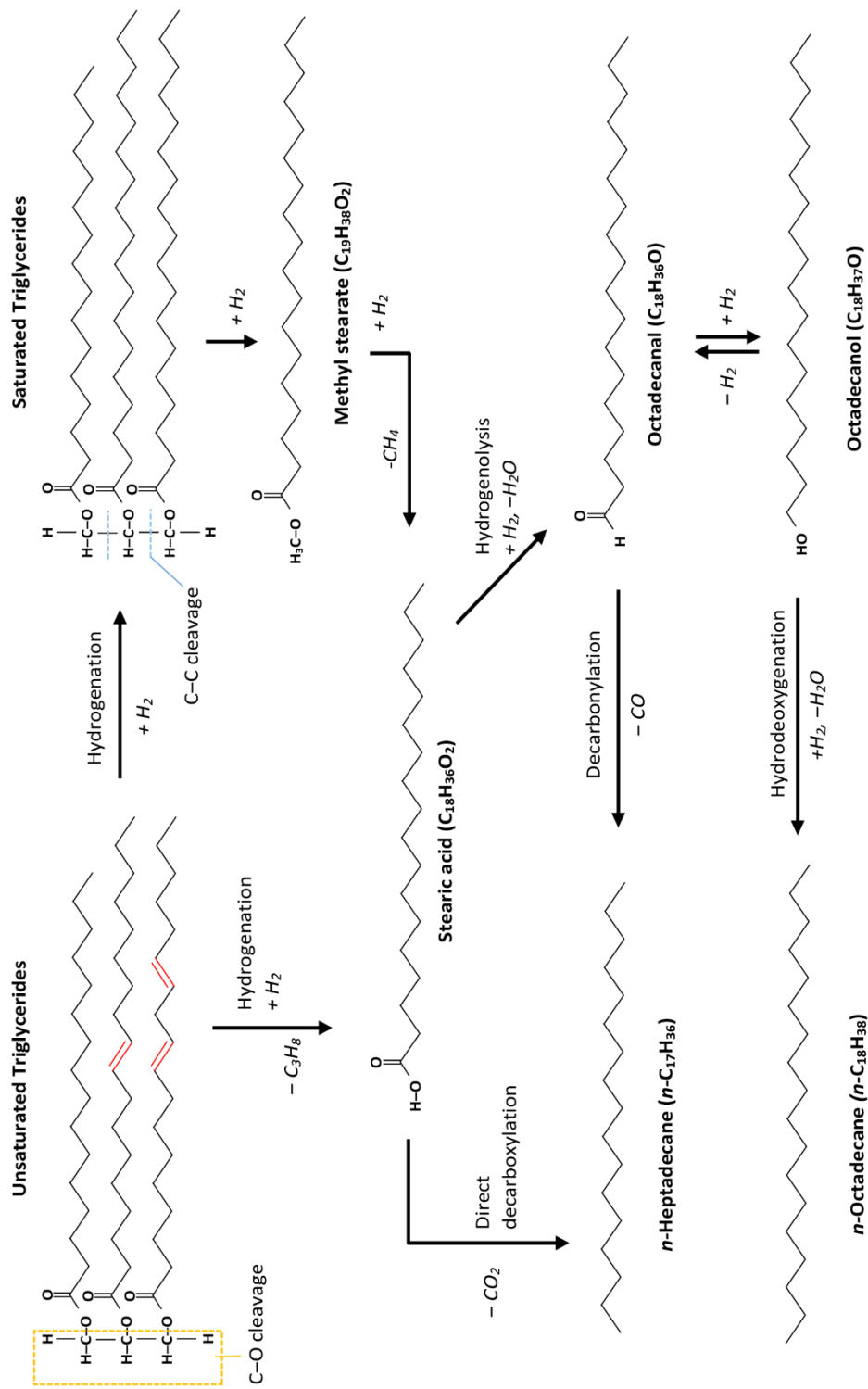
**Figure 3.** Possible reaction pathways of triglycerides over hydrotreating catalyst.

Subsequently, the intermediates are converted into alkanes by different pathways: decarboxylation (i), decarbonylation (ii), hydrodecarbonylation (iii), and hydrodeoxygenation (or dehydration/hydrogenation) (iv). Direct decarboxylation and decarbonylation produce n-alkane and alkenes, respectively. These two reactions do not require hydrogen for removing oxygen atom, while hydrodecabonylation and hydrodeoxygenation consume one and three moles per one fatty acid molecule, respectively.

*Liquid-phase Reaction* [32]

(i)      Decarboxylation (DCO$_2$)          $R\text{-}COOH \rightarrow R\text{-}H + CO_2$

(ii)     Decarbonylation (DCO)             $R\text{-}COOH \rightarrow R'\text{-}H + CO + H_2O$

(iii)    Hydrodecarbonylation (HDCO)       $R\text{-}COOH + H_2 \rightarrow R\text{-}H + CO + H_2O$

(iv)     Hydrodeoxygenation (HDO)          $R\text{-}COOH + 3H_2 \rightarrow R\text{-}CH3 + 2H_2O$

*R = saturated alkyl group*

*R' = unsaturated alkyl group*

*Gas-phase Reaction*

(v)      Methanation        $CO + 3H_2 \leftrightarrow CH_4 + H_2O$

(vi)     Methanation        $CO_2 + 4H_2 \leftrightarrow CH_4 + 2H_2O$

(vii)    Water-gas shift    $CO + H_2O \leftrightarrow CO_2 + H_2$

For eq (i)-(iii), the carboxyl group is removed from fatty acid by cleavage C-C bond as $CO_2$, CO and water, hence the hydrocarbon product from these reaction are contain odd numbers of carbon atom. On the contrary, linear alkanes with the full length of carbon from the fatty acid and water can be obtained from hydrodeoxygenation pathways by C-O scission (Eq. iv). Besides these main reactions, the hydrocarbon fuels production can undergo the consecutive reaction such as cracking, isomerization and cyclization, lead to formation of light hydrocarbon, iso-alkanes and aromatics.

The gaseous products from deoxygenation reaction composed of carbon monoxide (CO), carbon dioxide ($CO_2$), and water, can react with hydrogen and participate in a methanation, water-gas shift, and/or reverse water-gas shift, as shown in the equation (v)-(vii). Generally, the selective reaction pathway, the composition and quality of liquid product depend on catalyst type and operating conditions.

### 3.2.2 Supported Ni catalyst

The supported Ni catalyst for deoxygenation of fatty acid was proposed by Snare et al. (2006) who studied supported metal catalyst screening for deoxygenation of stearic acid. Several metal catalysts including Ni, Mo, Pd, Pt, Ru, Ir, Rh and Os supported on $Al_2O_3$, $Cr_2O_3$, MgO and $SiO_2$ as well as carbon were investigated under the same reaction conditions at 300°C under 6 bar He in a semi-batch reactor. In this study, 5%wt Pd/C was reported to be the most selective and active catalyst for deoxygenation of stearic acid, which complete conversion (100%) of stearic acid and 95% of C17 selectivity. In contrast, supported Ni catalysts showed very low activity (conversion <20%) even though it contained the highest active metal.

The result was in agree with [66] who investigated deoxygenation of waste fat by using oleic acid and tripalmitin as a model feed over various catalysts i.e. Pd, Pt and Ni on γ-$Al_2O_3$. Under the same condition, at 325 C, 20 bar hydrogen, 5 h reaction time in batch reactor, they found that Ni/γ-$Al_2O_3$ was less activity and less selective to deoxygenation than Pd/γ-$Al_2O_3$ and Pt/γ-$Al_2O_3$ so the efficiency of catalysts were reported to follow the order Pd>Pt>Ni. The poorest performance of Ni/γ-$Al_2O_3$ is result from the largest particle size of Ni (8.2 nm) with respect to Pd (4.6 nm) and Pt (5.4 nm) on average. However, Ni/C was reported the higher active and selective to deoxygenation more than Pd/C and Pt/C. This study, the reaction was performed over 20wt% Ni/C, 5wt% Pd/C and 1wt% Pt/C catalyst in deoxygenation of triglyceride and fatty acid (tristearin, triolein and soybean oil) under nitrogen atmosphere [82]. The higher activity of Ni/C was owing to the highest active metal loading of 20wt% of Ni compared to Pd and Pt. Moreover, 20wt% Ni/C is also higher active catalyst for C-C cracking activity due to its high acid sites [83].

The studied of supported Ni catalyst in the bio-oil upgrading process have also been reported. Witsuthammakul and Sooknoi [31] studied in screening metal supported catalysts for discovering the suitable catalyst for hydrodeoxygenation of ketones as a model compound of bio-oil derived product to produced olefins. Among various metal (Cr, Fe, Co, Ni, Cu, and Pd) supported on $SiO_2$, $Ni/SiO_2$ showed the highest activity at mild condition, but it also revealed the high selective for methane production which is an undesired product. Moreover, the effect of metal loading and support were also investigated. The activity of $Ni/SiO_2$ was enhanced when the metal loading was increased, due to the high number of active sites.

Though supported Ni-based catalyst have been reported to be potentially effective catalyst in hydrodeoxygenation of oxygen containing compound; the stability of catalyst is low due to carbon deposition on the catalyst surface and sintering of Ni metal lead to catalyst deactivation. The characteristics of catalyst (such as particle size, pore size, pore distribution, acid-base properties and etc.) are important factor which strongly affect to the activity, the stability of catalyst as well as product distribution. Therefore, the effect of supported, nickel loading and promoters on selective deoxygenation performance in nickel catalyst are reviewed.

### *3.2.2.1 Effect of supported and metal loading*

In 2012, Lercher's group proposed the series of Ni metal on various supports for hydrodeoxygenation of microalgae oil and fatty acid. Their first work [84] (*Table 3*, entry1) studied the deoxygenation of stearic acid and microalgae oil over 5 and 10 wt% of Ni loading supported on HBeta and HZSM-5 catalysts with different Si/Al ratio. The high Si/Al ratio or high Ni loading has affected to decrease the acid sites concentration of catalyst. The complete conversion was observed over 10wt% Ni/HZSM-5 (Si/Al=45) with n-C18 selectivity of 41.1% and 43% of cracking selective due to it contained strongly acid site, but the cracking rate was decreased by raising the Si/Al ratio. On the contrary, HBeta supported Ni catalyst showed full conversion of stearic acid but the Si/Al ratio was not affected to the cracking selectivity (lower than 0.7%). A comparative of Ni loading on HBeta support, the higher Ni loading displayed higher conversion and selectivity of alkane due to it

contained higher active metal, however, lower iso-alkanes was observed, indicating that high Ni concentration could be affected to lower acid site concentration causes a lower isomerization rate. 10wt% HBeta (Si/Al=180) was finally used in the hydrotreating of microalgae oil. The catalyst showed high total liquid alkane yield of 78wt% and good stability during 120 h.

In their second work [85] (*Table 3*, entry 2), the effect of Ni metal loading on $ZrO_2$ was studied. By varying Ni loading from 3 to 15wt%, the conversion and selectivity of n-C17 increased with increasing Ni loading, however, Ni loading to 15wt% does not affect catalytic performance. In addition, the effect of metal oxides support i.e., $ZrO_2$, $TiO_2$, $CeO_2$, $Al_2O_3$, and $SiO_2$ with 10% Ni loading was investigated. The complete conversion and high selectivity of n-C17 ($< 87\%$) was obtained over Ni catalyst supported on $ZrO_2$, $TiO_2$, $CeO_2$. Meanwhile, the catalyst supported on $Al_2O_3$, and $SiO_2$ showed the lower activity and selectivity. Because $ZrO_2$, $TiO_2$, $CeO_2$ are reducible supported, stearic acid could be adsorbed dissociatively on the oxygen vacancies of the support to form carboxylate and dihydrogen (route 2, *Figure 4*) to produce ketene intermediate which is hydrogenated to aldehydes over Ni particles. Moreover, Ni exhibited activity for hydrogenation of stearic to octadecanal (route 1, *Figure 4*). Therefore, the main reaction of Ni/$ZrO_2$ is following hydrogenation of fatty acid to form the aldehyde (in equilibrium with the corresponding alcohol), which is decarbonylated to heptadecane by CO removal. The deoxygenation of microalge oil was performed over the most active 10 wt% Ni/$ZrO_2$ catalyst at 270 °C and 40 bar $H_2$ in trickle bed reactor. More than 70% of n-C17 and total liquid alkane were observed. Besides, Ni/$ZrO_2$ catalyst showed high stability and no catalyst deactivation for a time on stream after 72 h.

In the comparison of their work, zeolite-supported catalysts exhibited the higher deoxygenated activity than metal oxide supported with the same Ni loading. However, $ZrO_2$ is a promising support due to it is able to adsorb the acid molecules at oxygen vacancy site, demonstrating its reducible property. Moreover, the deoxygenation of $ZrO_2$ as well as other oxide supported favored decarboxylation/decarbonylation, while hydrodeoxygenation reaction was enhanced over zeolite-supported.
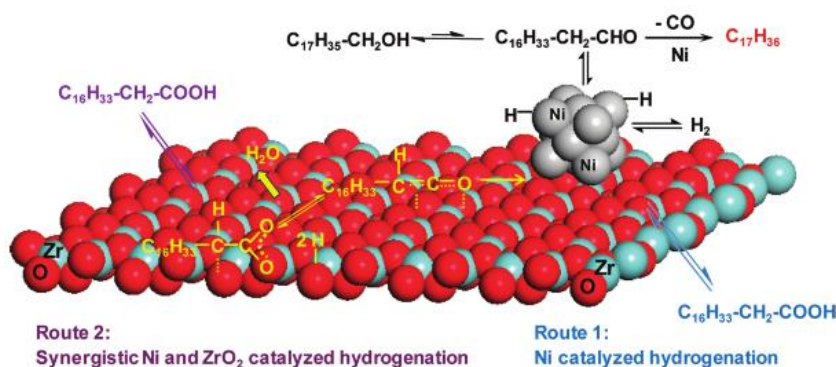
**Figure 4.** The reaction mechanism for deoxygenation of stearic acid to n-heptadecane via synergistic catalysis over Ni/ZrO$_2$. Source[85].

The effect of supported on nickel is continually investigated to seek the suitable supported on Ni catalyst for deoxygenation reaction. Zuo et al. [86], investigated the hydrodeoxygenation of methyl palmitate over Ni on various support namely SiO$_2$, γ-Al$_2$O$_3$, SAPO-11, HZSM-5, and HY, the same amount of Ni 7wt% was loaded into support. In all case, the mainly component in liquid product was n-pentadecane which represented by DCOx in **Table 3**, entry 3. The Ni/SiO$_2$ catalyst demonstrated the lowest activity (49.33% conversion) compared to other four support which the conversion are nearly 100%. However, the selectivity of C15 and C16 over 7wt% Ni/HZSM-5 and 7wt% Ni/HY were relatively low but more cracking activity was obviously observed, due to the strong acid site of HZSM-5 and HY. This results is consistent with [84]. In case of 7wt% Ni/SAPO-11 and 7wt% Ni/γ-Al$_2$O$_3$, not only high conversion was observed but also high selectivity of C15 and C16 (>90%). The high performance of 7wt% Ni/SAPO-11 was obtained with maximum diesel-like alkane yield of 93% due to the synergistic effect of Ni and the acidic sites of SAPO-11, showing its promising catalytic application in this reaction. Furthermore, the medium acidity of the catalysts could also inhibit carbon deposition which cause catalyst deactivation as comparing to the strong ones. The acidic sites and strength of the catalysts follows the order: 7 wt% Ni/SiO$_2$ < 7 wt% Ni/SAPO-11 < 7 wt% Ni/γ-Al$_2$O$_3$ < 7 wt% Ni/HZSM-5 < 7 wt% Ni/HY. Moreover, the high activity of Ni/γ-Al$_2$O$_3$ was exhibited due to the large surface areas and pore sizes of γ-Al$_2$O$_3$ which

lead to highly Ni dispersion and obtaining the very small particle size by no characteristic diffractions peak relative to Ni and NiO were observed.

In spite of the high performance of SAPO-11 in hydrodeoxygenation of methyl palmitate, amount of Ni loading on support was limited, high Ni loading led to low dispersion and large particle size, due to the small pore size and low surface area (85.6 $m^2$/g) of SAPO-11 [86]. Hence, the nano-sized SAPO-11 with high surface area was studied by the same author's group (*Table 3*, entry 4). The support was synthesized by a static hydrothermal method with using di-n-propylamine (DPA) as structure-directing agent and n-tetradecanoamine as surfactant. The nano-sized SAPO-11 support demonstrated larger surfaces and mesoporous volume with respect to the commercial SAPO-11. The Ni supported on the nano-sized SAPO-11 catalysts showed the higher liquid alkane yields and higher isomerization selectivities of more than 72% and 80%, respectively, with excellent catalytic stability, due to high active metal Ni dispersion and fast diffusion of the bulky palm oil and products as a consequence of the large surfaces and mesopores of the support. Moreover, the proper acidity by the functional of metal (Ni) and acid (SAPO-11) balancing could be suppressed the cracking reaction. Meanwhile it promoted the isomerization reaction and significantly reduced carbon deposition. TGA results revealed that the carbon deposition of the spent 7%Ni/SAPO-11 b was 6.5% which is much lower than the 21.3% of spent 7%Ni/SAPO-11 commercial [87].

According to their previous work, the different Ni loading on small particles of SAPO-11 with large surface area and mesoporosity was investigated. The support was synthesized by hydrothermally method, while 2 -9 wt% of Ni was loaded into support by incipient wetness impregnation [88], (*Table 3*, entry 5). The results showed that the liquid alkanes yield and isomerization selectivity were increased when increasing the Ni loading until reach to 7 wt%. 9%wt of Ni loading, the liquid alkane yield was similar, but the cracking reaction increased obviously as C1-C4 gas and C5-C18 liquid alkane yield were increased. Moreover, the stability of catalyst was test using 7wt% Ni/SAPO-11, the liquid alkane yield and isomerization selectivity were decreased after 35 h, indicating the excellent catalytic stability. After 35 h, the performance of catalyst was decreased due to the SAPO-11 particle size was

increased from <50 nm to 100 nm by sintering while the Ni particles was less than 20 nm. For transformation of palm oil, more than 85% of C15-C18 was found. Meanwhile, the fatty acid intermediates from HDO were detect as well as CO gas product from decarbonylation pathway. Hence, they concluded that the production of hydrocarbon over Ni/SAPO-11 catalyst was occurred via parallel hydrodeoxygenation (HDO) and decarbonylation pathway due to the proper acid value of SAPO-11 and the well balance between the Ni metal and acidic SAPO-11 functions (synergistic activation of C-O bond over acidic sites and hydrogenation over metal sites). In addition, the acid property and good match of metal and support can significantly inhibit cracking reaction and enhance isomerization selectivity likewise good stability. From this three work [86-88], it could be concluded that the properties of support including surface area and pore size as well as the acid value have affected the deoxygenation performance, besides, the acid value of support is essentially optimized to achieve the high activity and low cracking.

The acid value of catalyst is an important factor for production of biofuels including diesel, gasoline, and also jet range. Due to the acid value is related to cracking and isomerization reaction, which can convert long straight chain alkanes into many range of shorter alkanes depending on the acidity of catalyst. Moreover, high normal paraffin products from non-acidic catalysts present poor low-temperature properties, but it can improve by isomerization with moderate acidic catalyst. Bifunctional catalysts is the cooperation between different functionalities on the same system by the hydrogenation over transition metal and the hydrocracking and isomerization over acid site, offer the biofuel product with better characteristic in one step.

The influence of acidity of metal supported on acidic mesoporous material on the production of hydrocarbon was studied by Ochoa-Hernández et al. [89]. They studied in hydrotreating of methyl ester mixture over metal (Ni, Co) supported on SBA-15 and Al-SBA-15. Incorporation of aluminum into pure SBA-15 lead to existing of mild acid sites and higher metallic reduction temperatures. The higher reduction temperature of both of Ni and Co on Al-SBA-15 support was suggested the existence of smaller metal crystallite sizes and stronger metal-support interactions

between Ni and Co site with Al site. Both bifunctional Ni/Al-SBA-15 and Co/Al-SBA-15 catalysts demonstrated more hydrocarbon conversion and selectivity (including n-paraffins and iso-paraffins) than no acidity SBA-15 catalyst as shown in *Table 3*, entry 6. In addition, hydrodeoxygenation reaction is more favored over the acidic catalyst resulting in the formation of C18 and C16 majority product, and tendency to increase when Co as an active phase at low temperature (300 ∘C). Whereas the Ni, Co/SBA-15 produce more n-C17 than the acid ones. Regarding active phases, Co revealed good performance for production of hydrocarbon, especially for hydrodeoxygenation reaction. This result is good agreement to the reported by Srifa et al.[73] (*Table 3*, entry 7). They studied the catalytic behaviors of Ni/$\gamma$-Al$_2$O$_3$ and Co/$\gamma$-Al$_2$O$_3$ on the hydrodeoxygenation of palm oil. As their result, both catalysts exhibited good catalytic activity (complete conversion with more than 90% liquid alkanes yield) and high stability for 100 h on stream. Moreover, the reaction pathway for palm oil conversion was based on the active sites of catalyst, seeing that the dominant product contribution over Co was from decarboxylation/decarbonylation and hydrodeoxygenation pathway, while the Ni site was strongly promoted decarboxylation/decarbonylation pathway [73].

With regard to the high performance of Al-SBA-15 support in Ochoa-Hernández's report, Al-SBA-15 was employed in hydrodeoxygenation on bio-oil upgrading [90,91]. The effect of Ni supported on Al-SBA-15 compared to other support including zeolites, mesoporous material, transition metal oxide as well as microporous carbon support were reported by the author in the same group of Ochoa-Hernández. Yang et al.[91] focused on the Ni supported on various support i.e. SBA-15, Al-SBA-15, $\gamma$-Al$_2$O$_3$, TiO$_2$, CeO$_2$ and microporous carbon for producing aromatics from hydrodeoxygenation of anisole. They found that the complete conversion (100%) was observed over Ni supported on SBA-15, Al-SBA-15 and $\gamma$-Al$_2$O$_3$ and high selective to alkane and cycloalkanes. In contrast, the Ni/TiO$_2$, Ni/CeO$_2$ and Ni/C revealed high aromatic selectivity with mainly benzene, especially on Ni/TiO$_2$ catalyst. However, Ni/C is the most suitable catalyst for this study due to it showed high conversion (reach to 96%) compared to Ni/TiO$_2$ (<51%) and remarkable selectivity toward aromatics. This results can be attributed to the appropriate combination of strong acid

site and good dispersion of metal active site over Ni/C because the formation of aromatics can be promoted by hydrogenolysis of anisole which occurred on acid site while the hydrogenation was promoted on metallic site.

In the context of bifunctional catalyst as I mentioned earlier, the production of high quality hydrocarbon fuel via single-step over Ni supported on zeolites was reported by Wang et al.[92] (***Table 3***, entry 8). In this study, the Ni supported on different zeolites catalyst were employed in hydrodeoxygenation of soybean oil. From the results, 8 wt% Ni/SAPO-11 showed the best activity to produce diesel-ranged and high selective iso-alkanes. Over this catalyst, 100% conversion of soybean oil was obtained and 74.8% organic liquid yield was achieved with the 100% of alkanes- and 86.5 % isomerization selectivity. The good conversion, high liquid yield and superior isomerization selectivity were obtained over Ni/SAPO-11, owing to it has the suitable combination of structure including sufficiently meso-micropores with suitable pore size, and moderate acidity of the catalyst. In case of Ni/ZSM-5, the lowest conversion was observed, according to the characterization data, Ni/ZSM-5 contained smaller pore size diameter compared to the other catalysts, so triglyceride molecules can hardly react with the active sites located inside of the micropore. In addition, the lack of mesopores may be the reason for the low activity of Ni/ZSM-5 catalyst. For the low isoalkanes selectivity over Ni/Beta, they concluded that it was from the bigger micropores with three-dimentional pore structure of Beta zeolite, which could be promoted cracking reaction more than isomerization. Moreover, they proposed the reaction pathway for producing isoalkanes over Ni/SAPO-11 catalyst as shown in ***Figure 5***.

Briefly, the structure of pore and pore size distribution as well as acid value of catalyst strongly influence the distribution of hydrocarbon product. The sufficient mesopores distribution lead to completely alkanes conversion, while the one-dimensional micropore channel with suitable pore size together with the mild acidity of the support can enhance the isomeriztaion and suppress the cracking reaction. This is in strongly agreement with the reported already reviewed [86–88].
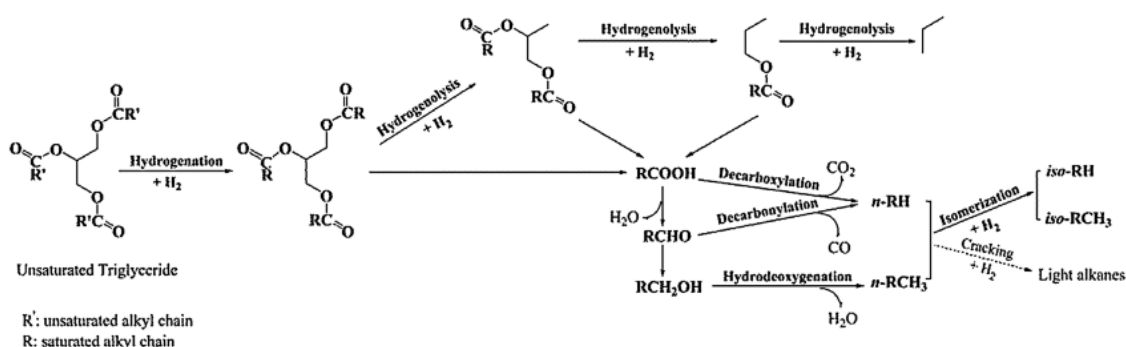
**Figure 5.** Reaction scheme of the hydrotreatment of soybean oil for producing isoalkanes over Ni/SAPO-11 catalyst [92].

Bifuctional Ni-based catalyst is also used in bio-jet fuel production from hydrodeoxygenation. The development of supported Ni catalyst on different zeolites to produces high quality bio-jet fuels in one-step was reported by Cen's group [93–95]. In the first report [95], they found that zeolite Y exhibited higher jet range alkanes selectivity and lower jet range aromatics than zeolite HZSM-5. The second work [93], zeolite Y was compared with other support (SAPO-34 and mesoporous zeolite Y) to convert waste cooking oil into jet range alkanes (C8-C16). Ni/SAPO-34 demonstrated a high jet range alkane yield of 40.8% and a low jet range aromatic hydrocarbon yield of 4.3% at 390 °C. The highest jet range aromatic was obtained over Ni/HY, which cause the low heating value of bio-jet fuel, while Ni/SAO-34 exhibited highest diesel range selectivity compare to other two catalyst, should be attributed to the low acid value of catalyst. The high activity of Ni/SAPO-34 was also observed in their third work [94], which compare to Ni supported on other four support namely MCM-41, SAPO-11, HY, and Hbeta. The Ni/SAPO-34 catalyst exhibited the highest alkane selectivity (65%) and lowest arene selectivity (11%), and the yield increased when increasing temperature. The activity of this five catalyst in term of high jet range alkanes selectivity are in following order: Ni/SAPO-34 > Ni/MCM-41 >Ni/HY >Ni/SAPO-11 >Ni/Hbeta.

Apart from zeolites supports, the good activity of deoxygenation over oxide support (such as SiO2, Al2O3, CeO2, ZrO2 and TiO2) have been report. Zirconium oxide is a promising support due to the activation of oxygen compound on surface

[71,85], but the textural properties is poor. Thus, the mixed oxide support has been revealed for improvement catalytic performance.

$SiO_2$-$ZrO_2$ mixed oxide was employed as supported in the study of hydrodeoxygenation of lignin-derived phenolic compound [96]. In the study, they compared the performance of catalyst between 10 wt% Ni supported on $ZrO_2$ and $SiO_2$/$ZrO_2$, in addition, the effect of Si/Zr ratio was observed (*Table 4*, entry 5). The Ni/SZ-n was represented Ni/ $SiO_2$-$ZrO_2$ (n is the molar ratio of Si/Zr). In the results, the activities of catalysts supported on SZ-n were obviously higher than that of catalysts supported on $ZrO_2$, due to the higher surface area (Ni/$ZrO_2$ = 6.21 $m^2$/g, Ni/SZ-n $\approx$ 220 $m^2$/g) was observed, lead to high Ni metal dispersion. Moreover, the acidity of SZ-n was higher than $ZrO_2$, which related to hydrogenation, dehydration isomerization and cracking reaction [97]. The Ni/SZ-3 exhibited the highest performance on HDO of phenolic compounds with complete conversion and more than 98% hydrocarbon selectivity (mainly cyclohexane) at 300 °C, 50 bar $H_2$ pressure. In addition, Ni/SZ-3 also showed the high recyclability which was repeatedly used for four runs with slightly dropped conversion, and excellent anti-coking formation due to the combination of $SiO_2$-$ZrO_2$ support exhibited amphoteric character which cause inhibition of coke formation. Significantly, the Ni/SZ-3 exhibited 54.99% alkane yield and 7.82% aromatic yield from HDO of the real lignin-derived phenolic compounds. According to the experimental results, they proposed the reaction pathway for HDO of guaiacol as shown in *Figure 6*, which could be that dehydroxylation, demethoxylation, demethylation and transmethylation might be parallel competing reaction at the beginning, which was proved by the detected product and intermediate component.
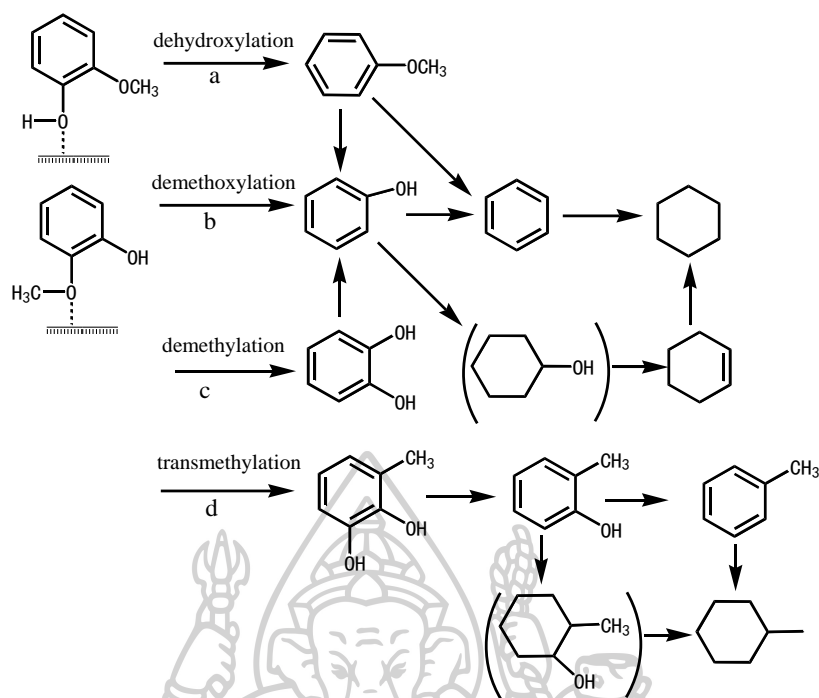
**Figure 6.** Tentative catalytic reaction pathways for the HDO of guaiacol [96].

The study of supported mixed oxide on HDO reaction was also reported by Shu et al., [98] (***Table 4***, entry 1). The synergistic effect of Ni and acid site on $SiO_2$-$Al_2O_3$ support for syringol hydrodeoxygenation was investigated. The results revealed that $Ni/SiO_2$ and $Ni/SiO_2$-$Al_2O_3$ were higher active on syringol HDO reaction more than $Ni/Al_2O_3$. The 98.4% conversion with 98.9% hydrocarbon selectivity was obtained over $Ni/SiO_2$-$Al_2O_3$, due to the mixing of $SiO_2$-$Al_2O_3$ oxide supported on Ni can increase the Ni dispersion and acid value of catalyst. Moreover, they also proposed the reaction pathway for syringol HDO which resemble the previously proposed [96]. However, the pathway for hydrogenated-deoxygenated phenol into cyclohexane was not detected, thus over this catalyst phenol can undergo only dehydroxylation, due to the synergistic effect of highly active Ni dispersion and acid site.

To summarize all above reviewed, support play an important role for the hydrodeoxygenation performance and also effect on product distribution. The proper textural properties including specific, surface area, pore size, and pore structure, together with acid-based properties of support is a key factor for development of

catalyst. The high surface area offer the high dispersion of active metal sites, while the pore size and pore structure affect to mass transfer of substrate and product molecules. Moreover, acidic supports offer high conversion, isomerization, and especially cracking reaction. Basic supports can decrease catalytic deactivation rate due to its offer high sintering and coking resistance [99], but the hydrodeoygenation activity is low compare to acidic support. Therefore, the optimization of acid-based support is necessary.

### 3.2.2.2 Effect of promoter

As mention in the last section, the supported monometallic Ni catalyst have many report about the high performance on hydrodeoxygenation of biomass-based material. However, the monometallic Ni catalysts was also reported to be strongly active in methanation reaction [31,73] which may cause the catalyst deactivation by carbon deposits due to the decomposition of methane [65,99]. The addition of promoters such as Cu, Fe and Co could be solved this problem. Recently, there are many report which reveal the superior catalytic properties of bimetallic Ni-Cu compare to monometallic Ni catalysts for HDO of vegetable oil [100], fatty acid and algal lipid [101] as well as bio-oil upgrading such as guaiacol [102–104], pyrolysis algae oil [105], anisole and fast pyrolysis oil [71,106]. Adding Cu in supported Ni catalysts can retard cracking reaction [101] and the carbon deposition and decrease methane yield during the HDO of oxygenated-compound [71]. In addition, Cu can reduce the reduction temperature of NiO at lower 350 °C [71,102], which can limit the sintering of active phase [107].

Aside from Cu, iron (Fe) was studies as promoter in Ni/SBA-15 catalyst in steam reforming of biomass derived tar reaction [108]. Compare to Ni/SBA-15, adding Fe can promote catalytic activity and stability, in addition, it is effective in suppressing the coking formation rate, due to its redox properties. For HDO of oxygenated-compound, the monometallic Fe was investigated in green diesel production from HDO of microalgal oil [109]. In this study, Fe nanoparticles supported on mesoporous silica nanoparticles (Fe-MSN) was employed, the hydrocarbon yield nearly 100% was obtained at 290 °C, 30 bar $H_2$ at 6 h reaction with mainly *n*-octadecane (*n*-C18). This suggest that the HDO of microalgal oil over Fe-MSN

underwent hydrodeoxygenation reaction as the major pathway, due to the partially oxidized by acid occurred on the surface of iron. The process involved the reduction of carboxylic acid to aldehydes, then it was continuously reduced by $H_2$ (under the study conditions) to form alcohol which is an intermediated of $n$-C18 production. From the results, the reaction mechanism on surface of Fe-MSN was proposed as shown in
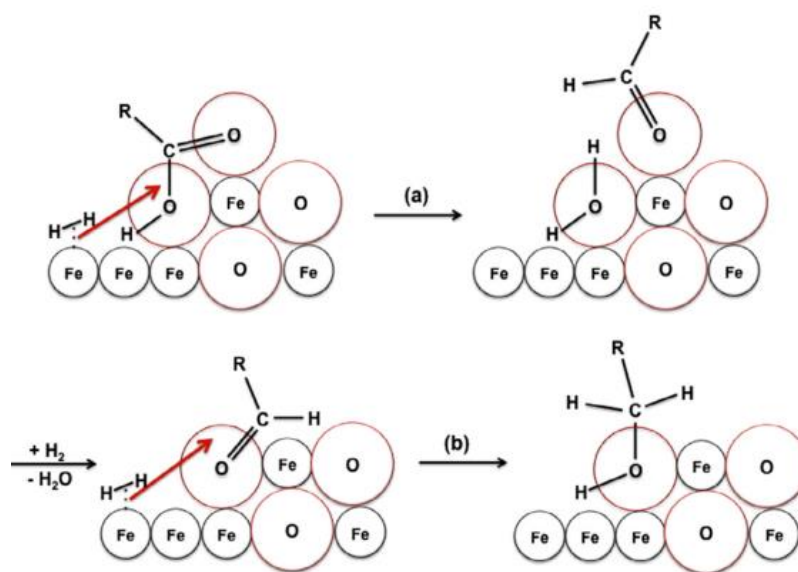


**Figure 7**. Proposed mechanism of the hydrogenation of carboxylic groups on the surface of the partially oxidized Fe nanoparticles of Fe-MSN: (a) reduction to aldehyde, and (b) further reduction to alcohol. The oxygen atoms eliminated from the FFA may either escap [109].

Moreover, NiFe catalyst exhibited the performance for improvement of heating value and pH of liquid fuel product by HDO of model compounds of bio-oil [110]. The conversion of furfuryl alcohol, benzene alcohol and ethyl oenanthate was 100, 95.48 and 97.89% at 400 °C. The major reaction pathway is the cleavage of C-O rather than C-C under the study condition. This result is consistent with [111,112].

As mentioned earlier, the precious metal such as Pd, Pt, and Ru were reported the higher catalytic performance compared to Ni-based catalyst, even small at small loading amounts. However, usage of the precious metal catalysts was limited by their

high cost. The adding a small quantities of precious metal on Ni-based bimetallic catalyst may be greatly improve the catalytic performance. As we known, Platinum (Pt) is very active for hydrogenation. When Pt is introduced in Ni-based catalyst to form bimetallic Ni-Pt, the Ni-Pt exhibit significantly higher hydrogenation activity of benzene [113], cyclohexene[114], and 1, 3-butadiene [115] at low-temperature compared to monometallic Ni and Pt monometallic Ni and Pt catalysts. Moreover, Pt has been reported as a promoter of bimetallic Ni-based catalyst for methane dissociation [116,117], The results demonstrated that adding Pt on Ni catalyst suppresses the coke formation.

Usage of promoters such as Rhenium (Re) was reported to help in decrease Ni particles size, lead to high dispersion of Ni and prevent coke formation, greatly improve the catalytic activity [118,119]. Yang et al., studied the geometric and electronic effects of bimetallic Ni–Re catalysts for selective deoxygenation of m-cresol to toluene [119]. The Ni-Re-support interaction was shown in *Figure 8*.
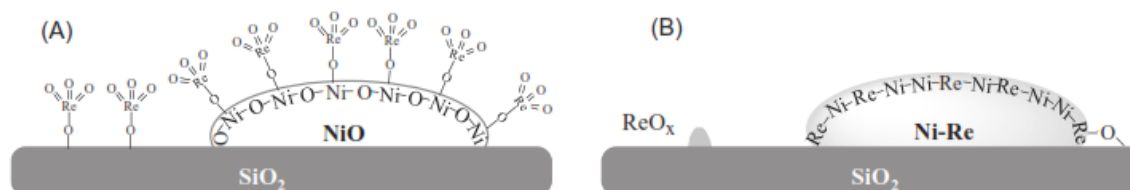


**Scheme 2.** Schematic representation of the structure of bimetallic Ni–Re catalyst before (A) and after (B) reduction at 450 °C for 1 h.

**Figure 8.** The structure of bimetallic Ni-Re catalyst before (A) and after (B) reduction at 450 °C for 1 h [119].

Adding Re to the Ni/SiO$_2$ catalyst increase NiO dispersion through the Ni-O-Re interactions. The proximity between NiO and ReOx species could prevent the NiO particle agglomeration during calcination and facilitate forming surface Ni–Re alloy during reduction. The presence of Ni-Re sites enhance the transformation of phenol via the C-O cleavage. It can be described by adsorption of phenol on surface. Over Ni-Re surface, the phenyl ring would adsorb on Ni site and O on Re sites facilitates C-O bond cleavage compared to that on single Ni catalyst which absorbed phenyl ring with O pointing away from the surface. Moreover, the Ni ensemble with a small size would inhibit the C-C hydrogenolysis that is favored by the transition state.

**Table 3.** Summary of the hydrodeoxygenation performance of triglycerides and related compound over supported Ni catalyst.

| Entry | Reactant | Catalyst | Reactor | Reaction condition | Conversion (%) | Selectivity (%) | | | |
|---|---|---|---|---|---|---|---|---|---|
| | | | | | | HDO | DCOx | cracking | iso-alkane |
| 1 [84] | Microalgae oil/Stearic acid | 10wt% Ni/HZSM-5 (Si/Al=45) | Batch | T= 260 °C, P =40 bar H$_2$, Time = 8h, Stearic acid 1.0 g in 100mL dodecane Catalyst weight 0.2g Stirring = 600 rpm | 100 | 41.1 | 9.2 | 42.7 | 6.7 |
| | | 10wt% Ni/HZSM-5 (Si/Al=120) | | | 65 | 67.5 | 8.8 | 15.9 | 7.6 |
| | | 10wt% Ni/HZSM-5 (Si/Al=200) | | | 60 | 80.1 | 6.1 | 7.2 | 6.3 |
| | | 5wt% Ni/HBeta (Si/Al = 75) | | | 96 | 66.5 | 13.8 | 0.7 | 18.8 |
| | | 10wt% Ni/HBeta (Si/Al = 75) | | | 100 | 72.6 | 14.8 | 0.6 | 11.7 |
| | | 5wt% Ni/HBeta (Si/Al = 180) | | | 96 | 82.8 | 10.2 | 0.4 | 16.2 |
| | | 10wt% Ni/HBeta (Si/Al = 180) | | | 98 | 84.6 | 9.5 | 0.4 | 5.2 |
| 2 [85] | Microalgae oil/Stearic acid | ZrO$_2$ | Batch | T= 260 °C, P =40 bar H$_2$, Time = 8h, Stearic acid 1.0 g in 100 mL dodecane Catalyst weight 0.5g Stirring = 600 rpm | 13 | - | 3.2 | - | n.d. |
| | | 3wt% Ni/ZrO$_2$ | | | 96 | 2.5 | 51 | 3.4 | |
| | | 5wt% Ni/ZrO$_2$ | | | 100 | 2.0 | 90 | 1.0 | |
| | | 10wt% Ni/ZrO$_2$ | | | 100 | 1.5 | 96 | 1.2 | |
| | | 15wt% Ni/ZrO$_2$ | | | 100 | 1.5 | 96 | 1.3 | |
| | | 10wt% Ni/CeO$_2$ | | | 100 | 0.4 | 93 | 2.8 | |
| | | 10wt% Ni/TiO$_2$ | | | 98 | 5.0 | 87 | 0.9 | |
| | | 10wt% Ni/Al$_2$O$_3$ | | | 63 | 0.7 | 81 | 0.9 | |
| | | 10wt% Ni/SiO$_2$ | | | 45 | 1.5 | 57 | 1.3 | |

| Entry | Reactant | Catalyst | Reactor | Reaction condition | Conversion (%) | Selectivity (%) | | | |
|---|---|---|---|---|---|---|---|---|---|
| | | | | | | HDO | DCOx | cracking | iso-alkane |
| 3 [86] | Methyl Palmitate | 7wt% Ni/SiO₂ | Semi-Batch | T= 220 °C, P =20 bar H₂, Time = 6h, H₂ flowing rate = 50 mL/min, Methyl palmitate 30 g, Catalyst weight 1.0 g, Stirring = 1000 rpm | 49.3 | 5.97 | 61.0 | 24.53 | 2.37 |
| | | 7wt% Ni/γ-Al₂O₃ | | | 90.9 | 16.72 | 71.71 | 5.08 | 0.0 |
| | | 7wt% Ni/SAPO-11 (Si/Al = 0.11) | | | 99.8 | 42.48 | 47.63 | 4.81 | 3.07 |
| | | 7wt% Ni/HZSM-5 (Si/Al = 38) | | | 99.7 | 22.47 | 30.54 | 42.0 | 8.41 |
| | | 7wt% Ni/HY (Si/Al = 2.9) | | | 98.5 | 9.97 | 20.17 | 63.64 | 5.69 |
| 4 [87] | Palm oil | 7wt% Ni/SAPO-11 Commercial* | Fixed-bed | T= 280 °C, LSHV = 2 h⁻¹, P =40 bar H₂, flowing rate 50 mL/min, Palm oil feeding rate = 0.05 mL/min, Catalyst weight 1.0 g (1.5 mL) of 40-60 mesh | Not report | 85.1** | | 12.4 | 35.0 |
| | | 7wt% Ni/SAPO-11 a | | | | 57.5** | | 38.7 | 79.5 |
| | | 7wt% Ni/SAPO-11 b | | | | 62.4** | | 33.9 | 81.2 |
| | | 7wt% Ni/SAPO-11 c | | | | 49.6** | | 46.7 | 81.7 |
| 5 [88] | Palm oil | 2wt% Ni/SAPO-11 | Fixed-bed | T= 360 °C, LSHV = 1 h⁻¹, P =40 bar H₂, flowing rate 50 mL/min, Palm oil feeding rate = 0.05 mL/min, Catalyst weight 2.0 g (3 mL) of 40-60 mesh | Not report | 70.0** | | 28.2 | 46.2 |
| | | 5wt% Ni/SAPO-11 | | | | 71.8** | | 26.4 | 54.0 |
| | | 7wt% Ni/SAPO-11 | | | | 75.3** | | 23.4 | 61.5 |
| | | 9wt% Ni/SAPO-11 | | | | 49.0** | | 49.5 | 83.4 |
| 6 [89] | Methyl oleate | 5wt% Ni/SBA-15 | Fixed-bed | T= 340 °C, WSHV = 20.4 h⁻¹, P =30 bar H₂, feeding rate = 0.1 mL/min of 70wt%f of methyl oleate in n-heptane, Catalyst weight 2.0 g of 400-250 μm. | 73 | 5 | 88.5 | | 2.0 |
| | | 5wt% Ni/Al-SBA-15 (Si/Al=68) | | | 99 | 15.0 | 66.0 | n.d. | 15.0 |
| | | 5wt% Co/SBA-15 | | | 90 | 25.0 | 64.0 | n.d. | 2.0 |
| | | 5wt% Co/Al-SBA-15 (Si/Al=68) | | | 98 | 41.5 | 40.0 | | 10.0 |

| Entry | Reactant | Catalyst | Reactor | Reaction condition | Conversion (%) | Selectivity (%) | | | |
|---|---|---|---|---|---|---|---|---|---|
| | | | | | | HDO | DCOx | cracking | iso-alkane |
| 7 [73] | Palm oil | 10wt% Ni/$\gamma$-Al$_2$O$_3$ | Trickle bed | T= 300 °C, LSHV = 1 h$^{-1}$, P =50 bar H$_2$, H$_2$/oil feed ratio = 1000 N(cm$^3$/cm$^3$), Catalyst weight 5.5 g | 100 | 2.1 ± 0.3 | 89.2 ± 2.4 | n.d. | n.d. |
| | | 10wt% Co/$\gamma$-Al$_2$O$_3$ | | | 100 | 45.8 ± 3.0 | 43.0 ± 3.3 | | |
| 8 [92] | Soybean oil | 4wt% Ni/SAPO-11 | Three phase, trickle bed | T= 370 °C, LSHV = 1 h$^{-1}$, P =40 bar H$_2$, flowing rate 300 mL/min, Catalyst volume 10 mL of 20-40 mesh with Inert silica 40-60 mesh | 98.9 | 98.1[+] | | 13.3 | 76.9 |
| | | 8wt% Ni/SAPO-11 | | | 100 | 100[+] | | 16.0 | 86.5 |
| | | 12wt% Ni/SAPO-11 | | | 100 | 100[+] | | 15.4 | 83.2 |
| | | 8wt% Ni/ZSM-22 | | | 100 | 100[+] | | 60.5 | 89.7 |
| | | 8wt% Ni/ZSM-23 | | | 100 | 100[+] | | 55.8 | 90.8 |
| | | 8wt% Ni/ZSM-5 | | | 80.1 | 67.4[+] | | 52.3 | 68.9 |
| | | 8wt% Ni/Beta | | | 100 | 97.6[+] | | 67.2 | 58.7 |
| 9 [120] | Stearic acid | H-Y-80 | Batch | T= 300 °C, P = 30 bar H$_2$, Time = 6 h, Stearic acid 1.0g in dodecane 100 mL, Catalyst weight 0.25 g, Stirring = 1200 rpm | 2 | - | - | n.d. | n.d. |
| | | 5wt% Ni/SiO$_2$ | | | 100 | 0.9 | 96.3 | | |
| | | 5wt% Ni/$\gamma$-Al$_2$O$_3$ | | | 100 | 1.9 | 96.2 | | |
| | | 5wt% Ni/H-Y-80 | | | 100 | 61.6 | 38.3 | | |
| | | Pd/C | | | 53.74 | 1.5 | 98.4 | | |
| 10 [121] | Mixture of ethyl caprate and methyl palmitate | 13Ni-5Cu/Al$_2$O$_3$ | Fixed-bed reactor | T= 300 °C, P = 25 bar H$_2$, LSHV = 3 h$^{-1}$, H$_2$ flow rate 5 L/h, Substrate rate 3 mL/h, Catalyst volume 1 cm$^3$ | 60 | 1.3 | 44.3 | 2.0 | n.d. |
| | | 12.4Ni-4.8Cu-2.2Mo/Al2O3 | | | 63 | 1.3 | 48.0 | 1.5 | |
| | | 11.7Ni-4.5Cu-3.9Mo/Al2O3 | | | 78 | 3.5 | 40.0 | 1.5 | |
| | | 11.3Ni-4.3Cu-5.6Mo/Al2O3 | | | 81 | 4.0 | 43.0 | 1.2 | |
| | | 10.1Ni-3.8Cu-6.9Mo/Al2O3 | | | 90 | 4.5 | 37.0 | 1.2 | |
| | | 7Mo/Al$_2$O$_3$ | | | 18 | 0.5 | - | - | |
| | | 9Ni-11Mo/Al$_2$O$_3$ | | | 90 | 21 | 150 | 1.5 | |

* The reaction temperature was 220 °C, ** It was reported as a selectivity of C15-C18, entry 4 and 5 are the report of nano-particle size SAPO-11, + Selectivity of alkanes

**Table 4.** Summary of the hydrodeoxygenation performance of bio-oil upgrading and model compound over supported Ni catalyst.

| Entry | Reactant | Catalyst | Reactor | Reaction condition | Conversion (%) | Hydrocarbon Selectivity (%) |
|---|---|---|---|---|---|---|
| 1 [98] | Syringol | 20wt% Ni/SiO$_2$<br>20wt% Ni/SiO$_2$-Al$_2$O$_3$ (Si/Al=5)<br>20wt% Ni/Al$_2$O$_3$ | Batch | T= 200 °C, P = 20 bar H$_2$,<br>0.2 g syringol in 20 mL decalin<br>Catalyst 0.1 g | 95.4<br>98.4<br>59.1 | 35.4<br>98.9<br>29.4 |
| 2 [104] | Guaiacol | 30.3wt% Ni-10.4wt% Cu/CeO$_2$-ZrO$_2$<br>14.1wt% Ni- 5.7wt% Cu/Al$_2$O$_3$<br>57.9wt% Ni- 7wt% Cu/SiO$_2$<br>36.5wt% Ni-2.3wt% Cu/ZrO$_2$-SiO$_2$-La$_2$O$_3$<br>55.4wt% Ni/SiO$_2$ | Batch | T = 320 °C, P = 17 bar H$_2$ initial<br>30 mL guaiacol<br>Catalyst 1 g<br>Stirring 2000 rpm | 94.2<br>80.3<br>87.1<br>85.6<br>97.5 | 1.6<br>49.9<br>72.7<br>80.1<br>90.9 |
| 3 [91] | Anisole | 20wt% Ni/C<br>20wt% Ni/CeO$_2$<br>20wt% Ni/SBA-15<br>20wt% Ni/Al-SBA-51<br>20wt% Ni/Al$_2$O$_3$<br>20wt% Ni/TiO$_2$ | Fixed-bed | T= 310 °C, WSHV = 20.4 h$^{-1}$<br>P = 3bar H$_2$, flowing rate 30 mL/min<br>Anisole in heptane (4wt %)<br>feeding rate = 6 mL/h | 96<br>98<br>100<br>99<br>99<br>51 | 96<br>98<br>97<br>98<br>98<br>98 |
| 4 [71] | Anisole | Ni/SiO$_2$<br>Ni/Cr$_2$O$_3$[a]<br>Ni/Al$_2$O$_3$<br>Ni/ZrO$_2$[a]<br>Ni-Cu/Al$_2$O$_3$<br>Ni-Cu/ZrO$_2$[b]<br>Ni-Cu/CeO$_2$[c] | Fixed-bed | T= 310 °C, LSHV = 1 h$^{-1}$<br>Feed gas 50vol% H$_2$ + 50vol% Ar<br>H$_2$ pressure 10 bar<br>feeding rate = 20 mL/h<br>Catalyst 0.5 mL diluted with 1 mL of quartz sand | 92.8<br>90.2<br>80.0<br>26.0<br>99.6<br>63.5<br>100 | 46.0[d]<br>15.7[d]<br>95.0[d]<br>69.0[d]<br>99.2[d]<br>60.0[d]<br>100[d] |
| 5 [96] | Lignin-derived phenolic compound | 10wt% Ni/ZrO$_2$<br>10wt% Ni/SiO$_2$-ZrO$_2$ (Si/Zr=1)<br>10wt% Ni/SiO$_2$-ZrO$_2$ (Si/Zr=3)<br>10wt% Ni/SiO$_2$-ZrO$_2$ (Si/Zr=5) | Batch | T = 300 °C, P =50 bar H$_2$<br>Reaction time 8 h<br>10 g reactants in dodecane<br>Catalyst 1.5 g, Stirring 800 rpm | 43.8<br>86.2<br>100<br>81.5 | ~95<br>~92<br>100<br>~96.5 |
| 6 [102] | Guaiacol | 10wt% Ni/ZrO$_2$<br>10wt% Ni-5wt% Cu/ZrO$_2$<br>10wt% Ni/SiO$_2$-ZrO$_2$ (Si/Zr=3)<br>10wt% Ni-5wt% Cu /SiO$_2$-ZrO$_2$ (Si/Zr=3)<br>10wt% Ni-15wt% Cu /SiO$_2$-ZrO$_2$ (Si/Zr=3) | Batch | T = 300 °C, P =50 bar H$_2$<br>Reaction time 8 h<br>10 g reactants in 100 gdodecane<br>Catalyst 1.5 g<br>Stirring 800 rpm | ~43<br>~39<br>100<br>100<br>~77 | ~94<br>~86<br>100<br>95.4<br>~88 |

# CHAPTER 4

# EFFECTIVE Cu/Re PROMOTED Ni-SUPPORTED γ-Al₂O₃ CATALYST FOR UPGRADING ALGAE BIO-CRUDE OIL PRODUCED BY HYDROTHERMAL LIQUEFACTION (HTL)

This chapter present the was to investigate the effect of Cu and Re addition on alumina supported Ni catalyst for upgrading of bio-crude produced from HTL of *Nannochloropsis* sp. Upgraded bio-oil yield, elemental content, and oil properties were here used to point out the activity of the catalysts. Moreover, the carbon efficiency and overall energy recovery ($ER_{overall}$) including ER from biomass algae to bio-crude ($ER_{HTL}$) and ER from bio-crude to upgraded bio-oil ($ER_{upgrade}$) are calculated. Finally, the reaction pathway of catalytic hydrotreating has been proposed.

## 4.1 Results and discussion

### 4.1.1 Catalyst characterization

To investigate textural properties of different γ-Al₂O₃-supported catalysts after the atmospheric-air calcination process, the morphology observation was performed for the synthesized catalysts by SEM as displayed in *Figure 9*. All catalysts are seemingly constructed from small quasi-spherical particles. An increase in the number of metal-type loading increased the size of particles, especially in the case of Ni-Cu-Re/γ-Al₂O₃, which is reasonably because of agglomeration of particles during heat treatment process [122]. From EDS elemental mapping analysis, a good dispersion of different active elements on γ-Al₂O₃ support was observed, indicating the perfect solution preparation and the wetting method subsequent with heat treatment process employed herein. The existing elemental compositions of catalysts are summarized in *Table 5*.
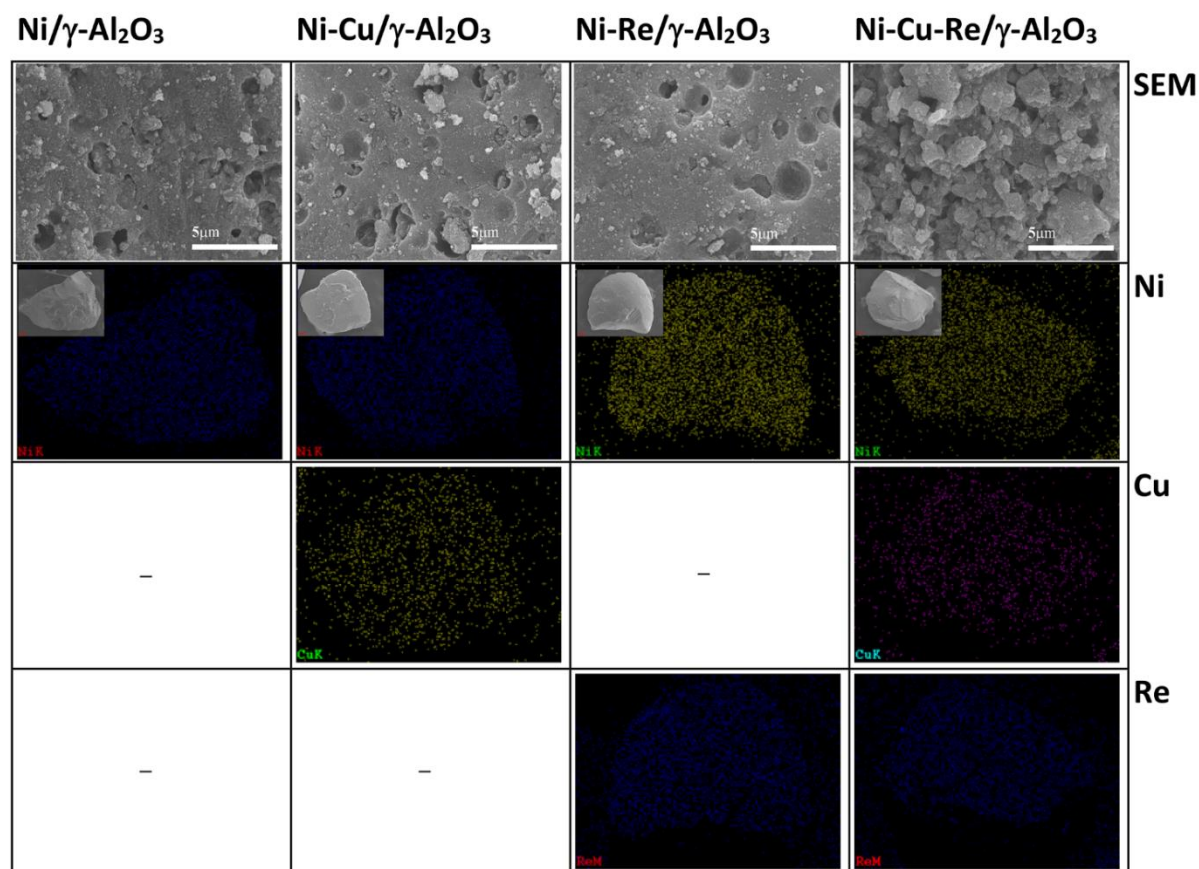
**Figure 9.** SEM micrographs and elemental mapping analysis of Ni/γ-Al₂O₃, Ni-Cu/γ-Al₂O₃, Ni-Re/γ-Al₂O₃, and Ni-Cu-Re/γ-Al₂O₃ catalysts. The insets show their corresponding high magnification SEM images of the catalyst particles.

**Table 5.** *Physicochemical properties of the support and catalysts.*

| Support/Catalysts | BET specific surface area* (m²/g) | Pore volume* (cm³/g) | Average pore diameter* (nm) | Metal content (SEM/TEM, wt%) | | |
|---|---|---|---|---|---|---|
| | | | | Ni | Cu | Re |
| γ-Al₂O₃ | 262 | 0.85 | 12.9 | - | - | - |
| Ni/γ-Al₂O₃ | 221 | 0.56 | 9.97 | 9.48/9.34 | - | - |
| Ni-Cu/γ-Al₂O₃ | 212 | 0.53 | 10.1 | 11.1/11.44 | 3.2/3.3 | - |
| Ni-Re/γ-Al₂O₃ | 211 | 0.54 | 10.2 | 9.29/8.1 | - | 0.7/2.12 |
| Ni-Cu-Re/γ-Al₂O₃ | 207 | 0.46 | 9.70 | 7.64/9.55 | 2.1/3.33 | 0.8/1.97 |

*Obtained from BET adsorption-desorption isotherm

The physical properties of the catalysts including porous structure along with the surface area were elucidated by the $N_2$ adsorption–desorption method. The $N_2$ adsorption–desorption profiles are shown in *Figure 10*. There was no different behavior observed among all the catalysts. All $\gamma$-$Al_2O_3$ supported samples exhibit isotherm type-IV with a pronounced type H2 hysteresis loop, indicating a characteristics of mesoporous materials with ink-bottle shape pores [123,124]. This result is consistent with the SEM results, implying an existence of irregular channel systems formed via assembling of quasi-spherical particles [125,126].

Data of pore volume, average pore diameter, and specific surface area are listed in *Table 5*. After the modification with Ni, Cu, and Re, the supported catalysts possessed the descended BET surface area, reasonably caused by partial blocking of the mesoporous structure by metal species. This is consistent with the decrease of pore volume and average pore diameters, which resulted from deposition of the metal layer on the $\gamma$-$Al_2O_3$ surfaces.
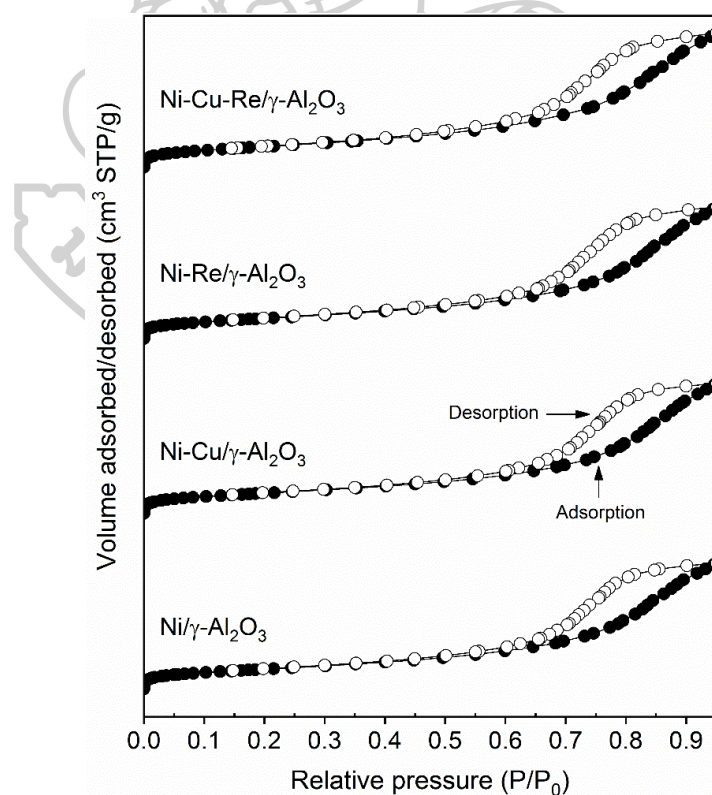


**Figure 10.** $N_2$ adsorption/desorption isotherms of catalysts: Ni/$\gamma$-$Al_2O_3$, Ni-Cu/$\gamma$-$Al_2O_3$, Ni-Re/$\gamma$-$Al_2O_3$, and Ni-Cu-Re/$\gamma$-$Al_2O_3$ catalysts.

The crystallographic features of the particle catalysts were also investigated by XRD as depicted in **Figure 11**. The commercial $\gamma$-$Al_2O_3$ used as catalyst support shows the diffraction peaks at $2\theta$ of around 37.6°, 39.3°, 45.7°, and 67°, which corresponds to (311), (222), (400), and (440) crystal planes (a face-centered cubic phase) of $\gamma$-$Al_2O_3$ with low crystallinity (JSPDS 00-010-0425) [126–128]. However, the (222) peak was clearly not observed in the case of all the doping catalysts. This is reasonably because of the phase transition of alumina taking place during the thermal treatment in atmospheric air [127,129]. Interestingly, no diffraction peaks around $2\theta$ of 37.2°, 43.3°, 62.9° and 75.4° corresponding to (111), (200), (220) and (311) crystal planes of NiO (JCPDS 44-1159) were detected, implying the highly dispersion of tiny NiO domains on the $\gamma$-$Al_2O_3$ surface.
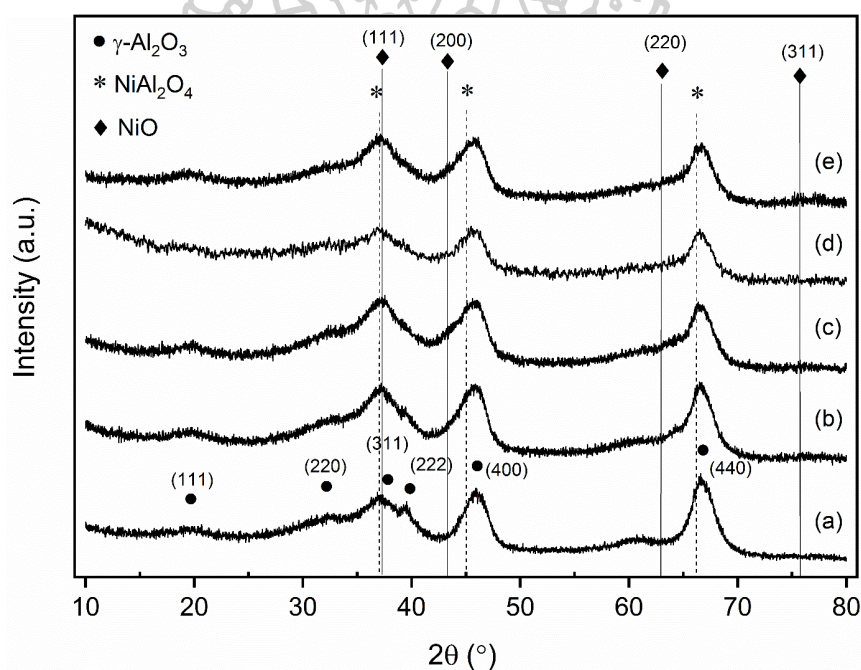


**Figure 11.** XRD patterns of support and fresh catalysts; (a) as-purchased $\gamma$-$Al_2O_3$ support, and as-prepared (b) Ni/$\gamma$-$Al_2O_3$, (c) Ni-Cu/$\gamma$-$Al_2O_3$, (d) Ni-Re/$\gamma$-$Al_2O_3$ and (e) Ni-Cu-Re/$\gamma$-$Al_2O_3$ catalysts.

Moreover, the peak shifting at around $2\theta = 66.5°$ for all doped catalysts from the $\gamma$-$Al_2O_3$ support also appeared, indicating nonstoichiometric $NiAl_2O_4$ spinel (JCPDS 10-0339) phase on the catalysts. This implies that the dispersion of Ni phase

trended to be preserved and a formation of $NiAl_2O_4$-like surface covering on the γ-$Al_2O_3$ support took place [126]. For the Ni–Cu/γ-$Al_2O_3$ catalysts, there were no diffraction peaks of CuO at 2θ = 35.5°, 38.7°, 48.6°, and 61.5° which correspond to (002), (111), (202), and (113) crystal planes (JCPDS 41-0254), present through all the XRD patterns. This might be reasonably because of good dispersion of Cu phase on the domains as also confirmed by EDS mapping (**Figure 9**), on the other hand, due to a lower metal content; as well for the circumstance of triple active metallic catalyst (Ni-Cu-Re/γ-$Al_2O_3$), the diffraction peak of Re phase was also absent.
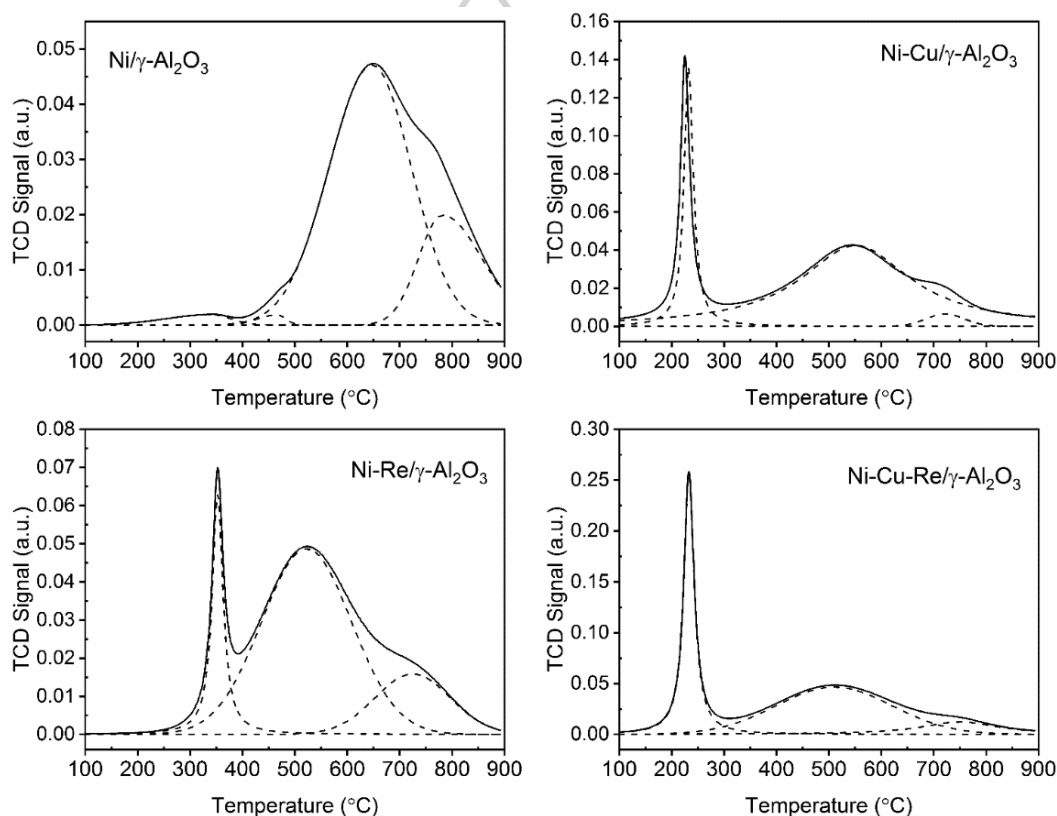


**Figure 12.** $H_2$-TPR profiles of catalysts; Ni/γ-$Al_2O_3$, Ni-Cu/γ-$Al_2O_3$, Ni-Re/γ-$Al_2O_3$, and Ni-Cu-Re/γ-$Al_2O_3$.

The XRD results also correspond to the TEM images and elemental mapping shown in Appendix A (**Figure 38**). It can be seen that Ni species are well dispersed on the surface of the alumina support. However, some NiO aggregation (Red dash-line circle) is observed over Ni/γ-$Al_2O_3$ (**Figure 38(a)**). On the other hand, the bi- and tri-metallic Ni catalysts show better dispersion of different metal species. This can be

explained that homogeneous distribution is obtained by the introduction of Re (*Figure 38(c-d)*), indicating that the interaction between Re and either Ni or Cu facilitates the dispersion of NiO. Also, the metal content was detected, which correspond to that obtained from the SEM analysis (**Table 5.** Physicochemical properties of the support and catalysts.*Table 5*).

In order to investigate the reducibility property of the various catalysts, $H_2$-TPR was carried out and the results are shown in *Figure 12*. Ni/$\gamma$-Al$_2$O$_3$ catalyst shows multiple broad peaks for the temperature range of 200–800 °C. The low-intensity shoulder peak at 350 °C representing a reduction of weak interacted-support bulk NiO to be Ni. Besides, the broad peaks at 400-750 °C are associated with reducing the strong interaction of NiO with Al$_2$O$_3$-support, while the reduction peak at higher 750 °C could be assigned to the reduction of difficultly-reduced species as bulk NiAl$_2$O$_4$ spinel [126,130]. Meanwhile, the reduction profiles of the bi- and tri-metallic catalysts are obviously different from that of the single Ni-metal catalyst. Ni-Re/$\gamma$-Al$_2$O$_3$ exhibits a sharp peak at 350 °C, and a broad peak at 527 °C, indicating the reduction of rhenium oxide or Ni-Re oxide, and NiO strongly bonded with $\gamma$-Al$_2$O$_3$-support, respectively. The same circumstance was also observed in the reduction profiles of Ni-Cu/$\gamma$-Al$_2$O$_3$ and Ni-Cu-Re/$\gamma$-Al$_2$O$_3$, the two reduction peaks at around 230-250 °C and 525-550 °C were found which could be attributed to the reduction of the dispersed CuO or Ni-Cu alloy species [38,79], and bulk NiO strongly interacted with the support, respectively. Interestingly, when introducing the Ni/$\gamma$-Al$_2$O$_3$ and Ni-Cu/$\gamma$-Al$_2$O$_3$ catalysts with Re metal, the reduction peak appeared with a high intensity compared with those of the mono- and bi-metallic with Re-free, suggesting that adding Re causes a positive effect on catalysts to enhance the reducibility of catalysts by hydrogen spillover [118,119,131].

## 4.1.2 Product distribution

The algae bio-crude oil was converted via catalytic hydrotreating process into four different phases; including oil phase (upgraded bio-oil), aqueous phase (water-soluble products), gas, and solid residue. The yields of product fractions from various

catalysts are presented in *Figure 13*. The mass balance closure is greater than 97 wt. %. The mass loss observed in all experiments could be occurred during product collection, extraction, and recovery.
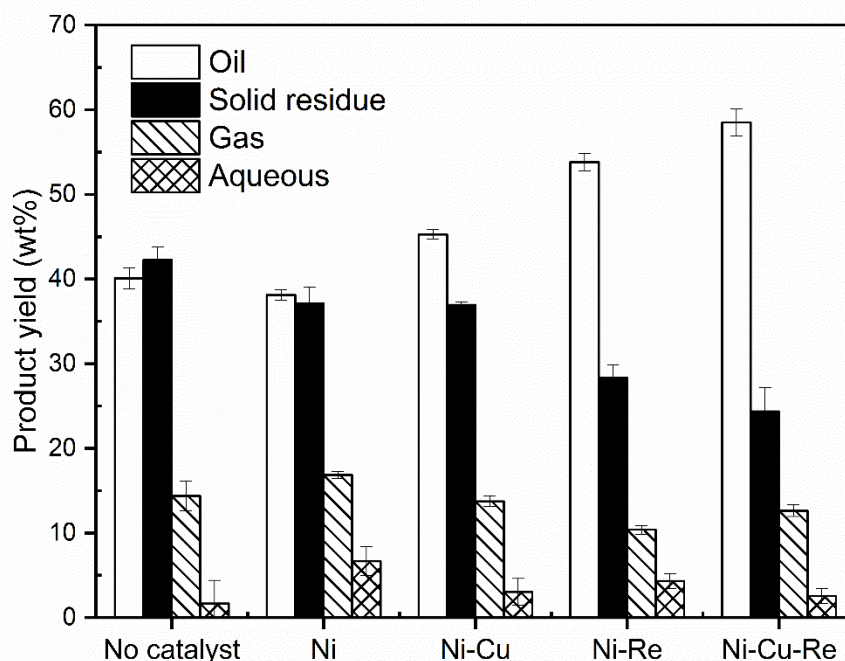


**Figure 13.** The product yields of non-catalytic ($H_2$ only) and catalytic upgraded bio-oil using different catalysts. All experiments were performed at 350 °C, initial hydrogen pressure of 75 bar and reaction time of 4 h.

The catalysts yielding a superior upgraded bio-oil yields are in the order of Ni-Cu-Re > Ni-Re > Ni-Cu > no catalyst > Ni. It is worth noting that the lowest bio-oil yield of 38 wt. % was observed over Ni/$\gamma$-$Al_2O_3$ catalyst due to high formation of gas and solid residue. This results from high secondary cracking to form gas phase, consistent with the highest gas yield (17 wt. %), which rather high selective over Ni metal catalyst [132]. In addition, relatively high solid residue yield (37 wt. %) over Ni/$\gamma$-$Al_2O_3$ could be attributed to recombination and further repolymerization of light organic compounds to form larger compounds toward coke formation [133,134]. This is reasonably because a small amount of low-boiling or volatile liquid medium was observed even though the high catalytic cracking was promoted over Ni metal

catalyst, which is confirmed by GC-MS and simulated distillation analysis (results will be shown later).

Compared with monometallic Ni catalysts, bi- and tri-metallic catalysts revealed higher bio-oil yield and lower solid residue yield. The highest bio-oil yield of 58 wt. % and lowest solid residue yield of 24 wt. % were obtained by Ni-Cu-Re/γ-$Al_2O_3$ catalyst. This result can be described by the synergistic effect of the different functioning metals loaded and the promising properties of catalysts after promoted with Cu and Re, which provide more active site for hydrotreating reaction. The addition of Cu also encouraged the activity of Ni catalyst which then increased the bio-oil yield. Surprisingly, Ni-Cu catalyst obtained solid residue yield as much as that of monometallic Ni catalyst, due to polymerization of aromatic compounds (confirmed by GC-MS). By adding Re, the performance of Ni and Ni-Cu catalyst could be enhanced, resulting in increasing the Ni and Cu metals dispersion. It also enhanced the reducibility of Cu and Ni on surface of catalyst. This assessment is confirmed by TPR results as mentioned in section 4.1. As a result of high metal dispersion, the active site would be exposed which increased the hydrogen dissociation and adsorption on surface, leading to the increased catalyst activity and bio-oil yield.

The gas yield obtained for all samples is slightly different. In comparison to the bi- and tri-catalytic experiments, the gas yield of non-catalytic runs are relatively high (as *Figure 13*). This result can suggest that the gas product could be produced not only through catalytic cracking but also thermal process. It is acknowledged that Ni metal catalyst is highly active for scission of C-C bond, leading to increasing gas formation [135,136]. The lower gas yield was produced by using bi- and tri-metallic Ni catalysts, which can be attributed to the positive effect of the promotion of Cu and Re by suppression of C-C bond scission, further lowering the cracking activity.

This study also revealed that the aqueous phase was the lowest fraction in upgraded products ranging from 2-7 wt. %, which could be formed via dehydration, hydrodeoxygenation and denitrogenation reaction. The highest aqueous yield of 7 wt. % was achieved by Ni/γ-$Al_2O_3$, which was attributed to the high removal activity of oxygen and nitrogen as confirmed by elemental analysis described further in

section 3.3. Hence, the dissimilarity of aqueous yield could be explained by removal of O and N in the bio-oil.

### 4.1.3 Upgraded bio-oil characterization

#### *4.1.3.1 Physical properties and elemental analysis*

The algae bio-crude oil contains large quantity of heteroatoms (S, N, and O) compared with those of petroleum fuel, which resulted in the low higher heating value (HHV) and high total acid number (TAN) as shown in ***Table 6***. The high amount of O-containing compounds can affect the combustion performance and cause an engine problem due to its low thermal stability, and high corrosion. Moreover, N- and S-containing oil causes the increase of air pollution by forming $NO_x$ and $SO_x$ after the combustion [20]. As a result of these properties, the bio-crude oil is not suitable to be used directly in motor engine as a transportation fuel.

The colors and viscosity of the upgraded bio-oil are rather different from the original bio-crude oil. By visual observation, the upgraded bio-oil flowed effortlessly than the bio-crude oil, indicating that the large/heavy compounds were degraded to be the small compounds during the hydrotreating. This inference was supported by the boiling point distribution data (as discussed in the detail in following section) which show that the lower fraction of vacuum gas oil and vacuum residue (larger compounds) can be achieved in upgraded bio-oil. For all the upgraded bio-oils, both non-catalytic and catalytic upgrading show no significant change in color (reddish-dark brown) but more translucent than the algae bio-crude oil. (See ***Figure 14***).
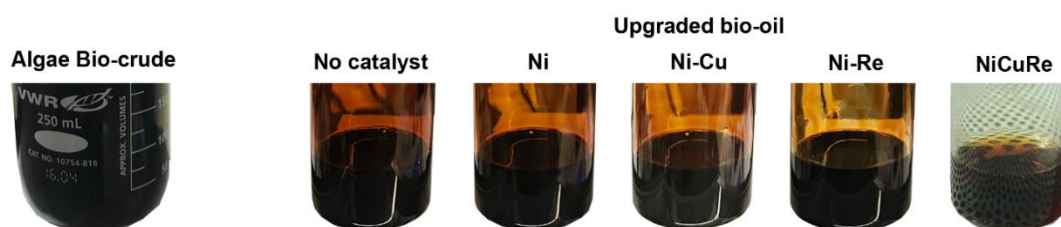


**Figure 14**. Photos of algae bio-crude oil and upgraded bio-oil.

As expected, after hydrotreating process, the properties of upgraded bio-oil were improved with increasing HHV, and simultaneously decreasing TAN value and

water content as accompanying with increasing of C and H and reducing of heteroatoms (**Table 6**). The catalytic upgraded bio-oil contained C and H between 81.7-86.1 wt. % and 11.8-12.9 wt. % which were higher than those of the algae bio-crude oil and one without catalyst, while S, N, and O heteroatoms are relatively low.

Remarkably, the relative high O content was observed over the Cu-promoted catalyst, indicating that the addition of Cu negatively affects the capability of deoxygenation. This is attributed to the selective reaction depending on a type of catalyst during the hydrotreating. The selective deoxygenation can be occurred via C-C and C-O bond scission of oxygen compounds. The scission of C-C bond favors over surfaces of Ni metal [135,136], while single Cu metal is more selective over hydrogenation of C=O and hydrogenolysis of C-O [31,137]. On the basis of the selectivity, by promotion with Cu, deoxygenation activity should be enhanced; however, it was observed to be less active than that of monometallic Ni. This effect can be explained by the existence of Cu causing the loss of Ni metal active sites due to a partial coverage by Cu and the formation of NiO-CuO alloy as observed by TPR. As unsupported Cu catalyst had been reported poor performance in deoxygenation of oxygen-containing hydrocarbon [132]. Additionally, decreasing the proportion of Ni surface results in hindrance of hydrogenation and C-C bond scission activities [37,38].

The low C content of 71.7 wt. % and high O content of 16.4 wt. % were presented in non-catalytic upgraded bio-oil, corresponding to higher TAN and lower HHV values. The TAN value directly correlates with the carboxyl groups from fatty acid containing in the oil. The TAN of non-catalytic upgraded bio-oil still remains high at 11.4 mg KOH/g which can be attributed to the low activity for deoxygenation occurred in absence of catalyst. Moreover, the decrease of acidic compounds (as shown by a decreasing of TAN approx. 49%) are not only from deoxygenation reaction (as O content decreased only approx. 15%) but might be dominated via esterification and condensation of the acids as indicated by the presence of esters and ketones.

**Table 6.** The water content, higher heating value (HHV), total acid number (TAN), and elemental analysis of algae bio-crude oil and upgraded bio-oils. (The value ± standard deviation)

| | Petroleum crude oil [138] | Algae bio-crude oil | Upgraded bio-oil | | | | |
| --- | --- | --- | --- | --- | --- | --- | --- |
| | | | No catalyst | Ni | Ni-Cu | Ni-Re | Ni-Cu-Re |
| Water content, wt. % | <1 | 3.01±0.89 | 1.88±0.21 | n.d. | 0.21±0.10 | 1.23±0.18 | 0.34±0.04 |
| TAN (as received), mg KOH/g | n/a | 22.45±0.17 | 11.46±0.31 | 0.98±0.22 | 2.95±0.16 | 3.37±0.02 | 3.27±0.11 |
| HHV (dry basis), MJ/kg | 42.7 | 34.40±0.42 | 35.67±0.35 | 44.77±0.09 | 40.07±0.01 | 41.03±0.10 | 41.02±0.05 |
| Oil yield (dry basis), % | n/a | - | 43.08±1.20 | 37.12±0.61 | 45.27±0.56 | 53.82±1.01 | 58.52±1.60 |
| $ER_{HTL}$, % | n/a | 71.91±0.67 | - | - | - | - | - |
| $ER_{upgrade}$, % | n/a | - | 42.58±0.89 | 44.61±0.35 | 50.61±0.16 | 59.11±0.44 | 64.58±1.08 |
| $ER_{overall}$, % | n/a | - | 30.62 | 32.08 | 36.39 | 42.51 | 46.44 |
| [a] $CE_{HTL}$, % | n/a | 64.16 | - | - | - | - | - |
| [a] $CE_{upgrade}$, % | n/a | - | 48.21 | 49.85 | 57.73b | 69.00 | 74.30 |
| [a] $CE_{overall}$, % | n/a | - | 30.93 | 31.99 | 37.04 | 44.28 | 47.68 |
| [b] **Element composition, wt. % on dry basis** | | | | | | | |
| C | 80-87 | 64.10 | 71.73 | 86.09 | 81.74 | 82.19 | 81.39 |
| H | 11-15 | 9.56 | 10.45 | 12.88 | 11.87 | 12.28 | 12.11 |
| N | <2 | 5.13 | 1.41 | 1.03 | 1.29 | 3.67 | 1.25 |
| S | 0.05-5 [139] | 0.78 | 0.012 | n.d. | n.d. | 0.02 | 0.022 |
| [c] O | 1-3 | 20.43 | 16.41 | 0.002 | 5.10 | 1.85 | 5.23 |
| O/C, by mole | <0.05 | 0.24 | 0.17 | 0.00 | 0.05 | 0.02 | 0.05 |
| H/C, by mole | 1.65-1.8 [140] | 1.79 | 1.75 | 1.80 | 1.74 | 1.79 | 1.79 |

Abbreviations: n.d., not detected; n/a, not available; CE, carbon efficiency; ER, energy recovery; HTL, hydrothermal liquefaction
[a] calculated based on an average oil yield with one-point datum of carbon content in each oil; [b] one-point datum; [c] calculated by difference

In addition, small amount of water was observed in the oil phase, which may be on account of an incomplete removal of O and N containing compounds of bio-crude oil [141]. This is possible because the incomplete removal of heteroatoms causes the remaining of some polar compound having the hydrophilic groups (e.g. -COOH, -OH, -CO, and -NH$_2$) in the oil, leading to the soluble of water in oil phase as observed by GC-MS and FT-IR.

Additionally, an increase in H/C accompanied with decrease in O/C which are consistent with the hydrogenation and deoxygenation reaction. The H/C and O/C ratios of catalytic upgraded bio-oil were in the range of 1.74-1.8 and 0-0.05, respectively, which are in the same range of petroleum based oil. Ni-upgraded bio-oil showed the high H/C ratio (1.8), and zero of O/C ratio which meet the ratio of diesel fuel (H/C = 1.80 and O/C = 0) [142]. The lowest H/C of 1.74 obtained over Ni-Cu/$\gamma$-Al$_2$O$_3$ mainly resulted from the highest aromatics content as confirmed by GC-MS. Apart from hydrodeoxygenation (HDO) reaction, the elemental analysis demonstrates the elimination of sulphur and nitrogen by the reactions of hydrodesulfurization (HDS), hydrodenitrogenation (HDN). The HDN activity over all the catalytic experiments was not achieved at the same levels of HDO and HDS. This is consistent with the heteroatom removal efficiency during hydroprocessing reported by Furimsky [143], which generally occurs in the following order: HDS > HDO > HDN.

Though Ni/$\gamma$-Al$_2$O$_3$ gave the lowest oxygen content with highest HHV, the obtained oil yield is lowest. Energy recovery (ER) refers to the chemical energy of algae biomass and bio-crude oil retaining in the bio-crude oil and upgraded bio-oil, which represented by ER$_{HTL}$ and ER$_{upgrading}$, respectively. It is calculated by the incorporation of energy (HHV value) and oil yield, and may be an indicator to explore the performance of catalysts in catalytic upgrading process for consideration to further study and potential to scale up [144]. The algae biomass was initially converted into bio-crude oil by HTL process, which remained the chemical energy (ER$_{HTL}$) of 71.9% in the bio-crude oil. Subsequently hydrotreating step, the energy recovery of upgraded bio-oil (ER$_{upgrade}$) relative to bio-crude oil was in the range of 42-65%. Higher values of energy recovery imply a greater recovery of contained feedstocks energy in bio-oil product. The highest energy ER$_{upgrade}$ of 64.6% was achieved for Ni-Cu-Re/$\gamma$-Al$_2$O$_3$

because the highest oil yield with high HHV was produced. Besides, the energy recovery of the overall process ($ER_{overall}$) which indicates the chemical energy of algae biomass remaining in upgraded bio-oil of 46.4% can be achieved for Ni-Cu-Re/$\gamma$-Al$_2$O$_3$ catalyst.

Carbon recovered in the oil phase was calculated as carbon efficiency (CE). A higher carbon efficiency implies that the most of carbon contained in feed is converted into oil phase product whereas carbon end ups more in solid, gas and some in aqueous phase resulting in lower CE value. The overall CE ($CE_{overall}$) from algae biomass to upgraded bio-oil product shows the similar trend as the value of energy recovery. The CE value of HTL ($CE_{HTL}$) process was about 64% which is in the same range reported in other studies (appox. 54%-69%, based on calculation of their reported yield and C content) [17,145–147]. A wide-range of carbon efficiency for upgrading step ($CE_{upgrade}$) as 48% for non-catalytic and to 74% for Ni-Cu-Re/$\gamma$-Al$_2$O$_3$ catalyst were achieved in this study. The values of $CE_{upgrade}$ calculated from literature are summarized in *Table 7* for comparison with our study. As shown in the table, Ni-Cu-Re/$\gamma$-Al$_2$O$_3$ catalyst exhibits relatively high $CE_{upgrade}$ but certainly less than NiMO/$\gamma$-Al$_2$O$_3$ [148] which deoxygenating mainly proceeds via HDO. However, it is worth to note that, mode of operation i.e. batch and continuous flow rather influences on $CE_{upgrade}$. As shown in *Table 7*, regardless of catalyst used, less carbon was recovered from batch operation comparing to flow operation. This could be mainly due to different interplay between hydrodynamics and mass transfer behavior. The H$_2$/oil ratio can be kept constant for flow operation while gradually decreased in batch operation as prolong reaction time.

**Table 7.** Summary of catalytic upgrading of bio-crude oil obtained from HTL.

| Biomass feedstock | Oil yield (wt. % dry basis) | Carbon content (%) | Carbon efficiency* (%) | Catalyst | T (°C) | P (bar) | Time (h) | Other conditions | Ref. |
|---|---|---|---|---|---|---|---|---|---|
| **Batch operation** | | | | | | | | | |
| *Chlorella pyrenoidosa* | 59.7 | 82.3 | 59.8 | Pt/C | 400 | 60 | 4 | | 17 |
| | 62.0 | 81.6 | 61.6 | Pd/C | 400 | 60 | 4 | | |
| | 64.7 | 80.9 | 63.7 | CoMoS/Al₂O₃ | 400 | 60 | 4 | | |
| | 65.3 | 82.8 | 65.9 | Raney-Ni | 400 | 60 | 4 | Water to oil ratio 1:2 | |
| | 66.4 | 82.8 | 67.0 | Pt/C (sulfided) | 400 | 60 | 4 | | |
| | 68.2 | 82.2 | 68.3 | Ni/SO₂-Al₂O₃ | 400 | 60 | 4 | | |
| | 68.5 | 84.5 | 70.5 | Ru/C | 400 | 60 | 4 | | |
| | 77.2 | 83.9 | 78.9 | Mixed Ru/C+Raney-Ni | 400 | 60 | 4 | | |
| *Chlorella pyrenoidosa* | 51.5 | 84.67 | 56.9 | Ru/C+MO₂/C (1:1) | 400 | 60 | 4 | Water to oil ratio 1:2.5 | 146 |
| Aspen wood | 57.5 | 84.1 | 60.1 | NiWS/Al₂O₃ | 350 | 75 | 2 | - | |
| | 66.0 | 86.5 | 70.9 | NiMoS/Al₂O₃ (low metal loading) | 350 | 75 | 2 | - | |
| | 70.3 | 87.8 | 76.7 | | 350 | 75 | 2 | | 148 |
| | 56.2 | 87.7 | 61.2 | | 350 | 50 | 4 | | |
| | 69.8 | 89.1 | 77.3 | NiMoS/Al₂O₃ (high metal loading) | 350 | 75 | 4 | | |
| | 62.6 | 89.5 | 69.6 | | 350 | 100 | 4 | - | |
| | 77.6 | 89.2 | 86.0 | | 350 | 100 | 2 | | |
| | 66.5 | 89.0 | 73.52 | | 350 | 100 | 1 | | |
| *Nannochloropsis* | 53.8 | 82.2 | 69 | Ni-Re/Al₂O₃ | 350 | 75 | 4 | - | This study |
| | 58.5 | 81.4 | 74 | Ni-Cu-Re/Al₂O₃ | 350 | 75 | 4 | - | |
| **Continuous operation** | | | | | | | | | |
| Woody | ~85 | n/a | 96 | n/a | | | | n/a | 147 |
| Chlorella (12-30% lipid) | 86 | 84.2 | 89.4 | CoMoS/Al₂O₃ | 400 | 103 | | Bio-crude feeds rate 0.133 ml/min, H₂ feed rate 188 SCCM, | 149 |
| Chlorella (57-64% lipid) | 90 | 86.0 | 99.2 | CoMoS/Al₂O₃ | 400 | 103 | | | |

*Calculated based on their reported oil yield and carbon content; n/a , not available; SCCM, standard cubic centimeters per minute

### 4.1.3.2 Molecular characterization

The chemical compositions of the algae bio-crude oil consisted of many complex compounds such as aliphatic hydrocarbon, substituted aromatic, heterocyclic, polycyclic aromatic hydrocarbons as well as oxygen-, nitrogen- and both oxygen-nitrogen containing compounds, which in principle are derived from the coexistence of carbohydrate, proteins and lipids in *Nannochloropsi*s sp. algae biomass [148,150].

FT-IR spectroscopy was employed to determine the comprehensive functional groups in the original bio-crude oil and upgraded bio-oils, which can be interpreted into relative chemical compounds listed in *Table 15* (Appendix A). *Figure 15(a)* shows strong intensity of FT-IR spectra at 3200-3650 cm$^{-1}$ in the bio-crude oil, corresponding to O-H group of (e.g.) water, phenol, and/or alcohol, and N-H stretching of amino group [33,151]. These corresponding spectral intensities were found weaker in the upgraded bio-oils (*Figure 15(b)* and *(c)*), indicating the reduction of alcohol, phenol, water as well as nitrogen compounds, corresponding to the GC-MS results. A noticeable reduction in spectral intensities at 1647-1780 cm$^{-1}$ and 1525-1590 cm$^{-1}$ were detected, indicating that carbonyl (C=O) of amide, ketone, and carboxylic acid and N-H of amide were removed [152,153]. The majority of absorbance at 2840-2970 cm$^{-1}$ was observed in both the bio-crude oil and upgraded bio-oil, which can be attributed to C-H stretching in aliphatic hydrocarbons.

The presence of absorbance attributed to symmetric =C-H stretching of alkene was found in the upgraded bio-oil by shoulder peaks at 3000-3100 cm$^{-1}$ [154]. Also, the absorbance at 1350-1480 cm$^{-1}$ attributed to the methyl (-CH$_3$) bending and methylene (-CH$_2$) scissoring of aliphatic or cyclic alkyl group. Compared with the bio-crude oil, lower intensities of absorbance at 700-815 cm$^{-1}$ were detected, attributed to C-H bending of an aromatic compound [144,155], which may be due to hydrogenation or hydrocracking of polyaromatic compounds during the hydrotreating. In all catalytic upgrading systems, FTIR results indicate an obvious removal of C=O, O-H, N-H bonds which conform to the decreased amides, acids, phenols and alcohols, whereas the content of hydrocarbons increased. This results in significant decreases of oxygen content, water content, and TAN with higher HHV which cannot be achieved from

non-catalytic upgrading. Moreover, for the upgraded bio-oil, the small O-H absorbance still exists, due to incomplete deoxygenation and denitrogenation, which can be confirmed by the results from CHNS/O elemental analysis and the GC-MS characterization.
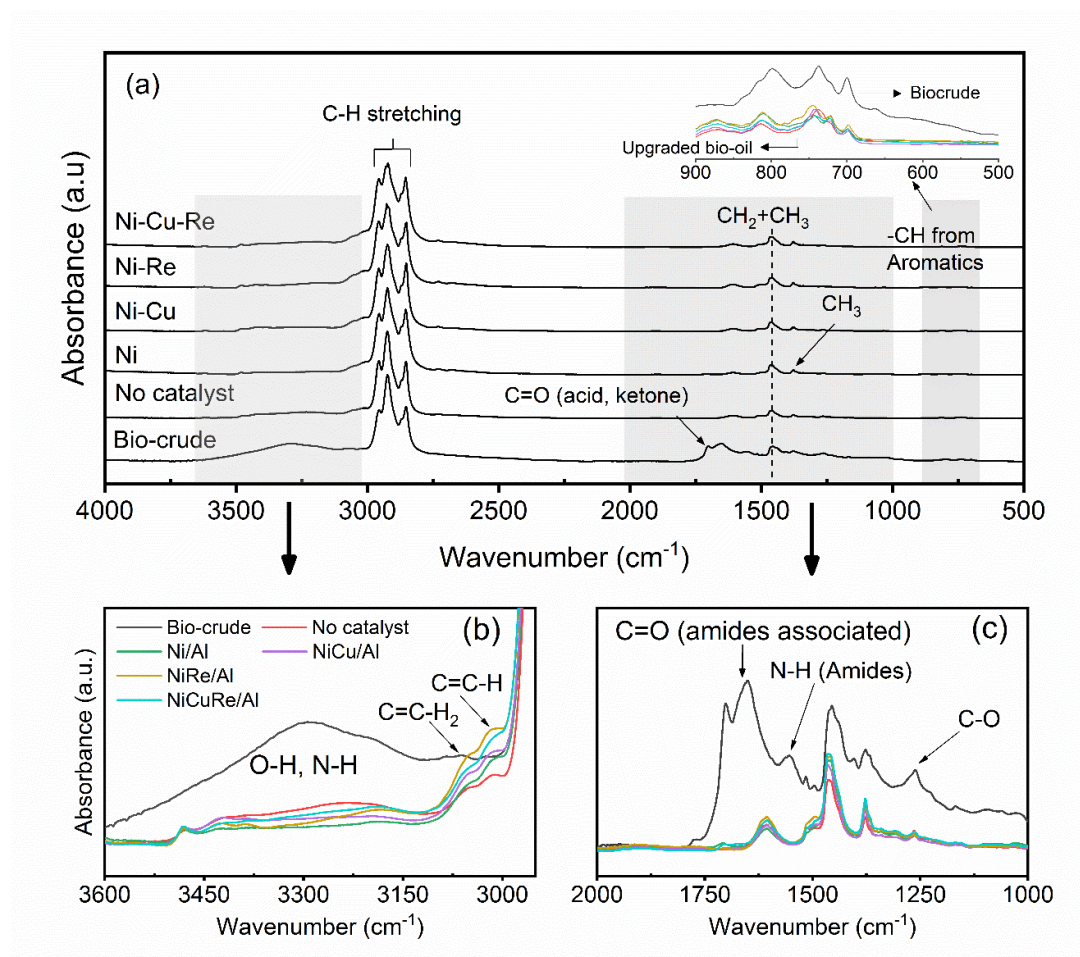


**Figure 15.** (a) FT-IR spectra of the algae bio-crude oil and upgraded bio-oil, (b) spectra zoom in at wave number values 2950 – 3600 cm$^{-1}$ and (c) spectra zoom in at wave number values 1000 – 2000 cm$^{-1}$. All experiments were performed at 350 °C, initial hydrogen pressure of 75 bar and reaction time of 4 h.

GC-MS was performed to identify the chemical compounds in the algae bio-crude oil and the upgraded bio-oil. Several hundreds of chromatograms of bio-crude oil and upgraded bio-oil were detected (Appendix A; ***Figure 39(a-f)***). Each individual peak was identified using the NIST mass spectral library (Appendix A; ***Table 16)***, the percentage of each peak area was classified and categorized as shown in ***Table 8***.

The algae bio-crude oil is composed mainly of nitrogen and oxygen compound, and a low amount of hydrocarbons. Amides compounds (mainly hexadecanamide) and heterocyclic nitrogen compounds (pyrroles, pyridines, and indoles) with various alkyl substituents are found as a dominant in the algae bio-crude oil, while carbonyl-containing compounds (such as 4,4,5-trimethoxy-2-Cyclohexen-1-one, Ethanol, 2,2'-[1,2-ethanediylbis(oxy)] bis-, diacetate, etc.) are predominant for oxygen compounds, as well as phenol and alkyl phenols.
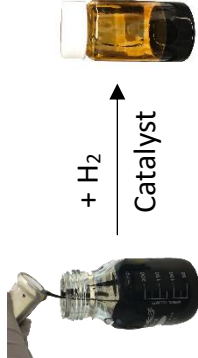
Subsequent to hydrotreating process, the aliphatic and aromatic hydrocarbons in all the upgraded bio-oils significantly increase, while the amount of nitrogen and oxygen compounds decrease, demonstrating that denitrogenation and deoxygenation were occurred during the reaction. The deoxygenation reaction possesses more effective in the presence of metal catalyst, which results in a great decrease of oxygen compounds. The majority of compound in the upgraded bio-oil is open-chain compounds which in detailed mainly straight chain alkanes (ranging from $C_7$-$C_{26}$). The minorities are aromatic hydrocarbons such as benzene, naphthalene. Among the catalytic upgrading, Cu-promoted catalysts show the higher oxygen compounds such as alcohols-, aldehyde-, and phenol-based structure since deoxygenation took place over Cu metal sites through C-O hydrogenolysis [31,137], which further evidenced by high water content in products. While the denitrogenation could not be completed because breaking of the C-N bond in aromatic ring is very difficult, resulting in finding some heterocyclic nitrogen compounds (benzenamine, carbazole, etc.) after hydrotreating process. In details, the elimination of nitrogen atoms that connected with π-electrons on aromatic ring in structural conjugation such as pyridine, pyrrole, and indole, is challenging because it has high strength of C-N bonds due to high structural stability of aromatic six member N-ring. In addition, highly condensed-aromatic nitrogen compounds such as quinoline and carbazole are less reactive than that of lower aromatic condensation due to the higher resonance energy of molecular structure [18,156].
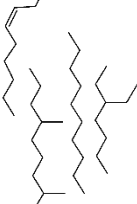
It is worthy noted that Ni-Re/γ-Al$_2$O$_3$ catalytic upgrading shows relative high N content compared to other catalysts (**Table 6**), which are mainly nitrile compounds such as tetradecane nitrile, hexadecane nitrile. This could be produced via dehydration

of amide to form nitrile which prefer over Ni-Re catalyst because oxophilic character of Re facilitates for oxygen atom adsorption over carbon atom adsorption, resulting in the promotion of C-O bond scission (dehydration) [119,157–159]. Besides, the high nitrogen content may attribute to the occurrence of reductive amination reaction. As it was reported by Ma *et al.* who investigated reductive amination of monoethanolamine and liquid ammonia over alumina supported Ni-based catalyst. They found that addition of Re as a promoter on Ni metal catalysts positively affect the activity for the reductive amination which facilitated by forming $Ni^0$-ReOx sites [126,160]. In our research, Ni-ReO$_x$ could be formed during the reduction step, which can be observed by the TPR; hence, it is reasonable to consider that the presence of Re promotes the reductive amination to produce amine, further undergo dehydrogenation to form nitriles.
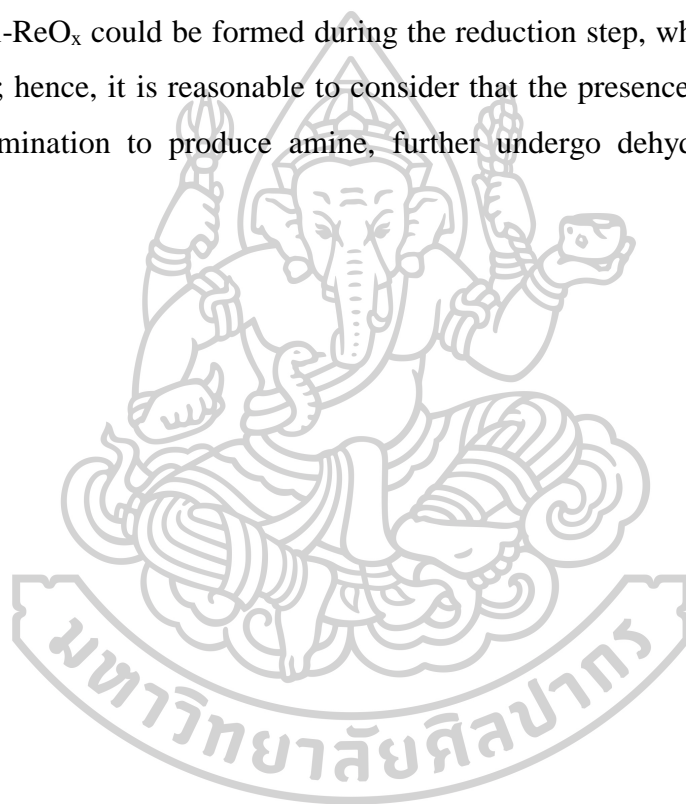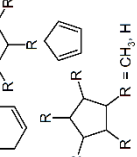
**Table 8.** The composition of algae bio-crude oil and upgraded bio-oils using different catalysts by GC-MS (% of Total peak area)
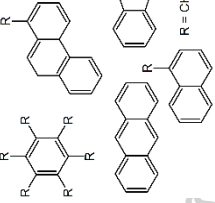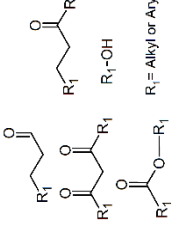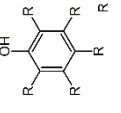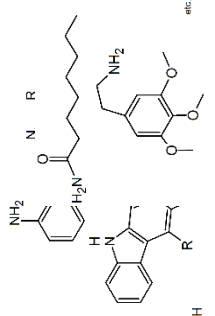
| Total peak area (%) | Bio-crude oil | Upgraded bio-oil | | | | |
|---|---|---|---|---|---|---|
| | | No catalyst | Ni | Ni-Cu | Ni-Re | Ni-Cu-Re |
| Open-chain hydrocarbons* | 26.65 | 51.34 | 75.28 | 62.03 | 56.21 | 65.94 |
| • Saturated | 12.63 | 51.34 | 75.28 | 62.03 | 55.26 | 65.94 |
| • Unsaturated | 14.02 | 0.00 | 0.00 | 0.00 | 0.95 | 0.00 |
| Cyclic hydrocarbons* | 1.37 | 1.83 | 3.94 | 3.45 | 1.76 | 1.97 |
| • Saturated | 0.68 | 1.31 | 1.64 | 2.12 | 1.58 | 1.97 |
| • Unsaturated | 0.69 | 0.52 | 2.31 | 1.33 | 0.19 | 0.00 |
| Aromatic hydrocarbons | 9.63 | 16.27 | 15.10 | 27.74 | 10.19 | 24.45 |
| O-containing compounds | 15.29 | 18.80 | 1.72 | 3.32 | 0.50 | 5.85 |
| • Phenols and alkyl phenols** | 8.89 | 1.93 | 0.00 | 0.95 | 0.50 | 2.47 |
| N-containing compounds | 14.64 | 6.03 | 3.95 | 1.71 | 22.19 | 0.24 |
| Hetero- (N and O) compounds*** | 32.43 | 5.73 | 0.00 | 1.74 | 9.14 | 1.54 |

*Sum of saturated and unsaturated hydrocarbons

** Phenols and alkyl-phenols are included in oxygenated compound

*** The peak area of heteroatom (N and O) compounds are separated from oxygen compounds and nitrogen compounds.

**4.1.4 Gas compositions**

As shown in *Figure 16*, $CH_4$ and $CO_2$ are found as primary components, while CO and light hydrocarbons ($C_2$-$C_5$) are also slightly observed. The light hydrocarbons ($C_2$-$C_5$) can be generated from hydrocracking of the large hydrocarbons in the bio-crude oil, while the CO and $CO_2$ were mainly produced through the decarbonylation (DCO) and decarboxylation ($DCO_2$). Moreover, $CO_2$ could be generated from water gas shift (WGS) reaction. The large $CH_4$ was observed for catalytic experiments, reasonably suggesting that the formation of $CH_4$ is through not only the cracking of the bio-crude oil but also the CO and $CO_2$ methanation in gas phase reaction. The lower content of $CH_4$ was found over Ni-Re and Ni-Cu-Re catalysts, which is attributed to the effect of adding Re, consistent with the investigation by Yang et al. [119]. They observed the positive effects of adding Re to Ni catalyst, increasing Ni dispersion and reducing Ni particle size by Ni-Re alloy formation. As a result of the Ni size decreased, the hydrogenolysis C-C would be suppressed, contributing to significantly less in methane production.

$$\text{Water gas shift (WGS): } CO + H_2O \leftrightarrow CO_2 + H_2$$
$$\text{Methanation: } CO + 3H_2 \rightarrow CH_4 + H_2O$$
$$: CO_2 + 4H_2 \rightarrow CH_4 + 2H_2O$$
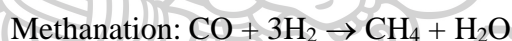
In addition, the hydrogen consumption during the hydrotreating was also determined. For all the upgrading experiments, unreacted hydrogen still remained in the gas product. Combined with the pressure change after the reaction, the hydrogen consumption could be determined according to the literature [140]. Obviously, higher hydrogen consumption was observed for catalytic hydrotreating. This suggests that the higher amount of hydrogen was consumed for hydrogenation of unsaturated hydrocarbons as well as methanation in gas phase, which preferably occurred over metal catalysts. Generally, DCO and $DCO_2$ consume less hydrogen than HDO; however, once reduction of $CO_x$ to $CH_4$ via methanation was occurred, the total hydrogen consumption is higher than HDO. Thus, hydrogen consumption is strongly dependent on methanation reaction as depicted in *Figure 16* and this leads to the

highest consumption of hydrogen for monometallic Ni catalyst. On the other hand, the lowest hydrogen consumption of Ni-Re is probably due to the internal generation of hydrogen through the water gas shift reaction as Ni-Re/$Al_2O_3$ is known as an active WGS catalyst [161], which had been reported to be achieved at around our study temperature (350-400 °C) [162]. Additionally, it has been reported dehydration reaction is more facilitated when Re is introduced [163,164], as observed the highest water content (**Table 6**) and highest $C_n/C_n+C_{n-1}$ (**Table 9**) among catalytic hydrotreating catalysts.
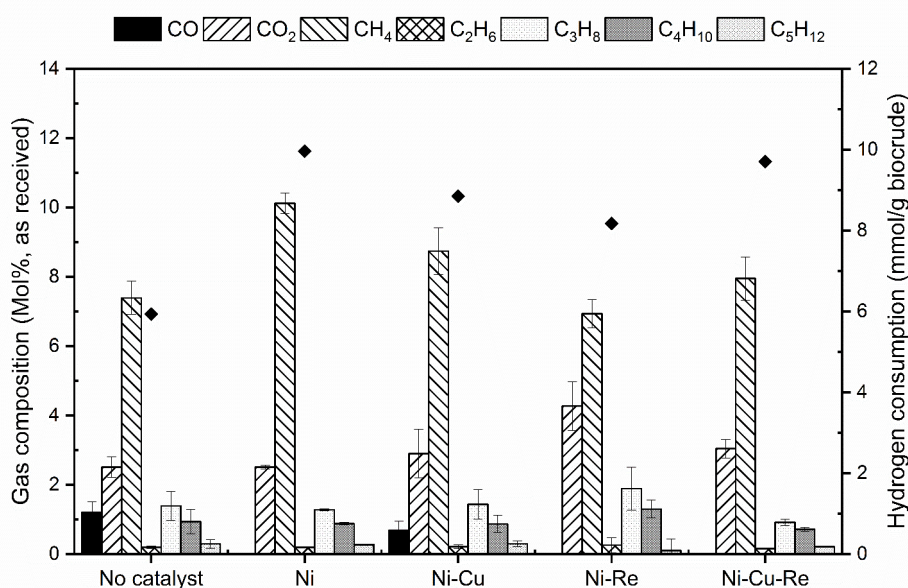


**Figure 16.** Hydrogen consumption and gas product composition of non-catalytic and catalytic upgraded bio-oil using different catalysts. All experiments were performed at 350 °C, initial hydrogen pressure of 75 bar and reaction time of 4 h.

**4.1.5 Simulated distillation analysis**

Boiling point (b.p.) distribution of the bio-crude oil and upgraded bio-oil was determined by Simulated distillation analysis following ASTM D2887. The boiling point range was grouped into five fraction corresponding to [33], including gasoline and heavy naphtha (b.p. < 193 °C), kerosene (b.p. 193-271 °C), diesel (b.p. 271-343 °C), vacuum gas oil (b.p. 343-538 °C), and vacuum residue (> 538 °C). **Figure 17** shows the boiling points of the algae bio-crude oil and upgraded bio-oil.

The highest vacuum gas oil of 78 wt. % and vacuum residue of 5 wt. %, as corresponding to the containing of heavy/large molecular compounds such as hexadecanamide and octadecanamide, were obviously found in the algae bio-crude oil. The non-catalytic upgraded bio-oil, the lower vacuum gas oil fraction and residue were observed compared with those of the algae bio-crude oil, suggesting that the heavy molecule of bio-crude oil was converted into these fractions via thermal process. Catalytic hydrotreating process led to a significant increase in gasoline, kerosene and diesel fractions, while the vacuum gas oil and vacuum residue fractions obviously decreased.
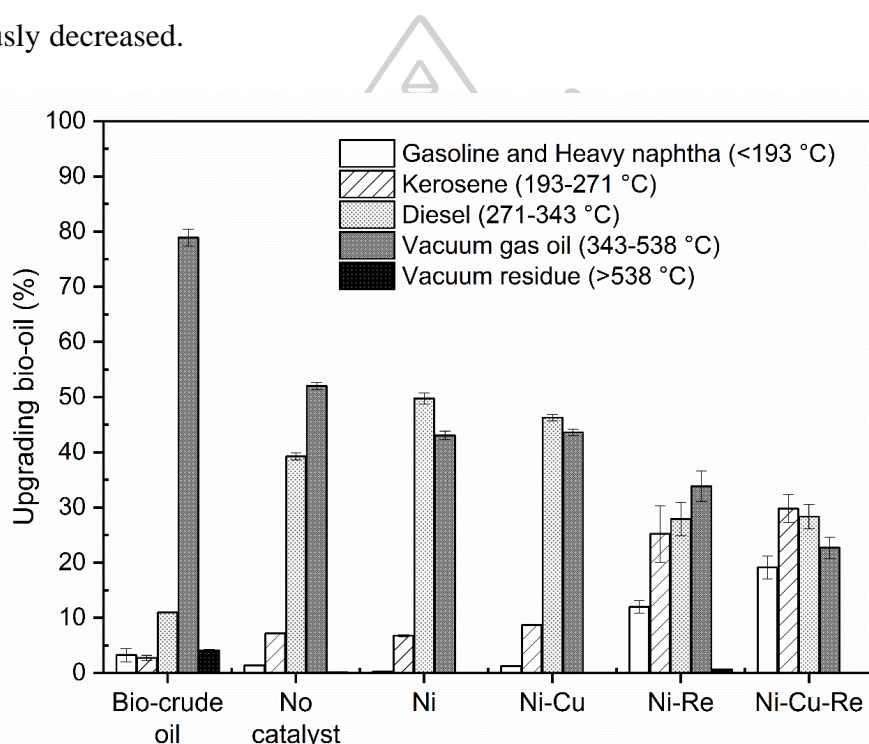


**Figure 17.** Boiling point distribution of algae bio-crude oil and upgraded bio-oil using different catalysts analyzed by Simulated Distillation analysis.

The relative high diesel fraction was presented in Ni and Ni-Cu, as a result of predominant $n$-$C_{15}$ and $n$-$C_{17}$ compositions (**Table 9**), which are in the diesel boiling range. The gasoline fraction was barely observed over Ni/$\gamma$-$Al_2O_3$, as in agreement with the GC-MS chromatogram (Appendix A, **Figure 39**), in spite of the severe cracking activity. This result can be explained by the recombination and polymerization of light/small molecular hydrocarbons into heavy molecules i.e.

alkanes containing carbon atom higher than $C_{20}$, which contributed to relative high vacuum gas oil fraction.

**Table 9.** Carbon number distribution of straight chain hydrocarbon products in upgraded bio-oils using different catalysts by GC-FID equipped with simulated distillation analysis (% of Total peak area).

| Upgraded bio-oil | Total peak area (%) | | | | | | | | | $C_n/C_n+C_{n-1}$ |
|---|---|---|---|---|---|---|---|---|---|---|
| | <C11 | C12-C14 | C15 | C16 | C17 | C18 | C19 | C20 | C21< | |
| No catalyst | 0.65 | 4.68 | 24.71 | 5.30 | 12.37 | 8.43 | 5.57 | 4.28 | 34.00 | 0.37 |
| Ni | 0.20 | 4.52 | 30.68 | 5.69 | 15.85 | 11.32 | 6.26 | 3.09 | 22.39 | 0.33 |
| Ni-Cu | 0.90 | 6.45 | 28.79 | 6.39 | 14.18 | 10.40 | 5.37 | 3.88 | 23.64 | 0.36 |
| Ni-Re | 4.18 | 11.22 | 17.89 | 11.38 | 11.70 | 18.21 | 6.26 | 5.86 | 13.30 | 0.51 |
| Ni-Cu-Re | 9.18 | 13.31 | 30.94 | 8.95 | 13.48 | 8.69 | 3.87 | 3.62 | 7.95 | 0.36 |

$C_n$ is summation of even carbon atoms in straight chain hydrocarbons

$C_{n-1}$ is summation of odd carbon atoms in straight chain hydrocarbons

Meanwhile, the lighter product was vastly generated over the Re-promoted catalyst, resulting in increasing the gasoline and kerosene fractions that of 10-20 wt. % and 25-30 wt. %, respectively. However, the gas product over Ni-Re and Ni-Cu-Re was observed at relative low level. This exhibits that moderate hydrocracking occurred during the hydrotreating of bio-crude oil over Ni-Re and Ni-Cu-Re.
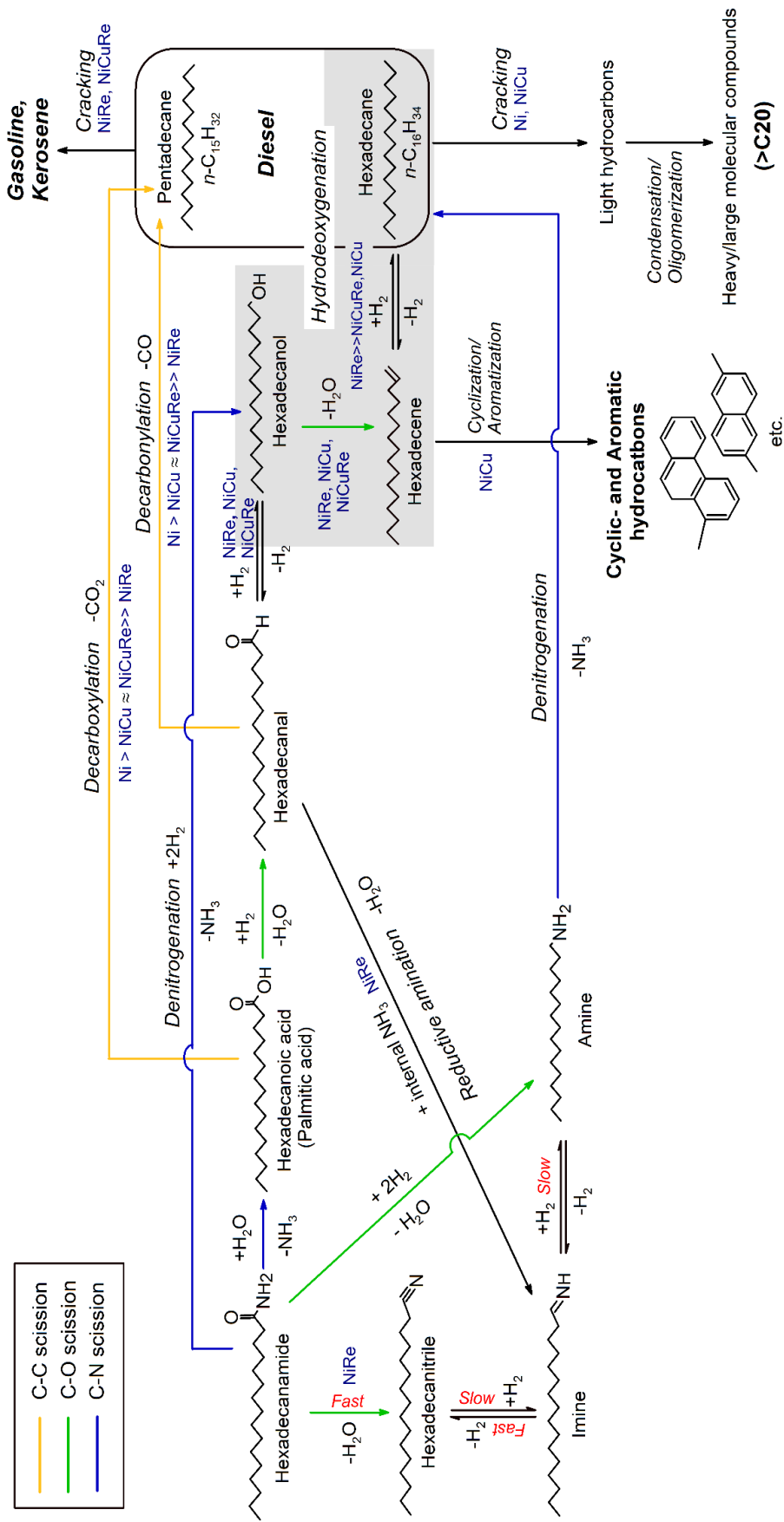
**Figure 18.** Proposed reaction pathways for upgrading of the algae bio-crude oil in hydrotreating process

**4.1.6 Reaction network**

Based on the product distribution described above, the overall of possible reaction pathways for hydrotreating of the algae bio-crude oil are proposed in ***Figure 18***. Such amides represent an important component where hexadecanamide ($C_{16}H_{33}NO$) and octadecanamide ($C_{18}H_{37}NO$) were observed as the main components in the bio-crude oil, while $n$-$C_{15}$/$n$-$C_{16}$ and $n$-$C_{17}$/$n$-$C_{18}$, respectively, are observed as main products in the upgraded bio-oil (See ***Table 9***). Amide is known as a rather more stable compound compared to other functional groups (ester, acid, amine, nitriles, etc.). In our study condition, breaking C-N bonds of amide possibly occurs through 3 different pathways: the first is hydrolysis of hexadecanamide to form hexadecanoic acid (palmitic acid); the second is hydrogenation of amide to form alcohol; the last one is hydrogenolysis of C-O in amide to amine, then further denitrogenation to alkane, as shown in ***Figure 19***.
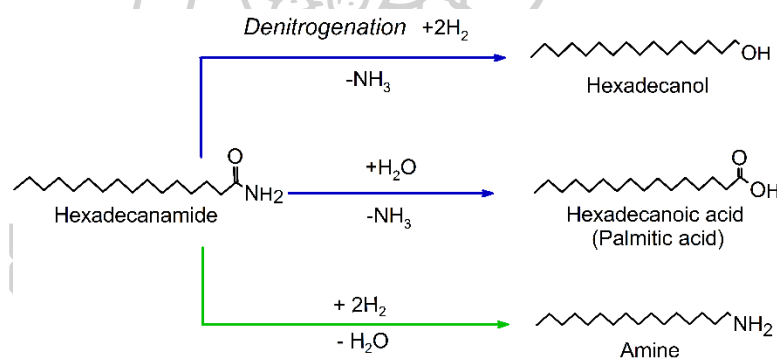


**Figure 19.** Possible reaction pathway for breaking C-N bonds of hexadecanamide

Even though hydrolysis of amide is known to be a thermodynamically unfavorable reaction; it can be occurred under acid or base condition at elevated temperature >100 °C [165–167]. In our system, operated at 350 °C, 75 bar of $H_2$, relatively high acidity atmosphere, and presence of water, could promote hydrolysis of hexadecanamide to form hexadecanoic acid at early stage, as sufficient water could be internally generated via dehydration or hydrodeoxygenation reaction. Hexadecanoic acid was further converted into hexadecanal via hydrogenolysis, which can be either deoxygenated to pentadecane via decarbonylation, or hydrogenated into hexadecanol.

Hexadecanol was subsequently dehydration to hexadecene ($C_{16}^=$) which further underwent hydrogenation to form hexadecane (n-$C_{16}$), as shown in *Figure 20(a)*. Alternatively, hexadecanamide could be hydrogenated into corresponding amine and alcohol which could be further decomposed into n-$C_{16}$ (See *Figure 20(b)*).

(a)



(b)
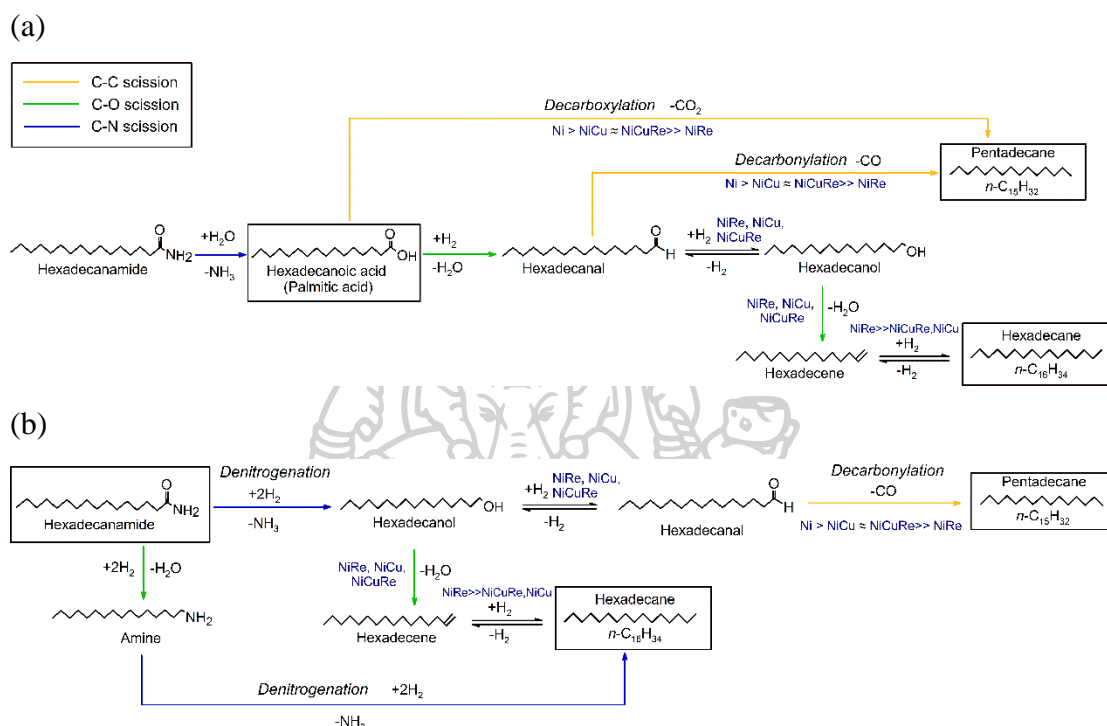


**Figure 20.** Formation of alkanes from hexadecanoic acid (a), and hexadecanamide (b).

Throughout the chemical compositions that have been mentioned in section 4.5 as well as literature information [168,169], we hypothesize that reductive amination can occur especially over Ni-Re catalyst, through dehydration of aldehydes intermediate and then react with internal ammonia to form imine (unstable amine). This imine further undergoes dehydrogenation to produce nitriles, or probably hydrogenation to the amine (See **Figure 21**). Due to rather high amount of nitriles discovering, we can presume that the dehydration of amide is more favorable than further hydrogenation to amine as well as dehydrogenation of imine. As our observation, hexadecanamide could be decomposed via at least three different routes. The finding in this study could elucidate and explain why hexadecanamide exhibits higher conversion compared to that of the intermediate, palmitic acid, as observed by [170].
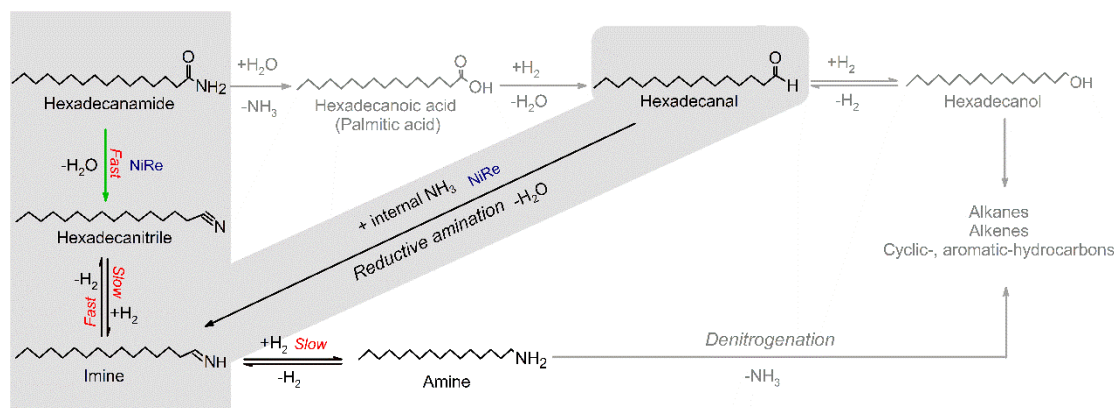
**Figure 21.** Reductive amination of aldehyde over Ni-Re catalyst.

Generally, $n$-$C_{15}$ are produced through direct decarboxylation of hexadecanoic acid which could favor over Ni catalyst due to C-C bond scission (to form $CO_2$), or decarbonylation of hexadecanal (releasing CO), which favorably occurs over Ni-Cu and Ni-Cu-Re catalysts. Simultaneously, hydrodeoxygenation of hexadecanol which is in equilibrium with hexadecanal [170–172], were occurred at C-O bond resulting in $n$-$C_{16}$ and water was generated, which apparently occur over Ni-Re catalyst confirmed by the highest of $C_n/C_n+C_{n-1}$ value (**Table 9**). Furthermore, some unsaturated- and cyclic-hydrocarbons as well as aromatics were also observed. This provided strong evidence for the occurrence of dehydrogenation, leading to cyclization and formation of aromatic compounds under the reaction atmosphere, which is more favorable active over Ni-Cu as its yielded the highest aromatic hydrocarbon.

## 4.2 Conclusion

Algae bio-crude oil produced from hydrothermal liquefaction (HTL) is an attractive third-generation biofuel. The bio-crude oil yield of 50 wt. % can be achieved from HTL of *Nannochloropsi*s sp. at 320 °C for 30 min with energy recovery ($ER_{HTL}$) of 71.8%. The hydrotreating upgrading of the bio-crude oil was investigated using Ni-based non-sulfided catalyst promoted by Cu and Re.

Among different catalysts, bare Ni/$\gamma$-$Al_2O_3$ catalyst exhibits the highest heteroatom removal activities (oxygen and nitrogen content of 0.002% and 1.03%) and thus the highest HHV of 44.8 MJ/kg. Nevertheless, the lowest yield of upgraded

bio-oil leads to the lowest $ER_{upgrade}$ (44.6%) which turned out to be an unpromising catalyst. The addition of Cu and Re in bimetallic, and both Cu and Re in trimetallic catalysts could increase the yield of upgraded bio-oil and thus improved ER.

By promotion with only Cu, the $ER_{upgrade}$ could be improved to 50.6%. This is because of the significant enhancement in the yield of upgraded bio-oil that could compromise in the decrease of deoxygenation activity. This effect can be explained by the favorable adsorption of C=O over Cu surface; and by the formation of NiO-CuO alloy which could decrease the Ni metal active sites. Hence, the hydrogenation takes place more at C=O bonds than cleavage of C-O and C-C bonds, resulting in more selective for aldehyde, alcohol as well as aromatic compounds.

Meanwhile with an addition of only Re, the $ER_{upgrade}$ could be further improved to 59.1% as increase of oil yield and oxygen removal activity compared to the Cu addition. Ni-Re/$\gamma$-Al$_2$O$_3$ catalyst offered rather high yields of $n$-C$_{16}$ and $n$-C$_{18}$ hydrocarbons, hydrodeoxygenation products containing the even number of carbon atoms in the molecule as the corresponding fatty acid amides i.e. hexadecanamide (C$_{16}$H$_{33}$NO) and octadecanamide (C$_{18}$H$_{37}$NO). This indicates the favorable dehydration and C-O hydrogenolysis over ReO$_x$ surface. However, Ni-Re/$\gamma$-Al$_2$O$_3$ presents a negative effect for nitrogen removal due to the reductive amination, then further nitriles formation.

The most impressive results can be achieved with the addition of both Cu and Re as trimetallic Ni-Cu-Re/$\gamma$-Al$_2$O$_3$. The increasing in the dispersion of Ni species and enhancing the reducibility of the catalyst are beneficial for the catalysis process. Ni-Cu-Re/$\gamma$-Al$_2$O$_3$ offers the highest oil yield of 58 wt. % with the utmost desirable $ER_{upgrade}$ of 64.6%. The carbon efficiency in the upgrading process ($CE_{upgrade}$) of 74.3% from Ni-Cu-Re/$\gamma$-Al$_2$O$_3$ exhibits relatively high $CE_{upgrade}$ compared to the literature performing in similar operating systems. The overall metrics from algae biomass to upgraded bio-oil of $ER_{overall}$ and $CE_{overall}$ as 46.4% and 47.7% can be achieved.

The reaction schemes depending on different metal catalysts have been proposed. Hexadecanamide, the O- and N-containing compound, which is the most component in bio-oil is illustrated in order to depict the reaction pathway. In

conclusion, O- and N- removal possibly occurs through 3 different pathways including 1) hydrolysis of hexadecanamide to form hexadecanoic acid, 2) hydrogenation of amide to form alcohol, and 3) hydrogenolysis of C-O in amide to amine.

# CHAPTER 5

# CATALYTIC BEHAVIORS OF MONO-, BI-, AND TRI-METALLIC SUPPORTED Ni/γ-Al₂O₃ IN HYDROTREATING OF *PONGAMIA PINNATA* OIL

In this chapter, the activity and stability of Ni, Ni-Cu, Ni-Re and Ni-Cu-Re supported on γ-Al₂O₃ were tested in a down-flow packed-bed reactor *using Pongamia pinnata* (*P.pinnata*) oil as a bio-oil feedstock. All studied were conducted under reaction condition: 330 °C. H₂ 50 bar, LHSV 1 h$^{-1}$ and H₂: oil 1000 Ncm$^3$/cm$^3$. The fresh and spent catalysts were characterized in order to understand the effect of Cu and Re on the catalyst deactivation.

*Pongamia pinnata (P.pinnata* oil*),* in English called "Indian beech" is a promising low-price feedstock for biodiesel production. *P.pinnata* oil is a fast growing tree in humid or subtropical area, such as Thailand, India, Malaysia, Australia, New Zealand, as well as parts of China and USA. The *P.pinnata* seed kernel contains about 27-40 wt % oil  which has potential in biodiesel production [173]. The oil has been investigated in biodiesel production via tranesterification reaction [174]; however, using of *P.pinnata* oil on bio-hydrotreated diesel or green diesel production was rarely disclosed.

## 5.1 Results and discussion

### 5.1.1 Oil extraction and yield

The extracted *P. pinnata* oil yield was 28% on dry weight of kernel seeds basis. The acid number and water content of crude *P. pinnata* oil were 7.8 mg KOH/g oil and 0.05 wt %, respectively. Fatty acid composition and the metallic and phosphorus content in crude *P. pinnata* oil were shown in ***Table 10*** and ***Table 11***,

respectively. The phospholipid content of degummed *P.pinnata* oil decreased from 570 to 187.9 ppm, which causes decreasing of viscosity from 48.01 to 37.06 cSt.

**Table 10.** Fatty acid distribution of *Pongamia pinnata (P.pinnata)* oil.

| Fatty acid | wt.% |
|---|---|
| C 16:0 (Palmitic acid) | 15.09 |
| C 18:0 (Steric acid) | 4.66 |
| C 18:1 (*n*-9 cis, Oleic acid) | 54.41 |
| C 18:2 (*n*-6 cis, Linoleic acid) | 13.45 |
| C 18:3 (*n*-3, Linolenic acid) | 0.205 |
| C 20:0 (Arachidic acid) | 1.05 |
| C 20:1 (*n*-9, Eicosenoic acid) | 1.46 |
| C 22:0 (Behenic acid) | 8.27 |

**Table 11.** The concentration of metallic and phosphorus impurities in crude *Pongamia pinnata (P.pinnata)* oil.

| Sample | Concentration (ppm) | | | | | Oil recovery (wt. %) | Viscosity (cSt) |
|---|---|---|---|---|---|---|---|
| | Na | K | Ca | Mg | P | | |
| Crude oil | 113 | 168 | 231.5 | 108.3 | 509.5 | - | 48 |
| Degummed oil | 23.2 | 21.3 | 88.3 | 47.5 | 188 | 90.2 | 37 |

**5.1.2 Catalytic activity**

The evolution of *P.pinnata* oil conversion, and product yields with time on stream for Ni, Ni-Cu, Ni-Re, and Ni-Cu-Re catalysts are shown in **Figure *22*** The complete conversion of 100% was achieved for all catalysts and it is stable along 15 h time on stream, however, Ni-Cu/$\gamma$-Al$_2$O$_3$ catalyst shows a slightly decline in the activity and yield after 15 h. The liquid product yield was divided into 3 range, including gasoline range (C$_7$-C$_{12}$), diesel range (C$_{13}$-C$_{22}$), and high molecular weight hydrocarbon (>C$_{23}$).
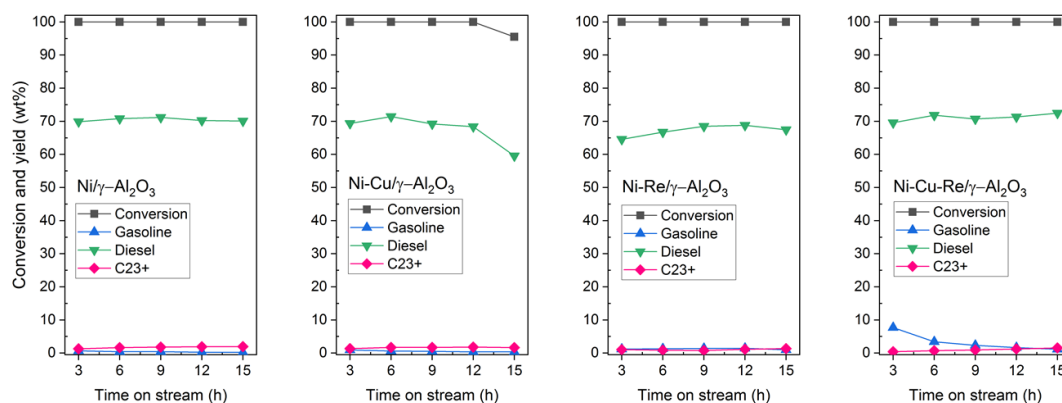


**Figure 22.** Conversion and product yield, over time on stream during hydrotreating of *P.pinnata* oil over Ni/$\gamma$-Al$_2$O$_3$, Ni-Cu/$\gamma$-Al$_2$O$_3$, Ni-Re/$\gamma$-Al$_2$O$_3$, and Ni-Cu-Re/$\gamma$-Al$_2$O$_3$ catalysts, All experiment were conducted at 330°C, 50 bar H$_2$, LHSV 1 h$^{-1}$, and H$_2$/oil ratio 1000 Ncm$^3$/cm$^3$.

The diesel range yield (C$_{13}$-C$_{22}$) is the majority product obtained over all the catalysts and small amount of gasoline yields were observed during the hydrotreating reaction, due to that the cracking reaction occurred over the Ni metal active site. Moreover, the C$_{23+}$ obtained from Ni-Cu catalyst was slightly high compared to the others, which is consistent with Loe et al studying the effect of Cu on deoxygenation of trioelin over supported Ni catalyst. They have been reported that adding Cu promoted the formation of long chain hydrocarbon led to higher selectivity of high molecular hydrocarbon range than monometallic Ni catalyst [175].
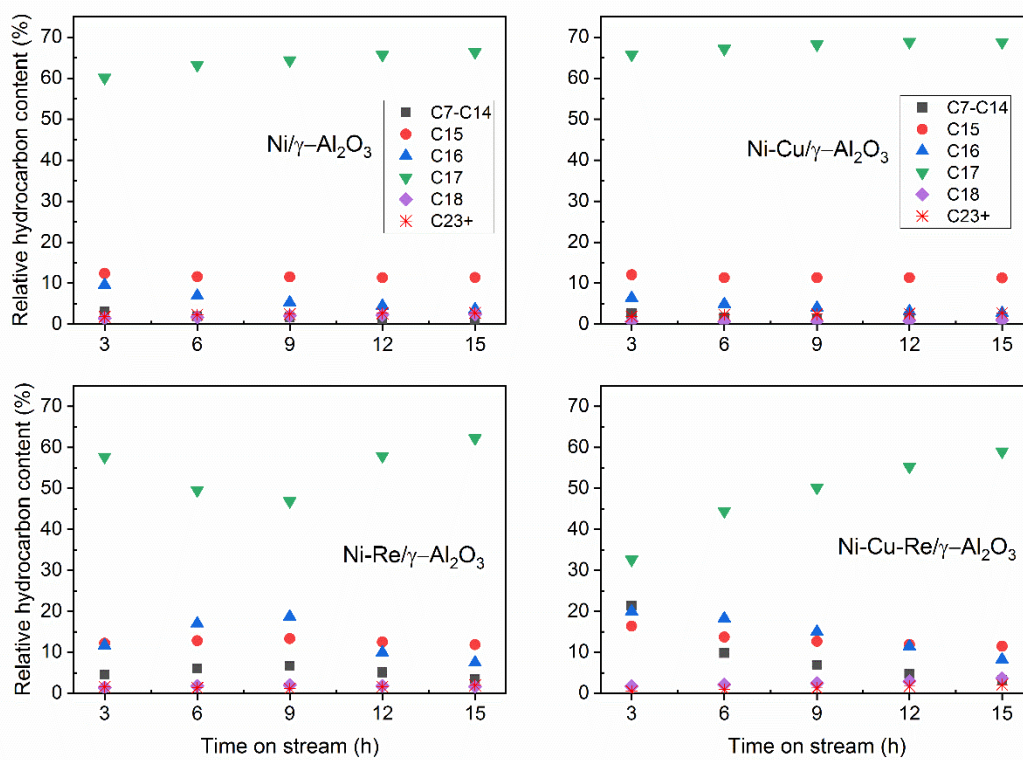
**Figure 23.** Relative hydrocarbon product distribution over Ni/γ-Al$_2$O$_3$, Ni-Cu/γ-Al$_2$O$_3$, Ni-Re/γ-Al$_2$O$_3$, and Ni-Cu-Re/γ-Al$_2$O$_3$ catalysts. All experiment were conducted at 330°C, 50 bar H$_2$, LHSV 1 h$^{-1}$, and H$_2$/oil ratio 1000 Ncm$^3$/cm$^3$

*Figure 23* presents hydrocarbon product distribution, *n*-C$_{17}$ hydrocarbon (C$_{n-1}$) are the major component which corresponding to oleic acid (C18:1), the main feed composition, for all catalysts. Over Ni and Ni-Cu supported on γ-Al$_2$O$_3$, the similar result of hydrocarbon distribution was observed: *n*-C$_{17}$ are the main product and very stable in the time interval test. This result could be indicated that the liquid product was produced mainly through decarboxylation/decarbonylation reaction rather than hydrodeoxygenation reaction [88,136], as shown by the relatively high contribution of decarboxylation/decarbornylation (DCO$_x$) compare to hydrodeoxygenation (HDO) (See *Figure 24*). The contribution of HDO and DCO$_x$ were calculated based on weight balance of C$_n$ and C$_{n-1}$ which represented by C$_{16}$/C$_{18}$ and C$_{15}$/C$_{17}$, respectively, following equation (9)-(10).
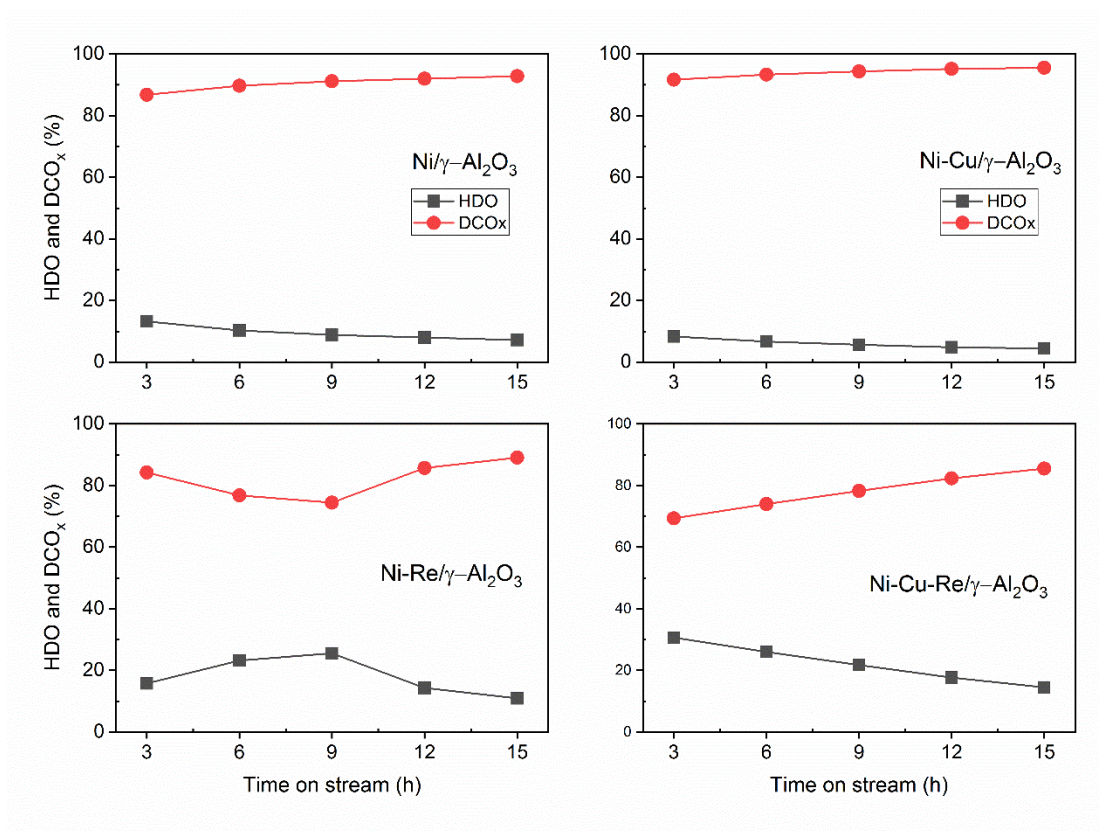
**Figure 24.** Contribution of HDO and $DCO_x$ over time on stream during hydrotreating of *P.pinnata oil* with continuous hydrogen feed. All experiment were conducted at 330°C, 50 bar $H_2$, LHSV 1 $h^{-1}$, and $H_2$/oil ratio 1000 $Ncm^3/cm^3$.

Although the $DCO_x$ was observed as a predominant reaction for all the catalyst. However, the addition of Re could be further improved the activity as well as enhanced the HDO reaction which offer relatively high yield of *n*-$C_{16}$ and *n*-$C_{18}$ hydrocarbons: this could explain via favorable dehydration and C-O hydrogenolysis over $ReO_x$ surface. The HDO activity have been reported favorable occurring on metal oxide site [38,41,158], and its rate depend on the accessibility of oxygen molecule on that site and feasibility of C-O bond scission. Meanwhile, the reaction that occurred over Ni metal favors scission of C-C bond, leading to increasing in $DCO_x$ activity.

The addition of Re catalysts shows the relative high fraction of light hydrocarbon composition ($C_7$-$C_{14}$), suggesting that adding Re could promote the cracking C-C bond over Ni active site [136,176] by increasing Ni dispersion and

enhancing the reducibility of Ni active site which is in good agreement with the TPR result in Appendix B (see *Figure 40*).

### 5.1.3 Catalyst characterization

**Table 12.** Physical properties of fresh and spent catalysts.

| Catalysts | BET surface area $(m^2/g)$ | Pore volume $(cm^3/g)$ | Average pore diameter (nm) |
|---|---|---|---|
| *Fresh catalysts* | | | |
| $\gamma\text{-Al}_2\text{O}_3$ | 202.0 | 0.54 | 10.64 |
| Ni | 181.0 | 0.43 | 9.58 |
| Ni-Cu | 176.2 | 0.42 | 9.24 |
| Ni-Re | 183.0 | 0.41 | 8.63 |
| Ni-Cu-Re | 180.4 | 0.40 | 8.83 |
| *Spent catalysts* | | | |
| Ni | 80.4 | 0.17 | 8.62 |
| Ni-Cu | 82.6 | 0.17 | 8.83 |
| Ni-Re | 95.4 | 0.19 | 7.95 |
| Ni-Cu-Re | 94.4 | 0.18 | 7.96 |

- The spent catalysts were conducted in degummed *P.pinnata* oil at 330°C, 50 bar $H_2$, LHSV 1 $h^{-1}$, $H_2$/oil ratio 1000 $Ncm^3/cm^3$ and collected at 15 h TOS.

As the Ni, Ni-Cu, Ni-Re and Ni-Cu-Re supported on alumina catalysts were comparatively studied for the performance of *P.pinnata* oil deoxygenation, which revealed the different activity and deactivation behaviors over these catalysts. In order to understand an effect of additional other metal promoter on stability and the reason for dropping in the activity of the catalysts, the spent catalysts were physicochemically characterized by $N_2$ sorption, SEM, XRD, TEM, $H_2$-TPR, and TGA. In addition, due to the different metal containing of catalyst compared to the chapter 4, hence, the fresh catalyst are also characterized and discussed.

*Table 12* presents the textural properties of fresh and spent catalysts Ni, Ni-Cu, Ni-Re, and Ni-Cu-Re supported on $\gamma\text{-Al}_2\text{O}_3$ catalyst, including surface area, total pore volume, and pore diameter. The surface area of commercial $\gamma\text{-Al}_2\text{O}_3$ support was measured as 202 $m^2/g$. After loading of metal into the support, the surface area and pore volume of fresh catalysts decreased, which could be due to coverage of surface

and partial pores blockage by incorporation of metal species. However, Ni-Re/γ-Al$_2$O$_3$ and Ni-Cu-Re/γ-Al$_2$O$_3$ show relatively high surface area and have no significantly different from monometallic Ni/γ-Al$_2$O$_3$. This could be due to adding Re could facilitate well dispersion of Ni metal on support.

A significant decrease in BET surface area by 55.5%, 53.1%, 47.9%, and 47.7% were observed from spent Ni/γ-Al$_2$O$_3$, Ni-Cu/γ-Al$_2$O$_3$, Ni-Re/γ-Al$_2$O$_3$, and Ni-Cu-Re/γ-Al$_2$O$_3$, respectively. This may be due to pore blockage and/or the coverage on external surface of catalyst by deposition of produced hydrocarbon molecules. In addition, the lower BET surface area was probably caused by agglomeration of metal species to large particles. The occurrence of large particle formation and pore blockage cause catalyst deactivation by decreasing in active sites and limiting mass transfer of reactant, intermediated as well as product from active site [73].

The XRD patterns of support and reduced catalysts at 500 °C are shown in *Figure 25(a)*. The characteristic peak at $2\theta$ of 37.2°, 39.1°, 45.6°, and 66.3° are found corresponding to (311), (222), (400), and (440) crystal planes of γ-Al$_2$O (JCPDS 29-0063), respectively. Monometallic Ni catalyst shows small intensity at $2\theta$ of 44.5°, 51.7°, and 76.2° which corresponds to (111), (200), and (220) crystal planes of metallic Ni (JSPDS 04-0850), respectively. In contrast, the diffraction peaks corresponding to Ni metal are not observed on Ni-Cu/γ-Al$_2$O$_3$ and Ni-Cu-Re/γ-Al$_2$O$_3$ catalysts, which could be ascribed by small fine Ni particle and high dispersion of Ni species on alumina surface, as can confirmed by particle size distribution estimated from TEM images, as shown in *Figure 26*. It should be noted that the average metal particle size was estimated from 50-120 particle at various magnification to ensure a significant population variance.
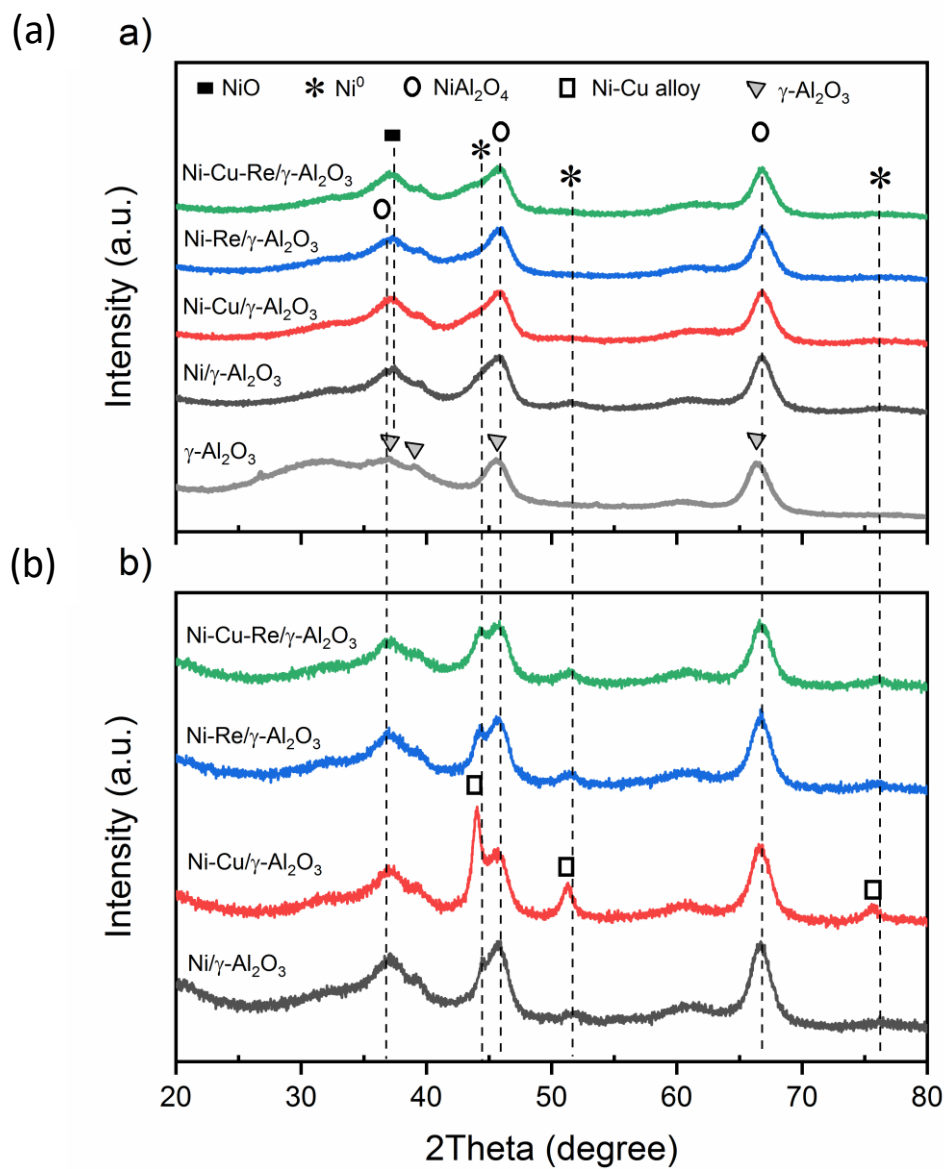
**Figure 25.** XRD patterns of (a) fresh $\gamma$-$Al_2O_3$ support and reduced Ni/$\gamma$-$Al_2O_3$, Ni-Cu/$\gamma$-$Al_2O_3$, Ni-Re/$\gamma$-$Al_2O_3$, and Ni-Cu-Re/$\gamma$-$Al_2O_3$ catalysts, and (b) spent catalyst after deoxygenation of *P. pinnata* oil for 15 h (TOS).
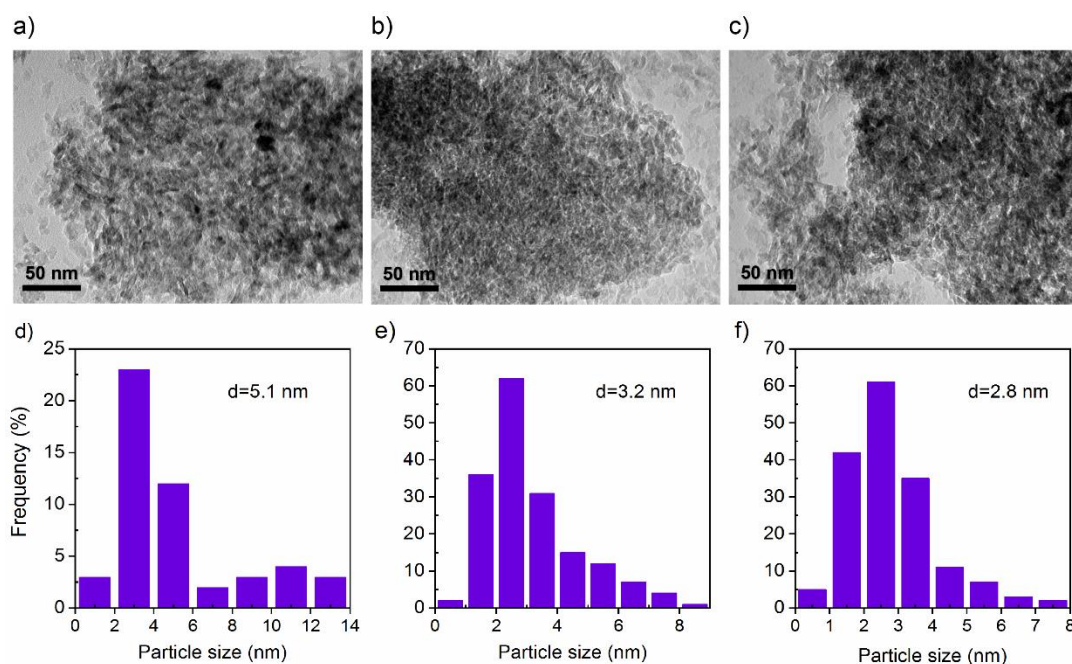
**Figure 26.** TEM image of (a) Ni/γ-Al$_2$O$_3$, (b) Ni-Cu/γ-Al$_2$O$_3$, and (c) Ni-Cu-Re/γ-Al$_2$O$_3$, and the particle size distribution of (d) Ni/γ-Al$_2$O$_3$, (e) Ni-Cu/γ-Al$_2$O$_3$, and (f) Ni-Cu-Re/γ-Al$_2$O$_3$.

For bi- and tri-metallic catalysts, no diffraction peaks at 43.3°, 50.4°, and 74.1° corresponding to Cu metal (JCPDS 04-0836) and Re are detected, probably because of its small percentage and low crystallinity, or also suggesting the high dispersion of Cu and Re species. This results could indicate that the introduction of Cu and Re could effectively improves the dispersion of Ni metal on alumina surface and the results are in agreement with other studies [38,126,177]. For all catalysts, weak diffraction peaks at 2θ of 37.4° originating from bulk NiO (JCPDS 44-1159) were detected, which could be described by the air exposure of catalyst surface during transfer from reduction process to XRD analysis. In addition, the peak shifting at around 2θ = 36.8°, 45.8°, and 66.8° for all impregnated catalysts from the γ-Al$_2$O$_3$ support also appeared, assigning to NiAl$_2$O$_4$ spinel phase (JCPDS 10-0339) on the catalysts [178], as confirmed by H$_2$-TPR.

For the spent catalyst, the intensity of diffraction peak of metallic Ni becomes gradually higher (at 44.5°, 51.7°, and 76.2°, *Figure 25(b)*, which seem to indicate that

the crystalize size of Ni particle increases due to agglomeration. However, the corresponding metallic Ni peaks are slightly shifted to lower angles at 44.0°, 51.2°, and 75.7° over Ni-Cu/$\gamma$-$Al_2O_3$ catalyst, which assigned to Ni-Cu alloy phase [38,179], and the formation of Ni-Cu alloy may result in relatively large crystalize size, leading to high diffraction peak intensity compare to other catalysts. The results are consistent with BET and SEM analysis. The agglomeration of Ni-Cu alloy could cause the declining of conversion and increasing the high molecular weight formation (see *Figure 22*).

The reducible behavior and interaction between metal-support were examined. The $H_2$-TPR profile of the calcined catalyst shows similar peak positions that were presented in chapter 4. However, the different in quantity of $H_2$ consumption was observed due to the different number metal loading. The Cu and Re can enhance the reducibility of Ni species. In addition, no observation the peak at high temperature peak around 700 °C when Re was added, implying that Re can also inhibit the $NiAl_2O_4$ formation by preventing $Ni^{2+}$ diffusion into $Al_2O_3$ lattice. The detail of $H_2$-TPR result was explained in Appendix B (see *Figure 40)*.

The morphology of both fresh and spent catalyst was examined by SEM image, as shown in *Figure 27*. For the fresh catalyst, it was calcined at 500 °C in atmospheric air prior to SEM analysis. High dispersion of metal species are observed on these four catalyst. Seemingly, a more porous structure was observed over Ni-Cu-Re/$\gamma$-$Al_2O_{3,}$ which may be ascribed to the $ReO_x$ incorporation into NiO structure, then more porous were generated due to the different atomic size of corresponding metal [180,181]. The agglomerated structure is clearly observed from SEM images of spent Ni/$\gamma$-$Al_2O_3$ and Ni-Cu/$\gamma$-$Al_2O_3$ catalyst, whereas morphological for spent Re-modified catalyst Ni-Cu-Re/$\gamma$-$Al_2O_3$ is slightly agglomerated, as consistent with BET and XRD results.
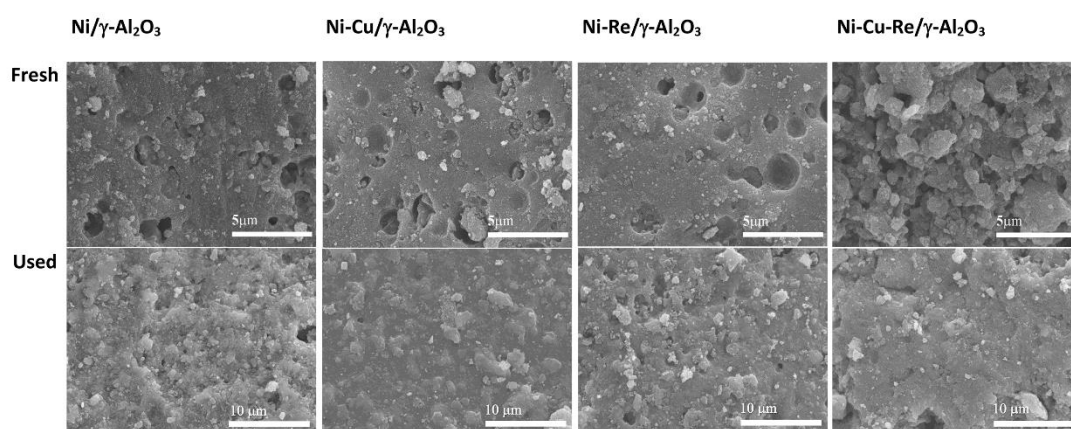
**Figure 27.** SEM images of fresh and spent Ni/γ-Al₂O₃, Ni-Cu/γ-Al₂O₃, Ni-Re/γ-Al₂O₃, and Ni-Cu-Re/γ-Al₂O₃ catalysts, performing in hydrotreating of *P.pinnata* oil.
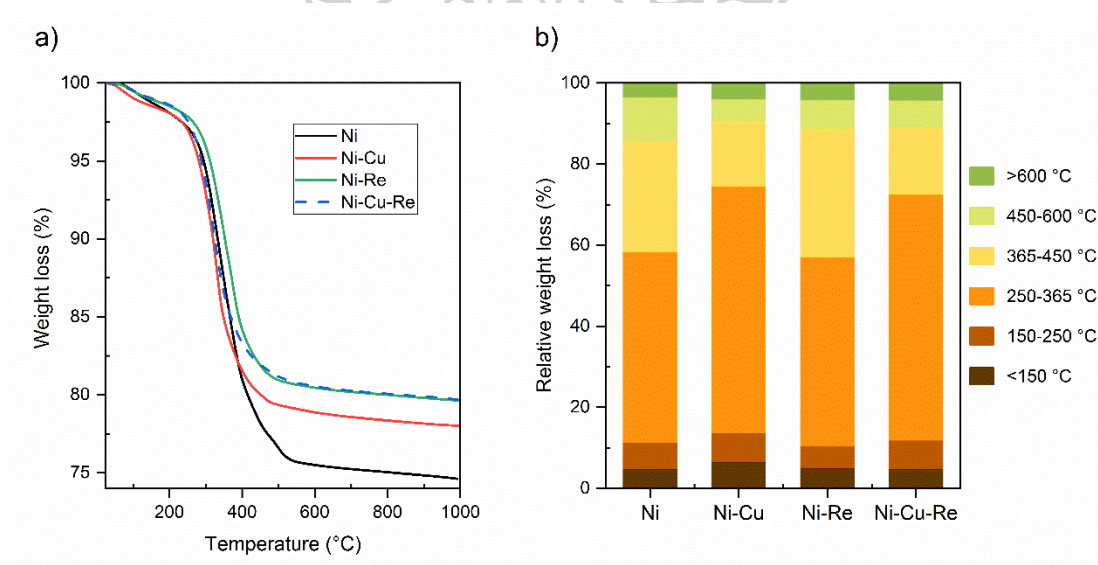


**Figure 28.** TGA curves and relative weight loss of spent catalysts after hydrotreated of *P.pinnata* oil

The spent catalysts were characterized using thermal gravimetric analysis to determine the coke formation on surface of catalysts. TGA curves of spent catalysts after hydrotreated of *P.pinnata* oil was shown in *Figure 28*, all samples exhibited about 2% weight loss at lower 150 °C due to the evaporation of moisture and water, and removal of physically adsorbed organic. Moreover, the combustion of deposited

carbon on surface of catalyst was existed at 250-550 °C, the weight loss at this temperature range was 21.6%, 18.1%, 17.4%, and 17.0% for Ni/γ-Al$_2$O$_3$, Ni-Cu/γ-Al$_2$O$_3$, Ni-Re/γ-Al$_2$O$_3$, and Ni-Cu-Re/γ-Al$_2$O$_3$, respectively. This coke formation causes the decreasing of catalyst surface area as shown in ***Table 12***. The Re-modified catalysts show lowest weight loss (17%), whereas the highest weight loss (20%) was achieved over the monometallic Ni catalyst, indicating the highest carbon deposit related to the lowest surface area compare to the other two catalysts. The ability of Re to reduce the metal particle size led to high metal dispersion on support and suppressed coke formation because large particle size will intensify carbon deposition [182,183]. Although the amount of carbon deposition is not considerably different implying the suppression of carbon formation is minority.

## 5.2 Conclusion

The catalytic behavior of Ni/γ-Al$_2$O$_3$, Ni-Cu/γ-Al$_2$O$_3$, Ni-Re/γ-Al$_2$O$_3$, and Ni-Cu-Re/γ-Al$_2$O$_3$ activity during hydrotreating of *Pongania pinnata* oil was studied in packed-bed reactor. The catalytic characterization results were exhibited, adding Cu and Re as promoters of Ni/Al$_2$O$_3$ catalyst can enhance the reduction of NiO. Moreover, the liquid product are all mainly in diesel boiling range (C$_{15}$-C$_{22}$) which contained hydrocarbons having *n*-C$_{17}$ as the main components for all catalysts, mainly produced from decarbonylation/decarboxylation. However, the hydrodeoxygenation was promoted when Re was added due to the favorable of C-O bonds scission over ReOx. The constant 100% conversion was obtained over all the catalyst, excepting Ni-Cu catalyst, due to the reduction of Ni active site by Ni-Cu alloy formation. The Ni-Re and Ni-Cu-Re show superior performance of complete conversion and high diesel yield, along 15 h time on stream. The spent catalyst Ni-Re and Ni-Cu-Re show rather low coke deposition and insignificant sintering, attributed to introduce Re can reduce both of Ni and Cu particle size and improve the metal dispersion.

# CHAPTER 6

# FACILE DEVELOPMENT OF ACCELERATED AGING
# METHODS FOR DEOXYGENATION CATALYST

During the hydrotreating of lipids based feedstock, coke formation is one of the most prevalent cause of catalyst deactivation as reported by many studies [73,184–187], which principally involves with decomposition, cyclization, aromatization, condensation, and polymerization of hydrocarbon in reactant/intermediate/product to form polyaromatic and heavy hydrocarbon compounds. The heavy compounds can accumulate either on external surface and inside pores of catalyst, leading to loss of active sites and block the pores which results to the reduction of catalyst activity, conversion, hydrocarbon yield, product selectivity, and catalyst's lifetime [185,188,189].

On this basis, to screen catalytic activity and stability of several catalysts are high time-consuming and costly due to the requirement of a massive number of bio-oil, hydrogen, and catalyst with highly energy-intensive. The accelerated test of catalyst deactivation were performed in order to test the performance and durability of catalyst in reduced time, typically via chemical aging or thermal aging. In case of chemical aging, the accelerating agents or coke precursor are usually added into the feed [190,191]. By the thermal aging, The catalysts are tested under accelerated conditions with relative high temperature > 450 °C [186,192,193].

In this work, the performance of monometallic Ni supported on alumina was tested for hydrodeoxygenation of *Pongamia pinnata* oil by comparison between two little different processes including continuous feed of $H_2$ and intermittent feed of $H_2$. It is interesting that the variation of hydrogen feed method affects and accelerates catalyst deactivation, which may benefit to use as an alternative less-time consuming method for further study of catalyst deactivation. During the analysis of the literature no studies on accelerating catalyst deactivation by the operating method were found. This new method is beneficial by avoiding the use of chemicals and their additional

operating cost during chemical aging and higher capital cost of tolerance material during thermal aging.

## 6.1 Setup Modifications

Some modifications to the original design (see ***Figure 2***) have been made in order to fit the purposes of this chapter. The experimental setup for this chapter is shown in
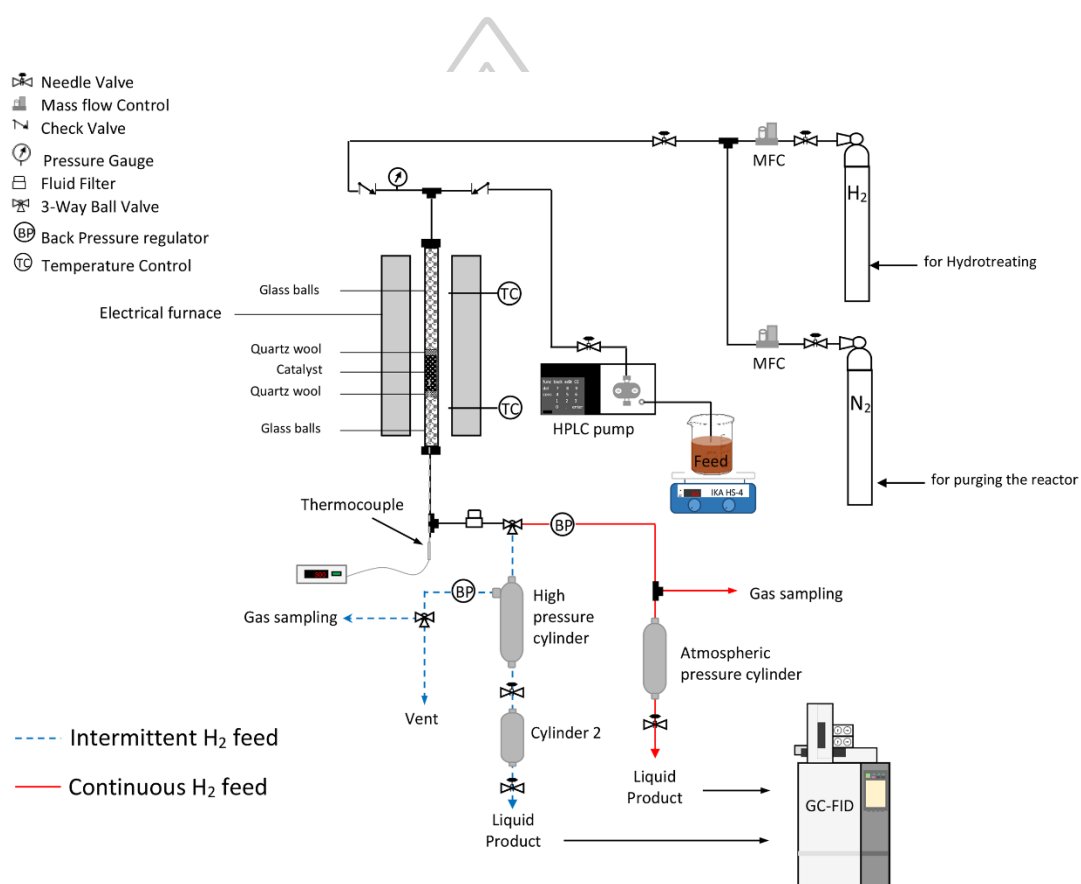


**Figure 29.** A modified configuration of packed-bed reactor for bio-hydrotreating diesel production.

For the intermittent feed of $H_2$, the experiment was conducted in the same condition as above. However, due to the different configuration of liquid product cylinder and back pressure regulator (BPR). As can be seen in ***Figure 29*** (dashed blue line), the liquid product was collected in high pressure cylinder due to the position of

BPR which placed before the cylinder, resulting in the pressure dropped approx. 5-10 bar during a product sampling step. Indeed, placing cylinder before BPR is also suitable for the specific BPR that allow only gas deliver through BPR. While the solid red line (*Figure 29*) shows the configuration of continuous feed system, which the product was collected in atmospheric pressure. Hence, the extremely high $H_2$ flowrate was introduced into the reactor only for the intermittent case, in order to make-up for the dropped system pressure. As this purpose, the discontinuous of hydrogen flow for each sampling time (every 3 hours in this study) which need intermittently high $H_2$ flowrate (taking time about 10 minutes) to restore the pressure of 50 bar.

## 6.2 Results and discussion

### 6.2.1 Catalytic activity
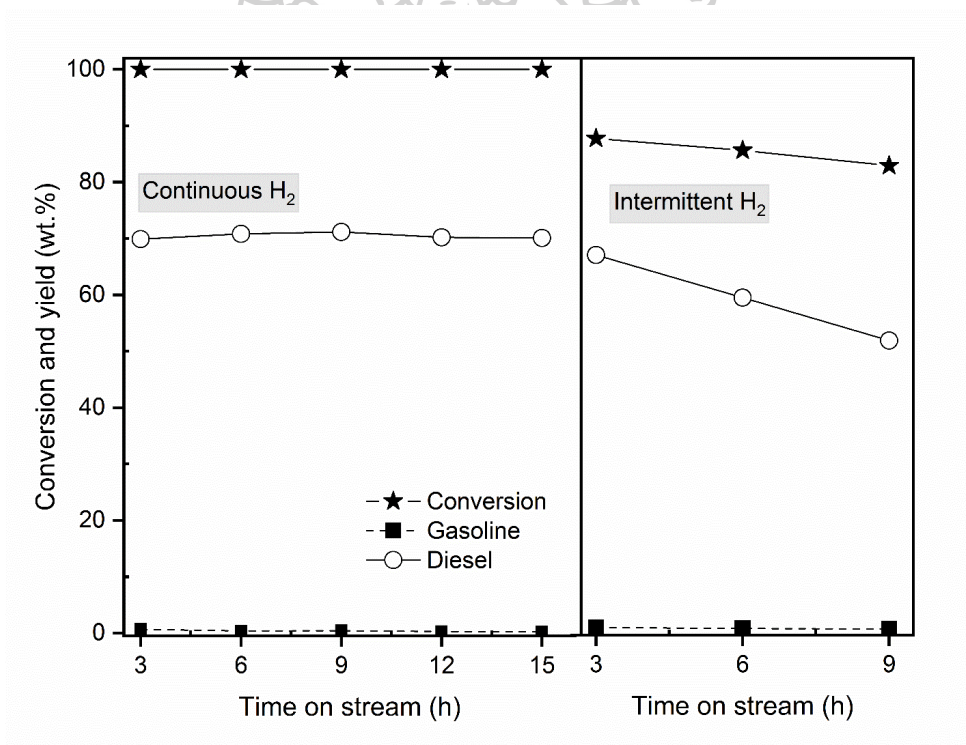


**Figure 30.** Conversion and liquid fuel yield (gasoline and diesel) as a function of TOS. All experiment were conducted at 330°C, 50 bar $H_2$, LHSV 1 h$^{-1}$, and $H_2$/oil ratio 1000 Ncm$^3$/cm$^3$.

*Figure 30* shows conversion, gasoline ($C_7$-$C_{12}$) yield, and diesel ($C_{13}$-$C_{20}$) yield, as a function of reaction time. During the continuous hydrogen feed, the complete conversion can be achieved without any deterioration during 15 h. The product yield which mainly diesel is almost constant. Meanwhile, the relatively low conversion of about 87% was observed during intermittent hydrogen feed and decreased to 82% at 9 h-on-stream. As it was observed on the liquid fuel yield that started decrease at 6 h and the lowest liquid yield of 54 wt. % was obtained at 9 h-on-stream.

In consideration of product distribution (*Table 13*), in both cases, the liquid product mostly composed of $n$-$C_{15}$ — $n$-$C_{18}$ hydrocarbons which are in diesel boiling range, corresponding to the liquid yield in *Figure 30*. In addition, $n$-$C_{17}$ is predominant hydrocarbon composition corresponding to oleic acid (C18:1) the main feed component. This result could be indicated that the liquid product was produced mainly through decarboxylation/decarbonylation ($DCO_x$/DCO) reaction rather than hydrodeoxygenation (HDO) reaction [88,136], as shown by the percent of contribution of HDO and $DCO_x$/DCO (*Table 13*) which were calculated using the ratio of weight percent of $n$-alkanes with even number ($n$-$C_{18}$) or odd number ($n$-$C_{17}$) to total weigh percent of $n$-$C_{18}$ and $n$-$C_{17}$ in product.
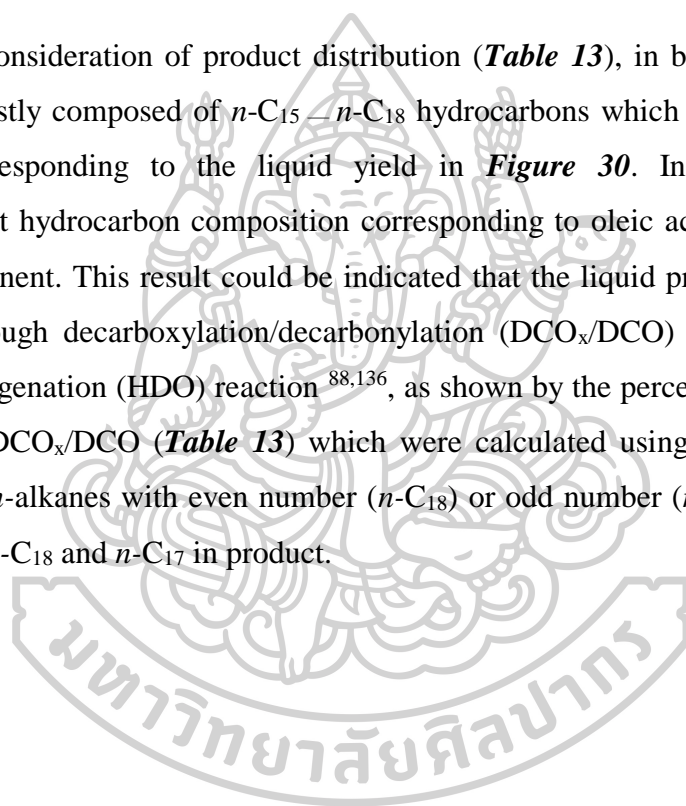
**Table 13.** Summary of conversion and composition of liquid product from hydrotreated *P.pinnata* oil over different catalysts. (All experiment were conducted at 330°C, 50 bar $H_2$, LHSV 1 $h^{-1}$, and $H_2$/oil ratio 1000 $Ncm^3/cm^3$ and collected at 9 h TOS)

| Catalysts | $H_2$ feed | Conversion (%) | Liquid product (wt. %) | Selectivity (wt. %) | | | | | | | | | | HDO (%) | $DCO_x$ /DCO (%) |
|---|---|---|---|---|---|---|---|---|---|---|---|---|---|---|---|
| | | | | $C_7$-$C_{14}$ | $C_{15}$ | $C_{16}$ | $C_{17}$ | $C_{18}$ | $C_{19}$-$C_{22}$ | $C_{23+}$ | 1-Octadecanal | 1-Octadecanol | Stearic acid | | |
| Ni | Inter. | 82.9 | 65.7 | 1.71 | 12.46 | 2.46 | 67.08 | 3.93 | 8.56 | 2.63 | 0.18 | 0.20 | 0.81 | 5.49 | 94.51 |
| Ni | Cont. | 100 | 73.5 | 1.73 | 11.54 | 5.30 | 64.37 | 2.04 | 12.52 | 2.50 | - | - | - | 3.07 | 96.93 |

**Table 14.** Physicochemical properties of fresh and spent catalysts using in the continuous and intermittent hydrogen feed.

| Catalysts | BET surface area ($m^2/g$) | Relative reduction of BET surface area (%) | Pore volume ($cm^3/g$) | Average pore diameter (nm) | The rate of carbon formation ($mg/g_{cat}/s$) | Carbon amount that accumulated on Sp catalyst ($mg/g_{cat}$) |
|---|---|---|---|---|---|---|
| **Fresh catalysts** | | | | | | |
| $\gamma$-$Al_2O_3$ | 202.0 | - | 0.54 | 10.64 | - | - |
| Ni | 181.0 | - | 0.43 | 9.58 | - | - |
| **Spent catalyst** | | | | | | |
| Ni-inter. $H_2$ | 95.3 | 47.3 | 0.21 | 8.70 | $5.53 \times 10^{-3}$ | 179.2 |
| Ni-cont. $H_2$ | 120.6 | 33.4 | 0.27 | 9.00 | $2.48 \times 10^{-3}$ | 134.0 |

Obviously, there is no significant change of product distributions and selective reaction pathway between these two different hydrogen feed methods, except the yield and its appearance. The visual colour of liquid products obtained from the continuous experiment are clear and colorless during the entire experiment, as shown in *Figure 31*. Whereas the intermittent experiment produced liquid product with light yellow at early stage, and turn into the dark yellow, then a half amount of product eventually became solid phase (wax, at room temperature) at 9 h-on-stream. The change of product's colour may be related to the existence of oxygen-containing compounds in the product, due to the color looked more similar to the feed. This indicates that the reduction in degree of deoxygenation, resulting from the losing catalytic activity during the reaction under intermittent hydrogen feed. It is evident by the detection of a small amount of 1-octadecanal at early stage, then 1-octadecanol and stearic acid gradually increased as a function of time-on-stream. The selectivity of the oxygen-containing compounds at 9 h-on-stream is presented in *Table 13*. Hence, the post-run catalyst was characterized via nitrogen-sorption, XRD, and TGA-DSC to examine the reason for loss of catalytic activity and effect of hydrogen feed mode on the catalysts. After the hydrotreating reaction, all experiments were fed by hexane at room temperature to clean the reactor system and facilitate unloading of catalyst.
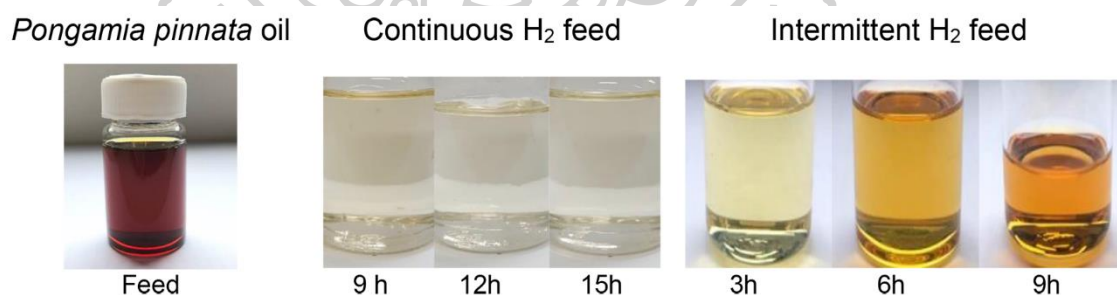


**Figure 31.** Pongamia pinnata oil and deoxygenated liquid product.

**6.2.2 Catalyst characterization**

*Table 14* presents the textural properties of fresh and used of Ni supported on γ-Al$_2$O$_3$ catalyst, including surface area, total pore volume, and pore diameter. The surface area of commercial γ-Al$_2$O$_3$ support was measured as 202 m$^2$/g. After loading of Ni metal into the support, the surface area and pore volume of fresh catalysts decreased, which could be due to coverage of surface and partial pores blockage by Ni incorporated. A significant decrease in BET surface area by 47.2% and 33.4% were observed from spent Ni/γ-Al$_2$O$_3$ used in the intermittent and continuous hydrogen, respectively, which could be due to the deposition of hydrocarbon molecules on surface and pores of catalyst (confirmed by TGA). In addition, the lower BET surface area were probably caused by thermal degradation, leading to agglomeration of metal species to large particles, which can be verified by XRD analysis. These occurrence are cause of a catalyst deactivation by decreasing in active sites [73]. The pore size distributions of fresh and spent Ni/γ-Al$_2$O$_3$ are shown in *Figure 32*. The rather large pore diameter with an average of 9.2 nm and pore volume were observed in case of fresh catalyst. After the reaction, the pore diameter and pore volume of spent catalysts significantly decrease. The lowest of pore diameter in an average of 6.1 nm was obtained from intermittent hydrogen, while for continuous mode, the higher pore diameter of 7.1 nm on average were noticed. This indicated that pore of the catalysts were highly blocked by the molecules of hydrocarbon reactant and products. In brief, it can be seen that the intermittent hydrogen has more influence on the rate of carbonaceous deposition compare to the continuous mode. The coke deposition is an obstacle of diffusion through the pores either reactant or product, which affect the catalytic activity.
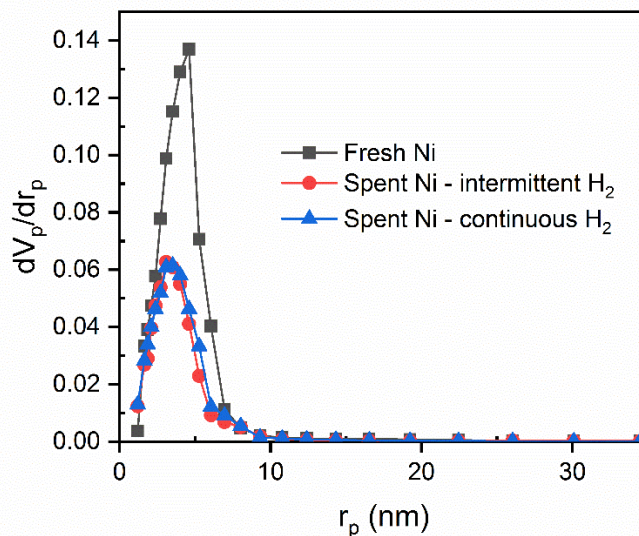
**Figure 32.** Pore size distribution of fresh and spent Ni/γ-Al$_2$O$_3$ after hydrotreating of *P.pinnata* oil in intermittent and continuous hydrogen feed mode. All experiment were conducted at 330°C, 50 bar H$_2$, LHSV 1 h$^{-1}$, and H$_2$/oil ratio 1000 Ncm$^3$/cm$^3$.

The XRD patterns of support and reduced catalysts at 500 °C were shown in *Figure 33(a)*. The characteristic peak at 2$\theta$ of 37.2°, 39.1°, 45.6°, 60.61°, and 66.3° are exhibited as dominant peak of all catalyst, corresponding to (311), (222), (400), (511), and (440) crystal planes of γ-Al$_2$O (JCPDS 29-0063), respectively. The diffraction of metallic Ni at 2$\theta$ of 44.4°, 51.8° and 76.3° (JSPDS 04-0850) are barely observed, which could be suggested by small particle size of Ni and well dispersion of Ni on surface catalyst. In addition, the peak shifting at around 2θ = 36.8°, 45.8°, and 66.8° for all impregnated catalysts from the γ-Al$_2$O$_3$ support also appeared, assigning to NiAl$_2$O$_4$ spinel phase (JCPDS 10-0339) on the catalysts [178]. For the spent catalyst, the intensity of diffraction peak of metallic Ni becomes gradually higher (at 44.5°, 51.7°, and 76.2°), angles zooming presented in *Figure 33(b)*, which indicate that the crystalize size of Ni particle increases due to agglomeration. However, crystallite size measurement via the Scherrer equation could not determine because the intensity of the peaks is rather low and no significant different is observed between intermittent and continuous hydrogen feed indicating that Ni metal agglomeration may not be the main cause for catalyst deactivation.
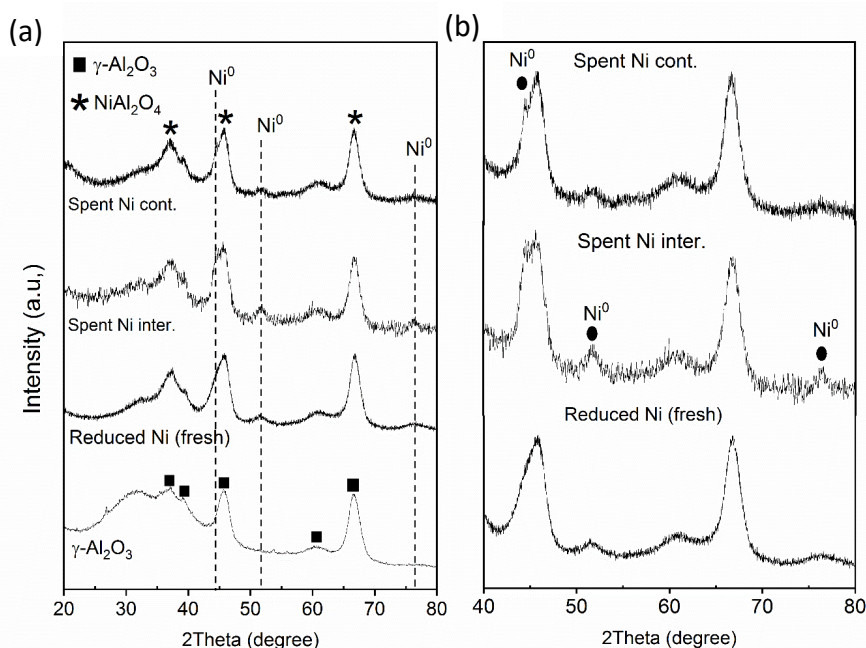
**Figure 33.** (a) XRD pattern of $\gamma$-$Al_2O_3$ support, reduced (fresh) and spent Ni/$\gamma$-$Al_2O_3$ catalyst for different hydrogen feed mode, and (b) angle zoom in at 2$\theta$ of 40° to 80°. All experiment were conducted at 330°C, 50 bar $H_2$, LHSV 1 $h^{-1}$, and $H_2$/oil ratio 1000 $Ncm^3/cm^3$. (Noted: cont. is continuous hydrogen feed and inter. is intermittent hydrogen feed)
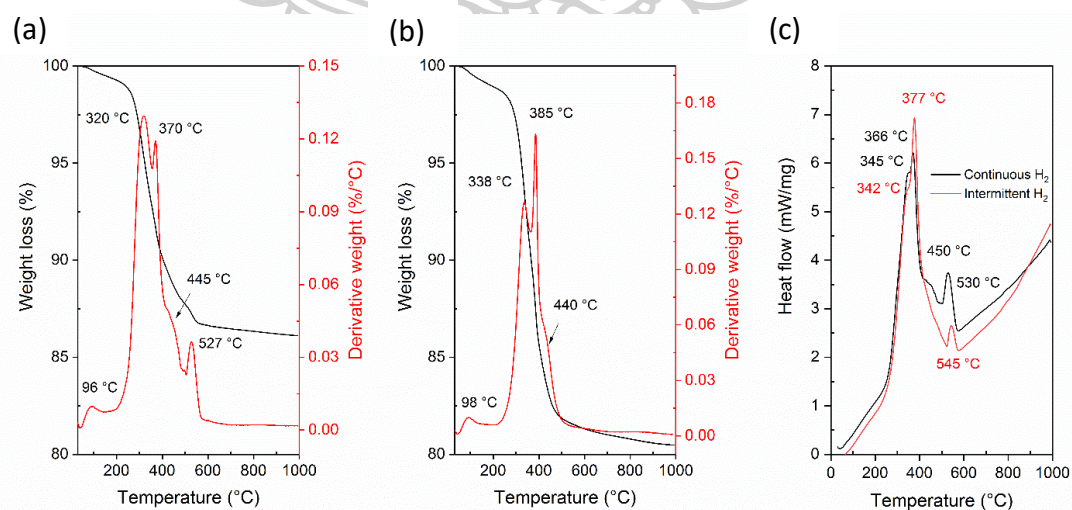


**Figure 34.** Thermogravimetric (TGA) - derivative weight loss (DTG) as function of temperature of the spent Ni/$\gamma$-$Al_2O_3$ catalysts spent in (a) continuous hydrogen feed mode, (b) intermittent hydrogen feed mode, and (c) differential scanning calorimetry (DSC) profiles.

Thermogravimetric analysis (TGA) was performed in atmospheric air to quantify the coke formation on the catalysts by monitoring the weight loss of catalyst as a function of temperature during its combusted. *Figure 34(a)* and *Figure 34(b)* show thermogravimetric (TG) and derivative thermogravimetric (DTG) curve of the Ni catalyst used in continuous and intermittent hydrogen feed, respectively. The initial weight loss approx. 1.3% at temperature ca. 100 °C, attributed to the vaporization of physical adsorbed water [194,195]. The maximum weight loss of both samples exhibit in temperature range of 250 - 550 °C; approx.18 % of intermittent hydrogen feed catalyst and 13% decreasing in continuous hydrogen feed.

As considering of DTG curves, two peaks around 320-340 °C and 370-385 °C attributed to either desorption and/or combustion of adsorbed residual molecules of heavy hydrocarbons over the external surface of catalyst. In addition, the higher temperature at 400-600 °C may correspond to the decomposition of heavy hydrocarbons deposited within the catalyst pores, and/or the oxidation of more stable amorphous coke [194,196–199].

The DTG profile of both continuous and intermittent experiment is well correlated with DSC curves presented in *Figure 34(c)*, indicating that the reactions corresponding to the exothermic (DSC peak) is influential effect on the change of weight loss. The exothermic peak reveals in temperature of 300 – 400 °C, assigned to the decomposition of the different reactive carbonaceous species which could be generated from the heavy hydrocarbons and/or fatty acids with corresponding boiling range temperature [200]. In case of continuous $H_2$ experiment, the other two small peaks exhibit at 445 °C and 527 °C, corresponding to the oxidation of slow reactive carbon species or the combustion of coke located within the pores of catalyst and amorphous coke, respectively [199], leading to more energy requirement. In case of the catalyst used in intermittent experiment, the DSC peak at 545 °C was observed, which assigned that there was the decomposition of the stable coke. However, there was no peak existing around 500 °C or higher were existed in the TGA-DTG profile in *Figure 34(b)*. This implies that the stable coke was formed but very small quantity, resulting in the overlapping with the peak around 440 °C. In comparison to the intermittent experiment, the DTG and DSC curves of continuous experiment are slightly shifted

toward the lower temperature, suggesting that its accumulated-carbon species more effortless to be removed.
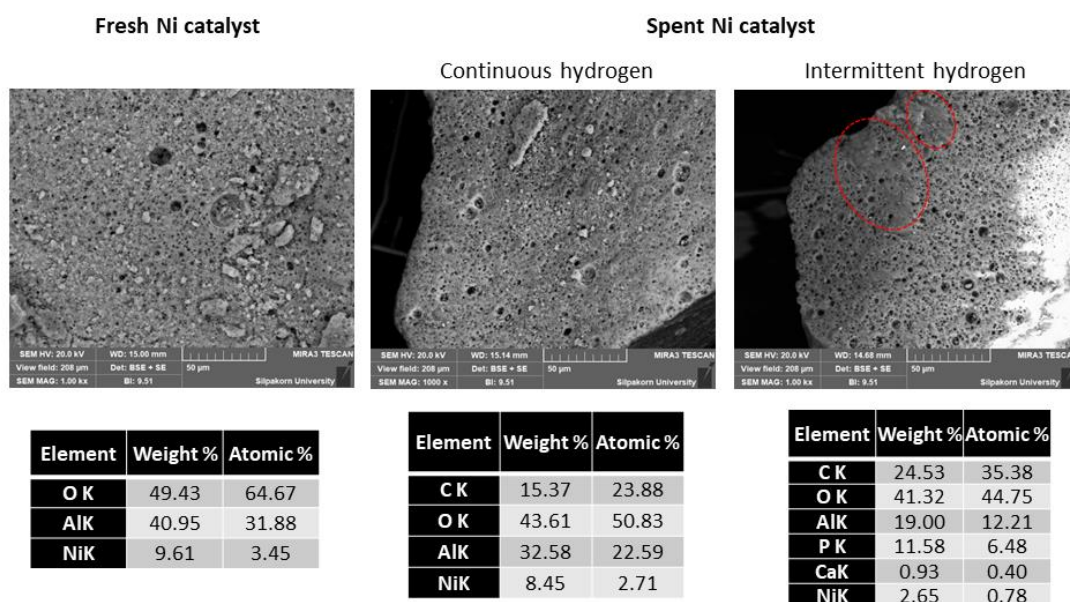


**Figure 35.** SEM image and elemental compositions of fresh and spent Ni/γ-Al$_2$O$_3$ catalysts.

Additionally, the morphology of fresh and spent catalyst using in both configuration system were characterized via SEM technique and the elemental deposition on the surface of catalysts were also examined by EDS analysis, as shown in *Figure 35*. The morphology of fresh and spent catalyst are quite similar; however, there has an observation of thick film covering on the surface of catalyst (red-dash circle), especially in the intermittent experiment. The EDS analysis clearly shows that higher amount of C selectively deposition on the catalyst using in the intermittent experiment, corresponding to the TGA result. Not only C but also phosphorus (P) and small amount of calcium (Ca) are observed in the intermittent catalyst. This could suggest that the thick film covering the surface of catalyst was generated from C and P, leading to loss of active site and plugging the catalyst's pores. The P deposition on the catalyst could be originated from the decomposition of phospholipid in the reactant during the reaction, which is reasonable due to an observation of high amount of P in *Pongamia pinnata* oil (See *Table 11*). As consider the relative effect between the amount of coke formation, P deposition, and the pore size distribution and pore

volume, the decreasing in pore size and volume may relate to deposition of C and P within the catalyst pores. In addition, the pore blockage may occur by a significant amount of elementals deposition on external surface at the beginning and thereby plugging the pores mouths. The deposited materials may expand and narrow the voids between catalyst particles in the bed, which result in feedstock uneven flow through the reactor or channeling through the bed, leading to increase in the pressure drop throughout the reactor. This induces a necessary of increasing liquid feed pressure to the reaction system, as shown in *Figure 36(a)*.

The rate of coke formation of $Ni/\gamma-Al_2O_3$ in the intermittent experiment is 5.53 x $10^{-3}$ mg $C/g_{cat}/s$, respectively, which higher than that of continuous experiment of 2.48 x $10^{-3}$ mg $C/g_{cat}/s$, as shown in *Table 14*. They are can be arbitrarily explained through a few existing experiment on inert gas which reported elsewhere by the fact that hydrogen gas has a crucial role not only for to enhance the deoxygenation activity but also to prevent catalyst deactivation by coke formation [201–203]. These results can be described by the role of hydrogen gas during deoxygenation reaction.

In case of the intermittent $H_2$, the reaction was interrupted by creation of pressure drop and extremely high inlet hydrogen velocity feed for restore the system pressure of 50 bar, which may causes the shorter contact time of the reactants and the catalyst, resulting in reducing of conversion and hydrotreating activity (*Figure 30*), as also confirm by increasing oxygen-containing molecules (*Table 13*). Moreover, the lack of pressure in reactor (for a while) during the pressure drop could accelerate other side reaction i.e. cracking, dehydrogenation reaction to form unsaturated hydrocarbons which is a coke precursor, after which the compound could be further cyclized and oligomerized to form the larger molecules. Besides, the oligomerization could be catalyzed by phosphoric acid containing in the oil[76], which may be enhanced due to the reduction of hydrotreaing activity. This is evident by the relatively high selectivity of high molecular weight hydrocarbons (> $C_{23}$) containing in the intermittent liquid product compare to the continuous (Table 1), which finally accumulate on the catalyst surface and further inside the pores [189,204], causing the catalyst deactivation. By this point, it is quite obvious that the $Ni/\gamma-Al_2O_3$ used in continuous hydrogen feeding and steady operating condition is rather more stable than

it is in the intermittent mode, due to the effect of hydrogen concentration and the operation method.

In addition, there is a pressure change observed during the reaction both in reactor and in liquid feed stream, as presented in *Figure 36(a)*. The operating pressure begins oscillating after reaction time of 5 h-on-stream, whereas the pressure in liquid stream gradually increased since 3 h-on-stream and reached the maximum pressure of HPLC pump after product collected at 9 h-on-stream. As a result, the reactor was instantly stopped operating and the experiment can no longer be conducted. This was only occurred in case of intermittent hydrogen, suggesting that the great amount of coke deposition could lead to reactor fouling by decreasing the bed porosity and plugging the reactor[189]. Also, we observed the gum formation on the glass beads used in the intermittent hydrogen feed mode, and no significant gum detected in continuous mode, as shown in **Error! Reference source not found.**, which could be originated form the phosphorus and alkali impurities in the reactant, leading to accumulation and plugging of the reactor[76]. However, somewhat small amount of phosphorus and alkali were detected on spent catalyst (See *Figure 35*), as well as the amount of gum formation on the glass beads. This is because some amount of P and alkali or gum were removed during the washing step after the reaction by using hexane in order to facilitate unloading of used catalyst and glass beads.
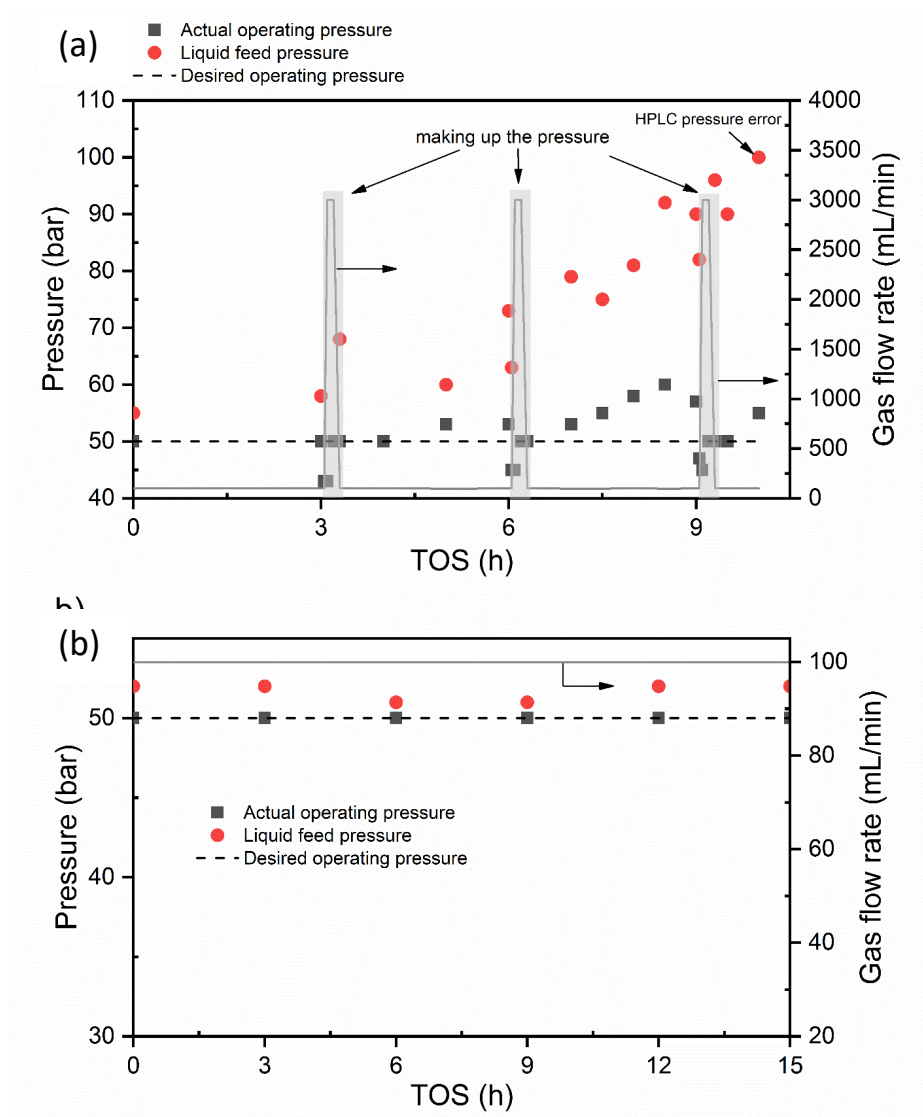
**Figure 36.** Change of pressure and hydrogen flow rate as a function of TOS during hydrotreating of *P.pinnata* oil of (a) intermittent hydrogen feed mode and (b) continuous hydrogen feed mode. All experiment were conducted at 330°C, 50 bar $H_2$, LHSV 1 $h^{-1}$, and $H_2$/oil ratio 1000 $Ncm^3/cm^3$.
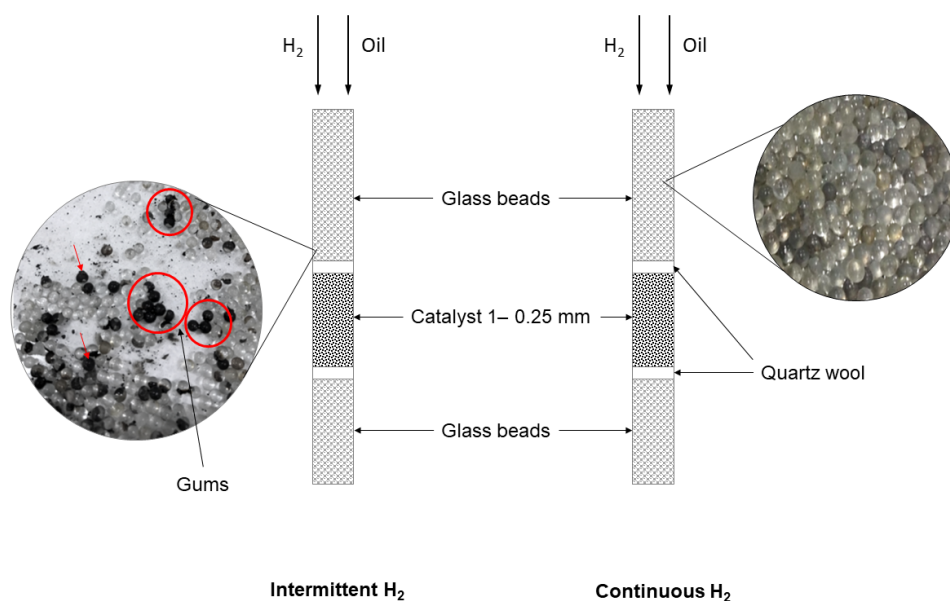
**Figure 37.** Interior view of packed bed reactor with gum formation on the glass beads.

## 6.3 Conclusion

In summary, the slightly different of hydrogen feed mode could affect the catalyst activity and its deactivation. In the intermittent hydrogen feed, conversion and product yield were lower than that obtained from continuous hydrogen feed system. In addition, a drop of liquid fuel yield was observed at long reaction time, whereas the complete conversion can be achieved in the continuous hydrogen feed without any deterioration during 15 h. The carbonaceous deposition seem to be a majority cause for catalyst deactivation in both case, besides, the coke formation is mostly reactive coke which can be removed effortless, especially when gasify agent ($H_2$) was introduced. Nevertheless, in the intermittent hydrogen feed mode, an extremely high inlet hydrogen velocity could cause the shorter contact time toward reduction of hydrotreating efficiency; and lacking of hydrogen can further accelerate aging of catalyst, leading to increasing rate of catalyst deterioration by coke deposit and gum formation results in plugging of reactor bed.

# CHAPTER 7

# SUMMARY AND RECOMMENDATIONS

.

This thesis contributes to the catalytic hydrotreating of non-edible biomass-derived oil with supported Ni on alumina catalysts showing high performance of catalyst activity and importance of promotion and $H_2S$ level during HDO.

The effect of Cu and Re addition on supported Ni/γ-Al2O3 catalyst were studied the performance for upgrading of algae bio-crude oil. The algae bio-crude oil is an attractive third-generation biofuel. The bio-oil yield of 50% can be obtained from HTL of *Nannochloropsis* sp. at 320 °C for 30 min with energy recovery ($ER_{HTL}$) of 71.8%. Catalytic hydrotreating of algae bio-crude oil from hydrothermal liquefaction (HTL) of *Nannochloropsis* sp. was performed at 350°C under hydrogen pressure of 75 bar for 4 h. Different Ni-based catalysts including Ni/γ-Al$_2$O$_3$, Ni-Cu/γ-Al$_2$O$_3$, Ni-Re/γ-Al$_2$O$_3$ and Ni-Cu-Re/γ-Al$_2$O$_3$, (10%Ni, 5%Cu, 2.5%Re) were used to examine the performance in upgrading of the bio-crude oil. Most catalytic systems could effectively eliminate S and decrease the N and O contents, and enhance more than 20% improvement in the higher heating value (HHV) of the bio-oil (34 to 41-45 MJ/kg) which is in the range of typical fossil fuels.

Addition of Re and Cu has significant influence on the product distribution and fuel characteristics. Introducing only Cu could enhance the C=O hydrogenation which results in high selectivity in aromatic and alcohol compounds. While adding Re is effective for hydrodeoxygenation but lowering denitrogenation due to amination reaction, then further nitriles formation. Adding both Cu and Re to form a Ni-Cu-Re/γ-Al$_2$O$_3$ ternary alloy offered the best results on the overall performance, achieving the highest upgraded bio-oil yield of 58 wt.% and the highest energy recovery in the upgrading process ($ER_{upgrade}$) of 64.6%. As ER in HTL process ($ER_{HTL}$) was ca. 71.8%, the overall ER ($ER_{overall}$) from algae biomass to upgraded bio-oil of 46.4% can be achieved for Ni-Cu-Re/γ-Al$_2$O$_3$ catalyst. Carbon efficiency approx. 47.7% can be

attained as the carbon in the algae biomass feedstock was retained in the upgraded bio-oil.

The catalytic behavior during hydrotreating of *Pongamia pinnata* oil was studied in packed-bed reactor at 330 °C, 50 bar $H_2$, $H_2$/oil ratio of 1000 $Ncm^3/cm^3$ and liquid hourly space velocity (LHSV) of 1 $h^{-1}$. The catalyst show a good activity and quite stable along 15 h, excepting Ni-Cu catalyst which the activity was declined at 15 h time on stream. According to the characterization, agglomeration of Ni-Cu alloy was observed in Ni-Cu catalyst, leading to reducing the active site toward loss of catalytic activity. Also, the carbonaceous deposition on the catalyst seem to be not the main reason of catalyst deactivation. The addition of Cu and Re on Ni/$\gamma$-$Al_2O_3$ catalyst exhibit the ability to improve catalytic activity and prevent coke formation compare to single metal Ni catalyst via promotion of the metal dispersion and enhancement of the reducibility NiO.

The accelerated coking deactivation was proposed by intermittent feed of hydrogen for hydrodeoxygenation reaction, in order to reducing feed and catalyst consuming, as well as its less and time-consuming. With intermittent feed of hydrogen, oil conversion sharply decreased to 80% in 9 h. The fresh and spent catalysts of continuous and intermittent hydrogen feed were analyzed by $N_2$ sorption, XRD, and TGA-DTG-DSC, which exhibited that coke formation were a reason of this rapid catalyst deactivation. The rate of carbon formation could be accelerated from 2.48 x $10^{-3}$ to 5.53 x $10^{-3}$ mg C $g_{cat}^{-1}$ $s^{-1}$ or over 120% rate increasing. Moreover, this accelerated deactivation technique does not alter the reaction pathway as the contribution of $DCO_x$ and HDO reactions are almost the same.

As our observation, we consider this method – the intermittent hydrogen feed – could effectively perform to be an accelerant for aging the catalyst in order to study the behavior of catalyst deactivation in hydrodeoxygenation of biomass with the beneficial to less-time consuming.

## Future recommended work

The catalytic upgrading of algae biomass is the promising pathway to produce bio-transportation fuel. Study and development of new catalyst in order to improve the catalyst's activity, selectivity, and stability under deoxygenation condition are necessary. Considering the work presented in this thesis, the other metal-modified show the positive effect on activity and selectivity of Ni/γ-Al₂O₃ catalyst in different ways. Also, the modified-Ni catalyst show the positive effect on the carbonaceous deposition during the deoxygenation process. Deactivation behavior and spent catalyst characterization of algae bio-crude upgrading should be further studied in detail compared with fresh catalyst. Nevertheless, we faced the issue about catalyst recovery, due to the solid residue formation. During the upgrading process, the solid residue was produced after the reaction which is an obstacle to recover the used catalyst, hence, the development of process should be conducted (e.g. study in packed-bed reactor or using the catalyst in pellet form) for further investigation on deactivation, reusability, and development of regeneration method.

In addition, the reaction mechanism of each catalysts was proposed via prediction on the predominant chemical containing in algae bio-crude and obtaining product, with the corresponding literature. However, the algae bio-crude oil contains very complicated chemical composition, which may result in unclarified some elementary reaction. The use of individual model compounds (e.g. hexadecanamide) or model mixture should be further investigated to clarify the occurred reaction mechanism and to more understand the role of other metal in deoxygenation process. Moreover, for the upgrading of algae bio-oil, Ni-Re seems to have an effect for N-containing compound, the effect of Re content and the mechanism for amination during the deoxygenation process should be further conducted.

As the accelerated catalyst deactivation have been accidentally observed in this work via operation in the different configuration of reactor. Coke formation seem to be a main reason for loss of activity; however, it was not clarified yet, because we also observed the formation of gum which caused the reactor plugging, leading to stop the run, only in the intermittent hydrogen feed experiment. Hence, the effect of

hydrogen flow rate and pressure drop during the operation on the gum and coke formation should be further investigated for more detail.

# REFERENCES

1.  Alemán-Nava GS, Casiano-Flores VH, Cárdenas-Chávez DL, et al. Renewable energy research progress in Mexico: A review. *Renew Sustain Energy Rev*. 2014;32:140-153. doi:10.1016/j.rser.2014.01.004

2.  Khan TMY, Atabani AE, Badruddin IA, Badarudin A, Khayoon MS, Triwahyono S. Recent scenario and technologies to utilize non-edible oils for biodiesel production. *Renew Sustain Energy Rev*. Published online 2014. doi:10.1016/j.rser.2014.05.064

3.  U.S. Energy Information Administration. *International Energy Outlook 2019*.; 2019. www.eia.gov/ieo

4.  Jagger A. Biofuels for transport in 2050. *Biofuels, Bioprod Biorefining*. 2011;5(5):481-485. doi:10.1002/bbb.330

5.  Morais RR, Pascoal AM, Pereira-Júnior MA, Batista KA, Rodriguez AG, Fernandes KF. Bioethanol production from Solanum lycocarpum starch: A sustainable non-food energy source for biofuels. *Renew Energy*. 2019;140:361-366. doi:https://doi.org/10.1016/j.renene.2019.02.056

6.  Thanapimmetha A, Saisriyoot M, Khomlaem C, Chisti Y, Srinophakun P. A comparison of methods of ethanol production from sweet sorghum bagasse. *Biochem Eng J*. 2019;151:107352. doi:https://doi.org/10.1016/j.bej.2019.107352

7.  Kiatkittipong W, Thipsunet P, Goto S, Chaisuk C, Praserthdam P, Assabumrungrat S. Simultaneous enhancement of ethanol supplement in gasoline and its quality improvement. *Fuel Process Technol*. 2008;89(12):1365-1370. doi:https://doi.org/10.1016/j.fuproc.2008.06.007

8.  European Technology and Innovation Platform Bio energy. ETBE. Accessed May 10, 2020. https://www.etipbioenergy.eu/value-chains/products-end-use/products/etbe

9.  Shrivastava P, Verma TN, Pugazhendhi A. An experimental evaluation of engine performance and emisssion characteristics of CI engine operated with Roselle and Karanja biodiesel. *Fuel*. 2019;254:115652. doi:https://doi.org/10.1016/j.fuel.2019.115652

10. Zhao S, Niu S, Yu H, et al. Experimental investigation on biodiesel production through transesterification promoted by the La-dolomite catalyst. *Fuel*. 2019;257:116092. doi:https://doi.org/10.1016/j.fuel.2019.116092

11. Al-Mashhadani HAM, Capareda SC, Lacey RE, Fernando SD. Catalytic valorization of glycerol for producing biodiesel-compatible biofuel blends. *Biofuels*. 2020;11(5):621-635. doi:10.1080/17597269.2017.1387746

12. Malaika A, Kozłowski M. Glycerol conversion towards valuable fuel blending compounds with the assistance of SO3H-functionalized carbon xerogels and spheres. *Fuel Process Technol*. 2019;184:19-26. doi:https://doi.org/10.1016/j.fuproc.2018.11.006

13. Kiatkittipong W, Phimsen S, Kiatkittipong K, Wongsakulphasatch S, Laosiripojana N, Assabumrungrat S. Diesel-like hydrocarbon production from hydroprocessing of relevant refining palm oil. *Fuel Process Technol*. 2013;116:16-26. doi:https://doi.org/10.1016/j.fuproc.2013.04.018

14. Stöcker M, Tschentscher R. Biomass to Liquid Biofuels via Heterogeneous Catalysis. In: *Fuel Production with Heterogeneous Catalysis*. CRC Press; 2014:213-252. doi:doi:10.1201/b17552-9

15. Arun N, Sharma R V., Dalai AK. Green diesel synthesis by hydrodeoxygenation of bio-based feedstocks: Strategies for catalyst design and development. *Renew Sustain Energy Rev*. Published online 2015. doi:10.1016/j.rser.2015.03.074

16. Pinto F, Varela FT, Gonçalves M, Neto André R, Costa P, Mendes B. Production of bio-hydrocarbons by hydrotreating of pomace oil. *Fuel*. 2014;116:84-93. doi:10.1016/j.fuel.2013.07.116

17. Bai X, Duan P, Xu Y, Zhang A, Savage PE. Hydrothermal catalytic processing of pretreated algal oil: A catalyst screening study. *Fuel*. 2014;120:141-149. doi:10.1016/j.fuel.2013.12.012

18. Tan XB, Lam MK, Uemura Y, Lim JW, Wong CY, Lee KT. Cultivation of microalgae for biodiesel production: A review on upstream and downstream processing. *Chinese J Chem Eng*. 2018;26(1):17-30. doi:https://doi.org/10.1016/j.cjche.2017.08.010

19. Zhao C, Brück T, Lercher JA. Catalytic deoxygenation of microalgae oil to green hydrocarbons. *Green Chem*. 2013;15(7):1720-1739. doi:10.1039/c3gc40558c

20. Guo Y, Yeh T, Song W, Xu D, Wang S. A review of bio-oil production from hydrothermal liquefaction of algae. *Renew Sustain Energy Rev*. 2015;48:776-790. doi:10.1016/j.rser.2015.04.049

21. Khoo CG, Dasan YK, Lam MK, Lee KT. Algae biorefinery: Review on a broad spectrum of downstream processes and products. *Bioresour Technol*. 2019;292:121964. doi:https://doi.org/10.1016/j.biortech.2019.121964

22. Thangalazhy-Gopakumar S, Adhikari S, Gupta RB, Tu M, Taylor S. Production of hydrocarbon fuels from biomass using catalytic pyrolysis under helium and hydrogen environments. *Bioresour Technol*. Published online 2011. doi:10.1016/j.biortech.2011.03.104

23. Widayatno WB, Guan G, Rizkiana J, et al. Upgrading of bio-oil from biomass pyrolysis over Cu-modified β-zeolite catalyst with high selectivity and stability. *Appl Catal B Environ*. Published online 2016. doi:10.1016/j.apcatb.2016.01.006

24. Sotelo-Boyas R, Trejo-Zarraga F, Jesus Hernandez-Loyo F de. Hydroconversion of Triglycerides into Green Liquid Fuels. *Hydrogenation*. Published online 2012. doi:10.5772/48710

25. Phimsen S, Kiatkittipong W, Yamada H, et al. Oil extracted from spent coffee grounds for bio-hydrotreated diesel production. *Energy Convers Manag*. 2016;126:1028-1036. doi:https://doi.org/10.1016/j.enconman.2016.08.085

26. Biller P, Sharma BK, Kunwar B, Ross AB. Hydroprocessing of bio-crude from continuous hydrothermal liquefaction of microalgae. *Fuel*. 2015;159:197-205. doi:10.1016/j.fuel.2015.06.077

27. Albrecht KO, Zhu Y, Schmidt AJ, et al. Impact of heterotrophically stressed algae for biofuel production via hydrothermal liquefaction and catalytic hydrotreating in continuous-flow reactors. *Algal Res*. 2016;14:17-27. doi:10.1016/j.algal.2015.12.008

28. Elliott DC, Hart TR, Schmidt AJ, et al. Process development for hydrothermal liquefaction of algae feedstocks in a continuous-flow reactor. *Algal Res*. 2013;2(4):445-454. doi:10.1016/j.algal.2013.08.005

29.  Duan P, Bai X, Xu Y, et al. Catalytic upgrading of crude algal oil using platinum/gamma alumina in supercritical water. *Fuel*. 2013;109:225-233. doi:10.1016/j.fuel.2012.12.074

30.  He Z, Jiao Y, Wang J, Chen Y. Effects of M (Zr, Nb, Y) modifiers on the catalytic performance of Ni/Ce-Al2O3 bimetallic catalyst in steam reforming of n-decane. *J Anal Appl Pyrolysis*. 2016;122:142-150. doi:10.1016/j.jaap.2016.10.007

31.  Witsuthammakul A, Sooknoi T. Selective Hydrodeoxygenation of Bio-Oil Derived Products: Ketones to Olefins. *Catal Sci Technol*. 2015;5:3639-3648. doi:10.1039/C5CY00367A

32.  Snare M, Kubickova I, Maki-Arvela P, Eranen K, Murzin DY. Heterogeneous Catalytic Deoxygenation of Stearic Acid for Production of Biodiesel. *Ind Eng Chem Res*. 2006;45(16):5708-5715. doi:10.1021/ie060334i

33.  Shakya R, Adhikari S, Mahadevan R, Hassan EB, Dempster TA. Catalytic upgrading of bio-oil produced from hydrothermal liquefaction of Nannochloropsis sp. *Bioresour Technol*. 2018;252(November 2017):28-36. doi:10.1016/j.biortech.2017.12.067

34.  De S, Zhang J, Luque R, Yan N. Ni-based bimetallic heterogeneous catalysts for energy and environmental applications. *Energy Environ Sci*. 2016;9(11):3314-3347. doi:10.1039/C6EE02002J

35.  Ardiyanti AR, Bykova M V., Khromova SA, et al. Ni-Based Catalysts for the Hydrotreatment of Fast Pyrolysis Oil. *Energy and Fuels*. 2016;30(3):1544-1554. doi:10.1021/acs.energyfuels.5b02223

36.  Boscagli C, Yang C, Welle A, et al. Effect of pyrolysis oil components on the activity and selectivity of nickel-based catalysts during hydrotreatment. *Appl Catal A Gen*. 2017;544:161-172. doi:https://doi.org/10.1016/j.apcata.2017.07.025

37.  Khromova SA, Smirnov AA, Bulavchenko OA, et al. Anisole hydrodeoxygenation over Ni-Cu bimetallic catalysts: The effect of Ni/Cu ratio on selectivity. *Appl Catal A Gen*. 2014;470:261-270. doi:10.1016/j.apcata.2013.10.046

38.  Dongil AB, Bachiller-Baeza B, Rodríguez-Ramos I, Fierro JLG, Escalona N. The effect of Cu loading on Ni/carbon nanotubes catalysts for hydrodeoxygenation of guaiacol. *RSC Adv*. 2016;6(32):26658-26667. doi:10.1039/C6RA00041J

39.  Kraiem T, Hassen A Ben, Belayouni H, Jeguirim M. Production and characterization of bio-oil from the pyrolysis of waste frying oil. *Environ Sci Pollut Res*. 2017;24(11):9951-9961. doi:10.1007/s11356-016-7704-z

40.  Leiva K, Martinez N, Sepulveda C, et al. Hydrodeoxygenation of 2-methoxyphenol over different Re active phases supported on SiO2 catalysts. *Appl Catal A Gen*. 2015;490:71-79. doi:https://doi.org/10.1016/j.apcata.2014.10.054

41.  Thongkumkoon S, Kiatkittipong W, Hartley UW, Laosiripojana N, Daorattanachai P. Catalytic activity of trimetallic sulfided Re-Ni-Mo/γ-Al2O3 toward deoxygenation of palm feedstocks. *Renew Energy*. 2019;140:111-123. doi:https://doi.org/10.1016/j.renene.2019.03.039

42.  Ma L, Yan L, Lu A-H, Ding Y. Effects of Ni particle size on amination of

monoethanolamine over Ni-Re/SiO2 catalysts. *Chinese J Catal*. 2019;40(4):567-579. doi:https://doi.org/10.1016/S1872-2067(19)63302-4

43. Shakya R, Adhikari S, Mahadevan R, et al. Influence of biochemical composition during hydrothermal liquefaction of algae on product yields and fuel properties. *Bioresour Technol*. 2017;243:1112-1120. doi:10.1016/j.biortech.2017.07.046

44. Singh R, Prakash A, Balagurumurthy B, Bhaskar T. Chapter 10 - Hydrothermal Liquefaction of Biomass. In: Pandey A, Bhaskar T, Stöcker M, Sukumaran RKBT-RA in T-CC of B, eds. Elsevier; 2015:269-291. doi:https://doi.org/10.1016/B978-0-444-63289-0.00010-7

45. Gollakota ARK, Kishore N, Gu S. A review on hydrothermal liquefaction of biomass. *Renew Sustain Energy Rev*. 2018;81:1378-1392. doi:https://doi.org/10.1016/j.rser.2017.05.178

46. Elliott DC. 19 - Production of biofuels via bio-oil upgrading and refining. In: Luque R, Lin CSK, Wilson K, Clark JBT-H of BP (Second E, eds. Woodhead Publishing; 2016:595-613. doi:https://doi.org/10.1016/B978-0-08-100455-5.00019-9

47. Kim J-Y, Lee HW, Lee SM, Jae J, Park Y-K. Overview of the recent advances in lignocellulose liquefaction for producing biofuels, bio-based materials and chemicals. *Bioresour Technol*. 2019;279:373-384. doi:https://doi.org/10.1016/j.biortech.2019.01.055

48. Zhang Y. Hydrothermal Liquefaction to Convert Biomass into Crude Oil. *Biofuels from Agric Wastes Byprod*. Published online August 13, 2010:201-232. doi:doi:10.1002/9780813822716.ch10

49. Tran K-Q. Fast hydrothermal liquefaction for production of chemicals and biofuels from wet biomass – The need to develop a plug-flow reactor. *Bioresour Technol*. 2016;213:327-332. doi:https://doi.org/10.1016/j.biortech.2016.04.002

50. Toor SS, Rosendahl L, Rudolf A. Hydrothermal liquefaction of biomass: A review of subcritical water technologies. *Energy*. 2011;36(5):2328-2342. doi:https://doi.org/10.1016/j.energy.2011.03.013

51. Jensen CU, Rodriguez Guerrero JK, Karatzos S, Olofsson G, Iversen SB. Fundamentals of Hydrofaction™: Renewable crude oil from woody biomass. *Biomass Convers Biorefinery*. 2017;7(4):495-509. doi:10.1007/s13399-017-0248-8

52. Demirbaş A. Mechanisms of liquefaction and pyrolysis reactions of biomass. *Energy Convers Manag*. 2000;41(6):633-646. doi:https://doi.org/10.1016/S0196-8904(99)00130-2

53. Fang Z, Sato T, Smith RL, Inomata H, Arai K, Kozinski JA. Reaction chemistry and phase behavior of lignin in high-temperature and supercritical water. *Bioresour Technol*. 2008;99(9):3424-3430. doi:https://doi.org/10.1016/j.biortech.2007.08.008

54. Miguel GS, Makibar J. New Advances in the Fast Pyrolysis of Biomass New Advances in the Fast Pyrolysis of Biomass. *J Biobased Mater Bioenergy*. 2012;6(April 2012):193-203. doi:10.1166/jbmb.2012.1209

55. Dabros TMH, Stummann MZ, Høj M, et al. Transportation fuels from biomass fast pyrolysis, catalytic hydrodeoxygenation, and catalytic fast hydropyrolysis.

*Prog Energy Combust Sci.* 2018;68:268-309. doi:https://doi.org/10.1016/j.pecs.2018.05.002

56.  Jiang W, Kumar A, Adamopoulos S. Liquefaction of lignocellulosic materials and its applications in wood adhesives—A review. *Ind Crops Prod.* 2018;124:325-342. doi:https://doi.org/10.1016/j.indcrop.2018.07.053

57.  Huber GW, Iborra S, Corma A. Synthesis of transportation fuels from biomass: Chemistry, catalysts, and engineering. *Chem Rev.* 2006;106(9):4044-4098.

58.  Anouti S, Haarlemmer G, Déniel M, Roubaud A. Analysis of Physicochemical Properties of Bio-Oil from Hydrothermal Liquefaction of Blackcurrant Pomace. *Energy & Fuels.* 2016;30(1):398-406. doi:10.1021/acs.energyfuels.5b02264

59.  Şenol Oİ, Viljava T-R, Krause AOI. Hydrodeoxygenation of methyl esters on sulphided NiMo/γ-Al2O3 and CoMo/γ-Al2O3 catalysts. *Catal Today.* 2005;100(3-4):331-335. doi:10.1016/j.cattod.2004.10.021

60.  Kubička D, Kaluža L. Deoxygenation of vegetable oils over sulfided Ni, Mo and NiMo catalysts. *Appl Catal A Gen.* 2010;372(2):199-208. doi:10.1016/j.apcata.2009.10.034

61.  Snåre M, Kubičková I, Mäki-Arvela P, Eränen K, Wärnå J, Murzin DY. Production of diesel fuel from renewable feeds: Kinetics of ethyl stearate decarboxylation. *Chem Eng J.* 2007;134(1-3):29-34. doi:10.1016/j.cej.2007.03.064

62.  Laurent E, Delmon B. Study of the hydrodeoxygenation of carbonyl, carboxylic and guaiacyl groups over sulfided CoMo/[gamma]-Al2O3 and NiMo/[gamma]-Al2O3 catalysts: I. Catalytic reaction schemes. *Appl Catal A Gen.* 1994;109(1):77-96. doi:Doi 10.1016/0926-860x(94)85005-4

63.  Kim SK, Han JY, Lee H, Yum T, Kim Y, Kim J. Production of renewable diesel via catalytic deoxygenation of natural triglycerides: Comprehensive understanding of reaction intermediates and hydrocarbons. *Appl Energy.* 2014;116:199-205. doi:10.1016/j.apenergy.2013.11.062

64.  Huber GW, O'Connor P, Corma A. Processing biomass in conventional oil refineries: Production of high quality diesel by hydrotreating vegetable oils in heavy vacuum oil mixtures. *Appl Catal A Gen.* 2007;329:120-129.

65.  Kordulis C, Bourikas K, Gousi M, Kordouli E, Lycourghiotis A. Development of nickel based catalysts for the transformation of natural triglycerides and related compounds into green diesel: a critical review. *Appl Catal B Environ.* 2016;181:156-196. doi:10.1016/j.apcatb.2015.07.042

66.  Madsen AT, Ahmed EH, Christensen CH, Fehrmann R, Riisager A. Hydrodeoxygenation of waste fat for diesel production: Study on model feed with Pt/alumina catalyst. *Fuel.* 2011;90(11):3433-3438. doi:10.1016/j.fuel.2011.06.005

67.  Rozmysłowicz B, Mäki-Arvela P, Tokarev A, Leino A-R, Eränen K, Murzin DY. Influence of Hydrogen in Catalytic Deoxygenation of Fatty Acids and Their Derivatives over Pd/C. *Ind Eng Chem Res.* 2012;51(26):8922-8927. doi:10.1021/ie202421x

68.  Mäki-Arvela P, Snåre M, Eränen K, Myllyoja J, Murzin DY. Continuous decarboxylation of lauric acid over Pd/C catalyst. *Fuel.* 2008;87(17-18):3543-3549. doi:10.1016/j.fuel.2008.07.004

69. Piqueras CM, Fernández MB, Tonetto GM, Bottini S, Damiani DE. Hydrogenation of sunflower oil on Pd catalysts in supercritical conditions: Effect of the particle size. *Catal Commun*. 2006;7(6):344-347.

70. Simakova I, Simakova O, Mäki-Arvela P, Simakov A, Estrada M, Murzin DY. Deoxygenation of palmitic and stearic acid over supported Pd catalysts: Effect of metal dispersion. *Appl Catal A Gen*. 2009;355(1-2):100-108.

71. Yakovlev VA, Khromova SA, Sherstyuk OV, et al. Development of new catalytic systems for upgraded bio-fuels production from bio-crude-oil and biodiesel. *Catal Today*. 2009;144(3):362-366. doi:10.1016/j.cattod.2009.03.002

72. Morgan T, Santillan-Jimenez E, Harman-Ware AE, Ji Y, Grubb D, Crocker M. Catalytic deoxygenation of triglycerides to hydrocarbons over supported nickel catalysts. *Chem Eng J*. 2012;189-190:346-355.

73. Srifa A, Viriya-empikul N, Assabumrungrat S, Faungnawakij K. Catalytic behaviors of Ni/γ-Al2O3 and Co/γ-Al2O3 during the hydrodeoxygenation of palm oil. *Catal Sci Technol*. 2015;5(7):3693-. doi:10.1039/C5CY00425J

74. Srifa A, Faungnawakij K, Itthibenchapong V, Assabumrungrat S. Roles of monometallic catalysts in hydrodeoxygenation of palm oil to green diesel. *Chem Eng J*. 2015;278:249-258. doi:10.1016/j.cej.2014.09.106

75. Kubičková I, Snåre M, Eränen K, Mäki-Arvela P, Murzin DY. Hydrocarbons for diesel fuel via decarboxylation of vegetable oils. *Catal Today*. 2005;106(1-4):197-200.

76. Kubička D, Horáček J. Deactivation of HDS catalysts in deoxygenation of vegetable oils. *Appl Catal A Gen*. 2011;394(1-2):9-17.

77. Bernas H, Eränen K, Simakova I, et al. Deoxygenation of dodecanoic acid under inert atmosphere. *Fuel*. 2010;89(8):2033-2039. doi:10.1016/j.fuel.2009.11.006

78. Snåre M, Kubičková I, Mäki-Arvela P, Chichova D, Eränen K, Murzin DY. Catalytic deoxygenation of unsaturated renewable feedstocks for production of diesel fuel hydrocarbons. *Fuel*. 2008;87(6):933-945.

79. Ambursa MM, Ali TH, Lee HV, Sudarsanam P, Bhargava SK, Hamid SBA. Hydrodeoxygenation of dibenzofuran to bicyclic hydrocarbons using bimetallic Cu-Ni catalysts supported on metal oxides. *Fuel*. 2016;180:767-776. doi:10.1016/j.fuel.2016.04.045

80. Dickinson JG, Savage PE. Stability and activity of Pt and Ni catalysts for hydrodeoxygenation in supercritical water. *J Mol Catal A Chem*. 2014;388-389:56-65. doi:10.1016/j.molcata.2013.08.003

81. Veriansyah B, Han JY, Kim SK, et al. Production of renewable diesel by hydroprocessing of soybean oil: Effect of catalysts. *Fuel*. 2012;94:578-585.

82. Morgan T, Grubb D, Santillan-Jimenez E, Crocker M. Conversion of triglycerides to hydrocarbons over supported metal catalysts. *Top Catal*. 2010;53(11-12):820-829.

83. Santillan-Jimenez E, Morgan T, Lacny J, Mohapatra S, Crocker M. Catalytic deoxygenation of triglycerides and fatty acids to hydrocarbons over carbon-supported nickel. In: *Fuel*. Vol 103. ; 2013:1010-1017.

84. Peng B, Yao Y, Zhao C, Lercher JA. Towards quantitative conversion of microalgae oil to diesel-range alkanes with bifunctional catalysts. *Angew Chemie - Int Ed*. 2012;51(9):2072-2075. doi:10.1002/anie.201106243

85. Peng B, Yuan X, Zhao C, Lercher JA. Stabilizing catalytic pathways via redundancy: Selective reduction of microalgae oil to alkanes. *J Am Chem Soc*. 2012;134(22):9400-9405. doi:10.1021/ja302436q

86. Zuo H, Liu Q, Wang T, Ma L, Zhang Q, Zhang Q. Hydrodeoxygenation of methyl palmitate over supported ni catalysts for diesel-like fuel production. *Energy and Fuels*. 2012;26(6):3747-3755. doi:10.1021/ef300063b

87. Liu Q, Zuo H, Wang T, Ma L, Zhang Q. One-step hydrodeoxygenation of palm oil to isomerized hydrocarbon fuels over Ni supported on nano-sized SAPO-11 catalysts. *Appl Catal A Gen*. 2013;468:68-74. doi:10.1016/j.apcata.2013.08.009

88. Liu Q, Zuo H, Zhang Q, Wang T, Ma L. Hydrodeoxygenation of palm oil to hydrocarbon fuels over Ni/SAPO-11 catalysts. *Chinese J Catal*. 2014;35(5):748-756. doi:10.1016/S1872-2067(12)60710-4

89. Ochoa-Hernández C, Yang Y, Pizarro P, De La Peña O'Shea VA, Coronado JM, Serrano DP. Hydrocarbons production through hydrotreating of methyl esters over Ni and Co supported on SBA-15 and Al-SBA-15. *Catal Today*. 2013;210:81-88. doi:10.1016/j.cattod.2012.12.002

90. Sankaranarayanan TM, Berenguer A, Ochoa-Hernández C, et al. Hydrodeoxygenation of anisole as bio-oil model compound over supported Ni and Co catalysts: Effect of metal and support properties. *Catal Today*. 2015;243(C):163-172. doi:10.1016/j.cattod.2014.09.004

91. Yang Y, Ochoa-Hernández C, de la Peña O'Shea VA, Pizarro P, Coronado JM, Serrano DP. Effect of metal-support interaction on the selective hydrodeoxygenation of anisole to aromatics over Ni-based catalysts. *Appl Catal B Environ*. 2014;145:91-100. doi:10.1016/j.apcatb.2013.03.038

92. Wang C, Liu Q, Song J, et al. High quality diesel-range alkanes production via a single-step hydrotreatment of vegetable oil over Ni/zeolite catalyst. *Catal Today*. 2014;234:153-160. doi:10.1016/j.cattod.2014.02.011

93. Li T, Cheng J, Huang R, Zhou J, Cen K. Conversion of waste cooking oil to jet biofuel with nickel-based mesoporous zeolite Y catalyst. *Bioresour Technol*. 2015;197:289-294. doi:10.1016/j.biortech.2015.08.115

94. Li T, Cheng J, Huang R, Yang W, Zhou J, Cen K. Hydrocracking of palm oil to jet biofuel over different zeolites. *Int J Hydrogen Energy*. 2016;41(47):21883-21887. doi:10.1016/j.ijhydene.2016.09.013

95. Cheng J, Li T, Huang R, Zhou J, Cen K. Optimizing catalysis conditions to decrease aromatic hydrocarbons and increase alkanes for improving jet biofuel quality. *Bioresour Technol*. 2014;158:378-382. doi:10.1016/j.biortech.2014.02.112

96. Zhang X, Zhang Q, Wang T, Ma L, Yu Y, Chen L. Hydrodeoxygenation of lignin-derived phenolic compounds to hydrocarbons over Ni/SiO2-ZrO2 catalysts. *Bioresour Technol*. 2013;134:73-80. doi:10.1016/j.biortech.2013.02.039

97. Rana MS, Srinivas BN, Maity SK, Murali Dhar G, Prasada Rao TSR. Origin of Cracking Functionality of Sulfided (Ni) CoMo/SiO2–ZrO2 Catalysts. *J Catal*. 2000;195(1):31-37. doi:10.1006/jcat.2000.2968

98. Shu R, Xu Y, Ma L, Zhang Q, Chen P, Wang T. Synergistic effects of highly active Ni and acid site on the hydrodeoxygenation of syringol. *Catal Commun*. 2017;91:1-5. doi:10.1016/j.catcom.2016.12.006

99.    Kumar R, Yadav A, Agrawal A, et al. Synthesis of highly coke resistant Ni nanoparticles supported MgO / ZnO catalyst for reforming of methane with carbon dioxide. *Appl Catal B Environ*. 2016;191:165-178. doi:10.1016/j.apcatb.2016.03.029

100.   Selishcheva SA, Babushkin DE. Studies on the Direct Hydrocracking of Fatty Acid Triglycerides on Ni-Cu/CeO2-ZrO2 Catalyst. 2011;19:181-186.

101.   Loe R, Santillan-jimenez E, Morgan T, et al. Effect of Cu and Sn promotion on the catalytic deoxygenation of model and algal lipids to fuel-like hydrocarbons over supported Ni catalysts. *Appl Catal B Environ*. 2016;191:147-156. doi:10.1016/j.apcatb.2016.03.025

102.   Zhang X, Wang T, Ma L, Zhang Q, Yu Y, Liu Q. Characterization and catalytic properties of Ni and NiCu catalysts supported on ZrO2–SiO2 for guaiacol hydrodeoxygenation. 2013;33:15-19. doi:10.1016/j.catcom.2012.12.011

103.   Bykova M V, Ermakov DY, Khromova SA, Smirnov AA, Lebedev MY, Yakovlev VA. Stabilized Ni-based catalysts for bio-oil hydrotreatment : Reactivity studies using guaiacol. *Catal Today*. 2014;220-222:21-31. doi:10.1016/j.cattod.2013.10.023

104.   Bykova M V, Ermakov DY, Kaichev V V, et al. Ni-based sol–gel catalysts as promising systems for crude bio-oil upgrading : Guaiacol hydrodeoxygenation study. *Appl Catal B Environ*. 2012;113-114:296-307. doi:10.1016/j.apcatb.2011.11.051

105.   Guo Q, Wu M, Wang K, Zhang L, Xu X. Catalytic Hydrodeoxygenation of Algae Bio-oil over Bimetallic Ni−Cu/ZrO2 Catalysts. *Ind Eng Chem Res*. Published online 2015. doi:10.1021/ie5042935

106.   Ardiyanti AR, Khromova SA, Venderbosch RH, Yakovlev VA, Heeres HJ. Catalytic hydrotreatment of fast-pyrolysis oil using non-sulfided bimetallic Ni-Cu catalysts on a δ-Al2O3 support.pdf. *Appl Catal B Environ*. 2012;117-118:105-117.

107.   Ardiyanti AR, Khromova SA, Venderbosch RH, Yakovlev VA, Melián-cabrera I V. Catalytic hydrotreatment of fast pyrolysis oil using bimetallic Ni – Cu catalysts on various supports. *Appl Catal A Gen*. 2012;449:121-130. doi:10.1016/j.apcata.2012.09.016

108.   Kathiraser Y, Ashok J, Kawi S. Synthesis and evaluation of highly dispersed SBA- 15 supported Ni–Fe bimetallic catalysts for steam reforming of biomass derived tar reaction†. *Catal Sci Technol*. 2016;6:4327-4336. doi:10.1039/C5CY01910A

109.   Kandel K, Anderegg JW, Nelson NC, Chaudhary U, Slowing II. Supported iron nanoparticles for the hydrodeoxygenation of microalgal oil to green diesel. *J Catal*. 2014;314:142-148. doi:10.1016/j.jcat.2014.04.009

110.   Leng S, Wang X, He X, et al. NiFe/γ-Al2O3: A universal catalyst for the hydrodeoxygenation of bio-oil and its model compounds. *Catal Commun*. Published online 2013. doi:10.1016/j.catcom.2013.06.037

111.   Fang H, Zheng J, Luo X, et al. Product tunable behavior of carbon nanotubes-supported Ni–Fe catalysts for guaiacol hydrodeoxygenation. *Appl Catal A Gen*. 2017;529:20-31. doi:10.1016/j.apcata.2016.10.011

112.   Shafaghat H, Rezaei PS, Daud WMAW. Catalytic hydrodeoxygenation of

simulated phenolic bio-oil to cycloalkanes and aromatic hydrocarbons over bifunctional metal/acid catalysts of Ni/HBeta, Fe/HBeta and NiFe/HBeta. *J Ind Eng Chem*. 2016;35:268-276. doi:10.1016/j.jiec.2016.01.001

113. Seridi F, Chettibi S, Keghouche N, Beaunier P, Belloni J. Structural study of radiolytic catalysts Ni-Ce/Al2O3 and Ni-Pt/Al2O3. *Radiat Phys Chem*. 2017;130:76-84. doi:10.1016/j.radphyschem.2016.07.029

114. Lu S, Lonergan WW, Bosco JP, et al. Low temperature hydrogenation of benzene and cyclohexene: A comparative study between γ-Al2O3 supported PtCo and PtNi bimetallic catalysts. *J Catal*. 2008;259(2):260-268. doi:10.1016/j.jcat.2008.08.016

115. Lonergan WW, Vlachos DG, Chen JG. Correlating extent of Pt–Ni bond formation with low-temperature hydrogenation of benzene and 1,3-butadiene over supported Pt/Ni bimetallic catalysts. *J Catal*. 2010;271(2):239-250. doi:10.1016/j.jcat.2010.01.019

116. Fan C, Zhu Y-A, Xu Y, Zhou Y, Zhou X-G, Chen D. Origin of synergistic effect over Ni-based bimetallic surfaces: A density functional theory study. *J Chem Phys*. 2012;137(1):14703. doi:10.1063/1.4731811

117. Niu J, Ran J, Du X, Qi W, Zhang P, Yang L. Effect of Pt addition on resistance to carbon formation of Ni catalysts in methane dehydrogenation over Ni-Pt bimetallic surfaces: A density functional theory study. *Mol Catal*. 2017;434:206-218. doi:http://doi.org/10.1016/j.mcat.2017.03.015

118. Feng B, Kobayashi H, Ohta H, Fukuoka A. Aqueous-phase hydrodeoxygenation of 4-propylphenol as a lignin model to n-propylbenzene over Re-Ni/ZrO2catalysts. *J Mol Catal A Chem*. 2014;388-389:41-46. doi:10.1016/j.molcata.2013.09.025

119. Yang F, Liu D, Wang H, et al. Geometric and electronic effects of bimetallic Ni – Re catalysts for selective deoxygenation of m-cresol to toluene. *J Catal*. 2017;349:84-97. doi:10.1016/j.jcat.2017.01.001

120. Hachemi I, Jeništová K, Mäki-Arvela P, et al. Comparative study of sulfur-free nickel and palladium catalysts in hydrodeoxygenation of different fatty acid feedstocks for production of biofuels. *Catal Sci Technol*. 2016;6(5):1476-1487. doi:10.1039/C5CY01294E

121. Kukushkin RG, Bulavchenko OA, Kaichev V V., Yakovlev VA. Influence of Mo on catalytic activity of Ni-based catalysts in hydrodeoxygenation of esters. *Appl Catal B Environ*. 2015;163:531-538. doi:10.1016/j.apcatb.2014.08.001

122. Suelves I, Lázaro MJ, Moliner R, Echegoyen Y, Palacios JM. Characterization of NiAl and NiCuAl catalysts prepared by different methods for hydrogen production by thermo catalytic decomposition of methane. *Catal Today*. 2006;116(3):271-280. doi:https://doi.org/10.1016/j.cattod.2006.05.071

123. Cychosz KA, Thommes M. Progress in the Physisorption Characterization of Nanoporous Gas Storage Materials. *Engineering*. 2018;4(4):559-566. doi:https://doi.org/10.1016/j.eng.2018.06.001

124. Cychosz KA, Guillet-Nicolas R, García-Martínez J, Thommes M. Recent advances in the textural characterization of hierarchically structured nanoporous materials. *Chem Soc Rev*. 2017;46(2):389-414. doi:10.1039/C6CS00391E

125. Dankeaw A, Gualandris F, Silva RH, et al. Amorphous saturated cerium–

tungsten–titanium oxide nanofiber catalysts for NOx selective catalytic reaction. *New J Chem*. 2018;42(12):9501-9509. doi:10.1039/C8NJ00752G

126. Ma L, Yan L, Lu A-H, Ding Y. Effect of Re promoter on the structure and catalytic performance of Ni–Re/Al2O3 catalysts for the reductive amination of monoethanolamine. *RSC Adv*. 2018;8(15):8152-8163. doi:10.1039/C7RA12891F

127. Benítez-Guerrero M, Pérez-Maqueda LA, Sánchez-Jiménez PE, Pascual-Cosp J. Characterization of thermally stable gamma alumina fibres biomimicking sisal. *Microporous Mesoporous Mater*. 2014;185:167-178. doi:https://doi.org/10.1016/j.micromeso.2013.11.012

128. Adamowska MB, Costa P Da. Structured Pd/γ-Al2O3 Prepared by Washcoated Deposition on a Ceramic Honeycomb for Compressed Natural Gas Applications. *J Nanoparticles*. 2014;2015:10-12. doi:http://dx.doi.org/10.1155/2015/601941

129. Ardiyanti AR, Khromova SA, Venderbosch RH, Yakovlev VA, Heeres HJ. Catalytic hydrotreatment of fast-pyrolysis oil using non-sulfided bimetallic Ni-Cu catalysts on a δ-Al2O3 support. *Appl Catal B Environ*. 2012;117-118:105-117. doi:https://doi.org/10.1016/j.apcatb.2011.12.032

130. Pudi SM, Biswas P, Kumar S, Sarkar B. Selective hydrogenolysis of glycerol to 1,2-propanediol over bimetallic Cu-Ni catalysts supported on γ-Al2O3. *J Braz Chem Soc*. 2015;26(8):1551-1564. doi:10.5935/0103-5053.20150123

131. Ghampson IT, Sepúlveda C, Dongil AB, et al. Phenol hydrodeoxygenation: effect of support and Re promoter on the reactivity of Co catalysts. *Catal Sci Technol*. 2016;6(19):7289-7306. doi:10.1039/C6CY01038E

132. Gurdeep Singh HK, Yusup S, Quitain AT, et al. Biogasoline production from linoleic acid via catalytic cracking over nickel and copper-doped ZSM-5 catalysts. *Environ Res*. 2020;186:109616. doi:https://doi.org/10.1016/j.envres.2020.109616

133. Furimsky E. Chemistry of Catalytic Hydrodeoxygenation. *Catal Rev*. 1983;25(3):421-458. doi:10.1080/01614948308078052

134. Kadarwati S, Hu X, Gunawan R, et al. Coke formation during the hydrotreatment of bio-oil using NiMo and CoMo catalysts. *Fuel Process Technol*. 2017;155:261-268. doi:10.1016/j.fuproc.2016.08.021

135. Miao C, Marin-Flores O, Dong T, et al. Hydrothermal Catalytic Deoxygenation of Fatty Acid and Bio-oil with In Situ H2. *ACS Sustain Chem Eng*. 2018;6(4):4521-4530. doi:10.1021/acssuschemeng.7b02226

136. Srifa A, Faungnawakij K, Itthibenchapong V, Assabumrungrat S. Roles of monometallic catalysts in hydrodeoxygenation of palm oil to green diesel. *Chem Eng J*. 2015;278:249-258. doi:10.1016/j.cej.2014.09.106

137. Sitthisa S, Resasco DE. Hydrodeoxygenation of Furfural Over Supported Metal Catalysts: A Comparative Study of Cu, Pd and Ni. *Catal Letters*. 2011;141(6):784-791. doi:10.1007/s10562-011-0581-7

138. Croce A, Battistel E, Chiaberge S, Spera S, De Angelis F, Reale S. A Model Study to Unravel the Complexity of Bio-Oil from Organic Wastes. *ChemSusChem*. 2017;10(1):171-181. doi:10.1002/cssc.201601258

139. Miao X, Wu Q, Yang C. Fast pyrolysis of microalgae to produce renewable fuels. *J Anal Appl Pyrolysis*. 2004;71(2):855-863.

doi:https://doi.org/10.1016/j.jaap.2003.11.004

140. Nam H, Kim C, Capareda SC, Adhikari S. Catalytic upgrading of fractionated microalgae bio-oil (Nannochloropsis oculata) using a noble metal (Pd/C) catalyst. *Algal Res*. 2017;24:188-198. doi:10.1016/j.algal.2017.03.021

141. Wang Z, Adhikari S, Valdez P, Shakya R, Laird C. Upgrading of hydrothermal liquefaction biocrude from algae grown in municipal wastewater. *Fuel Process Technol*. 2016;142:147-156. doi:10.1016/j.fuproc.2015.10.015

142. Alleman TL, McCormick RL, Christensen ED, Fioroni G, Moriarty K, Yanowitz J. *Biodiesel Handling and Use Guide*.; 2016. doi:10.2172/938562

143. Furimsky E. Catalytic hydrodeoxygenation. *Appl Catal A Gen*. 2000;199(2):147-190. doi:10.1016/S0926-860X(99)00555-4

144. Patel B, Arcelus-Arrillaga P, Izadpanah A, Hellgardt K. Catalytic Hydrotreatment of algal biocrude from fast Hydrothermal Liquefaction. *Renew Energy*. 2017;101:1094-1101. doi:10.1016/j.renene.2016.09.056

145. Duan P, Savage PE. Catalytic hydrotreatment of crude algal bio-oil in supercritical water. *Appl Catal B Environ*. 2011;104(1-2):136-143. doi:10.1016/j.apcatb.2011.02.020

146. Duan P, Wang B, Xu Y. Catalytic hydrothermal upgrading of crude bio-oils produced from different thermo-chemical conversion routes of microalgae. *Bioresour Technol*. 2015;186:58-66. doi:10.1016/j.biortech.2015.03.050

147. Holladay J. *Liquefaction Technologies for Producing Biocrude for Jet, Diesel and Gasoline*.; 2014.

148. Yu J, Biller P, Mamahkel A, et al. Catalytic hydrotreatment of bio-crude produced from the hydrothermal liquefaction of aspen wood: a catalyst screening and parameter optimization study. *Sustain Energy Fuels*. 2017;1(4):832-841. doi:10.1039/C7SE00090A

149. Albrecht KO, Zhu Y, Schmidt AJ, et al. Impact of heterotrophically stressed algae for biofuel production via hydrothermal liquefaction and catalytic hydrotreating in continuous-flow reactors. *Algal Res*. 2016;14:17-27. doi:https://doi.org/10.1016/j.algal.2015.12.008

150. Xu D, Guo S, Liu L, et al. Ni-Ru/CeO2 Catalytic Hydrothermal Upgrading of Water-Insoluble Biocrude from Algae Hydrothermal Liquefaction. *Biomed Res Int*. 2018;2018. doi:10.1155/2018/8376127

151. Li H, Hu J, Zhang Z, et al. Insight into the effect of hydrogenation on efficiency of hydrothermal liquefaction and physico-chemical properties of biocrude oil. *Bioresour Technol*. 2014;163:143-151. doi:https://doi.org/10.1016/j.biortech.2014.04.015

152. Mayers JJ, Flynn KJ, Shields RJ. Rapid determination of bulk microalgal biochemical composition by Fourier-Transform Infrared spectroscopy. *Bioresour Technol*. 2013;148:215-220. doi:https://doi.org/10.1016/j.biortech.2013.08.133

153. Viêgas CV, Hachemi I, Freitas SP, et al. A route to produce renewable diesel from algae: Synthesis and characterization of biodiesel via in situ transesterification of Chlorella alga and its catalytic deoxygenation to renewable diesel. *Fuel*. 2015;155:144-154. doi:https://doi.org/10.1016/j.fuel.2015.03.064

154. Kraiem T, Hassen A Ben, Belayouni H, Jeguirim M. Production and

characterization of bio-oil from the pyrolysis of waste frying oil. *Environ Sci Pollut Res*. 2017;24(11):9951-9961. doi:10.1007/s11356-016-7704-z

155.  Aboulkas A, Hammani H, El Achaby M, Bilal E, Barakat A, El harfi K. Valorization of algal waste via pyrolysis in a fixed-bed reactor: Production and characterization of bio-oil and bio-char. *Bioresour Technol*. 2017;243:400-408. doi:https://doi.org/10.1016/j.biortech.2017.06.098

156.  Sun J, Yang J, Shi M. Review of Denitrogenation of Algae Biocrude Produced by Hydrothermal Liquefaction. *Trans Tianjin Univ*. 2017;23(4):301-314. doi:10.1007/s12209-017-0051-4

157.  Zhou L, Lin W, Liu K, et al. Hydrodeoxygenation of ethyl stearate over Re-promoted Ru/TiO2 catalysts: rate enhancement and selectivity control by the addition of Re. *Catal Sci Technol*. 2020;10(1):222-230. doi:10.1039/C9CY01909J

158.  Tomishige K, Nakagawa Y, Tamura M. Selective hydrogenolysis and hydrogenation using metal catalysts directly modified with metal oxide species. *Green Chem*. 2017;19(13):2876-2924. doi:10.1039/C7GC00620A

159.  Said A, Da Silva Perez D, Perret N, Pinel C, Besson M. Selective C−O Hydrogenolysis of Erythritol over Supported Rh-ReOx Catalysts in the Aqueous Phase. *ChemCatChem*. 2017;9(14):2768-2783. doi:10.1002/cctc.201700260

160.  Ma L, Sun K, Luo M, et al. Role of ReOx Species in Ni-Re/Al2O3 Catalyst for Amination of Monoethanolamine. *J Phys Chem C*. 2018;122(40):23011-23025. doi:10.1021/acs.jpcc.8b06748

161.  Zhu M, Ge Q, Zhu X. Catalytic Reduction of CO2 to CO via Reverse Water Gas Shift Reaction: Recent Advances in the Design of Active and Selective Supported Metal Catalysts. *Trans Tianjin Univ*. 2020;26(3):172-187. doi:10.1007/s12209-020-00246-8

162.  Houston R, Labbé N, Hayes D, Daw CS, Abdoulmoumine N. Intermediate temperature water–gas shift kinetics for hydrogen production. *React Chem Eng*. 2019;4(10):1814-1822. doi:10.1039/C9RE00121B

163.  Chia M, Pagán-Torres YJ, Hibbitts D, et al. Selective Hydrogenolysis of Polyols and Cyclic Ethers over Bifunctional Surface Sites on Rhodium–Rhenium Catalysts. *J Am Chem Soc*. 2011;133(32):12675-12689. doi:10.1021/ja2038358

164.  Ciftci A, Ligthart DAJM, Hensen EJM. Aqueous phase reforming of glycerol over Re-promoted Pt and Rh catalysts. *Green Chem*. 2014;16(2):853-863. doi:10.1039/C3GC42046A

165.  Smith AM, Whyman R. Review of Methods for the Catalytic Hydrogenation of Carboxamides. *Chem Rev*. 2014;114(10):5477-5510. doi:10.1021/cr400609m

166.  Ouellette RJ, Rawn JD. 22 - Carboxylic Acid Derivatives. In: Ouellette RJ, Rawn JD, eds. *Organic Chemistry Second Edition*. Academic Press; 2018:665-710. doi:https://doi.org/10.1016/B978-0-12-812838-1.50022-0

167.  Beamson G, Papworth AJ, Philipps C, Smith AM, Whyman R. Selective Hydrogenation of Amides using Ruthenium/ Molybdenum Catalysts. *Adv Synth Catal*. 2010;352(5):869-883. doi:10.1002/adsc.200900824

168.  Wang Y, Furukawa S, Zhang Z, Torrente-Murciano L, Khan SA, Yan N. Oxidant free conversion of alcohols to nitriles over Ni-based catalysts. *Catal*

*Sci Technol*. 2019;9(1):86-96. doi:10.1039/C8CY01799A

169. Shimizu K, Kon K, Onodera W, Yamazaki H, Kondo JN. Heterogeneous Ni Catalyst for Direct Synthesis of Primary Amines from Alcohols and Ammonia. *ACS Catal*. 2013;3(1):112-117. doi:10.1021/cs3007473

170. Liu M, Shi Y, Wu K, et al. Upgrading of palmitic acid and hexadecanamide over Co-based catalysts: Effect of support (SiO2, γ-Al2O3 and H-ZSM-22). *Catal Commun*. 2019;129:105726. doi:https://doi.org/10.1016/j.catcom.2019.105726

171. Peroni M, Lee I, Huang X, Baráth E, Gutiérrez OY, Lercher JA. Deoxygenation of Palmitic Acid on Unsupported Transition-Metal Phosphides. *ACS Catal*. 2017;7(9):6331-6341. doi:10.1021/acscatal.7b01294

172. Bie Y, Lehtonen J, Kanervo J. Hydrodeoxygenation (HDO) of methyl palmitate over bifunctional Rh/ZrO2 catalyst: Insights into reaction mechanism via kinetic modeling. *Appl Catal A Gen*. 2016;526:183-190. doi:https://doi.org/10.1016/j.apcata.2016.08.030

173. Scott PT, Pregelj L, Chen N, Hadler JS, Djordjevic MA, Gresshoff PM. Pongamia pinnata: An Untapped Resource for the Biofuels Industry of the Future. *BioEnergy Res*. 2008;1(1):2-11. doi:10.1007/s12155-008-9003-0

174. Panpraneecharoen S, Punsuvon V. Biodiesel from crude Pongamia pinnata oil under subcritical methanol conditions with calcium methoxide catalyst. *Energy Sources, Part A Recover Util Environ Eff*. 2016;38(15):2225-2230. doi:10.1080/15567036.2015.1038669

175. Loe R, Santillan-Jimenez E, Morgan T, et al. Effect of Cu and Sn promotion on the catalytic deoxygenation of model and algal lipids to fuel-like hydrocarbons over supported Ni catalysts. *Appl Catal B Environ*. 2016;191:147-156. doi:10.1016/j.apcatb.2016.03.025

176. Zhang H, Lin H, Zheng Y. The role of cobalt and nickel in deoxygenation of vegetable oils. *Appl Catal B Environ*. 2014;160-161(1):415-422. doi:10.1016/j.apcatb.2014.05.043

177. Cheephat C, Daorattanachai P, Devahastin S, Laosiripojana N. Partial oxidation of methane over monometallic and bimetallic Ni-, Rh-, Re-based catalysts: Effects of Re addition, co-fed reactants and catalyst support. *Appl Catal A Gen*. 2018;563:1-8. doi:https://doi.org/10.1016/j.apcata.2018.06.032

178. Hossain MZ, Chowdhury MBI, Jhawar AK, Xu WZ, Biesinger MC, Charpentier PA. Continuous Hydrothermal Decarboxylation of Fatty Acids and Their Derivatives into Liquid Hydrocarbons Using Mo/Al2O3 Catalyst. *ACS Omega*. 2018;3(6):7046-7060. doi:10.1021/acsomega.8b00562

179. Wu Y, Gui W, Liu X, et al. Promotional Effect of Cu for Catalytic Amination of Diethylene Glycol with Tertiarybutylamine over Ni–Cu/Al2O3 Catalysts. *Catal Letters*. 2020;150(8):2427-2436. doi:10.1007/s10562-020-03145-8

180. Dankeaw A, Gualandris F, Silva RH, et al. Highly porous Ce–W–TiO2 free-standing electrospun catalytic membranes for efficient de-NOxvia ammonia selective catalytic reduction. *Environ Sci Nano*. 2019;6(1):94-104. doi:10.1039/C8EN01046C

181. Dankeaw A, Gualandris F, Silva RH, et al. Amorphous saturated cerium–tungsten–titanium oxide nanofiber catalysts for NOx selective catalytic reaction. *New J Chem*. 2018;42(12):9501-9509. doi:10.1039/C8NJ00752G

182. Chang-jun L, Jingyun Y, Jiaojun J, Yunxiang P. Progresses in the Preparation of Coke Resistant Ni-based Catalyst for Steam and CO2 Reforming of Methane. *ChemCatChem*. 2011;3(3):529-541. doi:10.1002/cctc.201000358

183. Xu L, Song H, Chou L. Mesoporous nanocrystalline ceria-zirconia solid solutions supported nickel based catalysts for CO2reforming of CH4. *Int J Hydrogen Energy*. 2012;37(23):18001-18020. doi:10.1016/j.ijhydene.2012.09.128

184. Srifa A, Viriya-empikul N, Assabumrungrat S, Faungnawakij K. Catalytic behaviors of Ni/γ-Al2O3 and Co/γ-Al2O3 during the hydrodeoxygenation of palm oil. *Catal Sci Technol*. 2015;5(7):3693-3705. doi:10.1039/C5CY00425J

185. Cheng S, Wei L, Zhao X, Julson J. Application, Deactivation, and Regeneration of Heterogeneous Catalysts in Bio-Oil Upgrading. *Catalysts*. 2016;6(12):195. doi:10.3390/catal6120195

186. Hita I, Cordero-Lanzac T, Bonura G, Frusteri F, Bilbao J, Castaño P. Dynamics of carbon formation during the catalytic hydrodeoxygenation of raw bio-oil. *Sustain Energy Fuels*. Published online 2020. doi:10.1039/D0SE00501K

187. Zhang X, Wang T, Ma L, Zhang Q, Yu Y, Liu Q. Characterization and catalytic properties of Ni and NiCu catalysts supported on ZrO2–SiO2 for guaiacol hydrodeoxygenation. *Catal Commun*. 2013;33:15-19. doi:https://doi.org/10.1016/j.catcom.2012.12.011

188. Karnjanakom S, Bayu A, Hao X, et al. Selectively catalytic upgrading of bio-oil to aromatic hydrocarbons over Zn, Ce or Ni-doped mesoporous rod-like alumina catalysts. *J Mol Catal A Chem*. Published online 2016. doi:10.1016/j.molcata.2016.06.001

189. Argyle MD, Bartholomew CH. Heterogeneous Catalyst Deactivation and Regeneration: A Review. *Catalysts*. 2015;5(1):145-269. doi:10.3390/catal5010145

190. Dadyburjor DB, Liu Z, Matoba S, Osanai S, Shiro-oka T. Accelerated tests of catalyst coking: What do they tell us? In: Delmon B, Froment GFBT-S in SS and C, eds. *Catalyst Deactivation 1994*. Vol 88. Elsevier; 1994:273-280. doi:https://doi.org/10.1016/S0167-2991(08)62750-0

191. Tanaka Y, Shimada H, Matsubayashi N, Nishijima A, Nomura M. Accelerated deactivation of hydrotreating catalysts: comparison to long-term deactivation in a commercial plant. *Catal Today*. 1998;45(1):319-325. doi:https://doi.org/10.1016/S0920-5861(98)00239-9

192. Cordero-Lanzac T, Palos R, Hita I, et al. Revealing the pathways of catalyst deactivation by coke during the hydrodeoxygenation of raw bio-oil. *Appl Catal B Environ*. 2018;239:513-524. doi:https://doi.org/10.1016/j.apcatb.2018.07.073

193. Wong KS, Vazhnova T, Rigby SP, Lukyanov DB. Temperature effects in benzene alkylation with ethane into ethylbenzene over a PtH-MFI bifunctional catalyst. *Appl Catal A Gen*. 2013;454:137-144. doi:https://doi.org/10.1016/j.apcata.2013.01.012

194. Zhang H, Shao S, Xiao R, Shen D, Zeng J. Characterization of Coke Deposition in the Catalytic Fast Pyrolysis of Biomass Derivates. *Energy & Fuels*. 2014;28(1):52-57. doi:10.1021/ef401458y

195. Moon C, Sung Y, Ahn S, Kim T, Choi G, Kim D. Thermochemical and combustion behaviors of coals of different ranks and their blends for

pulverized-coal combustion. *Appl Therm Eng*. 2013;54(1):111-119. doi:https://doi.org/10.1016/j.applthermaleng.2013.01.009

196. Cao Y, Maitarad P, Gao M, et al. Defect-induced efficient dry reforming of methane over two-dimensional Ni/h-boron nitride nanosheet catalysts. *Appl Catal B Environ*. 2018;238:51-60. doi:https://doi.org/10.1016/j.apcatb.2018.07.001

197. Nataj SMM, Alavi SM, Mazloom G. Modeling and optimization of methane dry reforming over Ni–Cu/Al2O3 catalyst using Box–Behnken design. *J Energy Chem*. 2018;27(5):1475-1488. doi:https://doi.org/10.1016/j.jechem.2017.10.002

198. Botas JA, Serrano DP, García A, de Vicente J, Ramos R. Catalytic conversion of rapeseed oil into raw chemicals and fuels over Ni- and Mo-modified nanocrystalline ZSM-5 zeolite. *Catal Today*. 2012;195(1):59-70. doi:https://doi.org/10.1016/j.cattod.2012.04.061

199. Prasongthum N, Chaiya C, Samart C, Guan G, Natewong P, Reubroycharoen P. Co-production of hydrogen and carbon nanotube-silica fiber composites from ethanol steam reforming over an Ni-silica fiber catalyst. *Monatshefte für Chemie - Chem Mon*. 2017;148(7):1311-1321. doi:10.1007/s00706-017-1989-6

200. Gabbott P. A Practical Introduction to Differential Scanning Calorimetry. *Princ Appl Therm Anal*. Published online January 1, 2008:1-50. doi:doi:10.1002/9780470697702.ch1

201. Hermida L, Abdullah AZ, Mohamed AR. Deoxygenation of fatty acid to produce diesel-like hydrocarbons: A review of process conditions, reaction kinetics and mechanism. *Renew Sustain Energy Rev*. Published online 2015. doi:10.1016/j.rser.2014.10.099

202. Mäki-Arvela P, Rozmysłowicz B, Lestari S, et al. Catalytic Deoxygenation of Tall Oil Fatty Acid over Palladium Supported on Mesoporous Carbon. *Energy & Fuels*. 2011;25(7):2815-2825. doi:10.1021/ef200380w

203. Madsen AT, Rozmys B, Simakova IL, Kilpi T, Er K, Murzin DY. Step Changes and Deactivation Behavior in the Continuous Decarboxylation of Stearic Acid. *Ind Eng Chem Res*. 2011;50(19):11049-11058.

204. Alzaid A, Wiens J, Adjaye J, Smith KJ. Catalyst Deactivation and Reactor Fouling during Hydrogenation of Conjugated Cyclic Olefins over a Commercial Ni–Mo–S/γ-Al2O3 Catalyst. *Energy & Fuels*. 2018;32(5):6213-6223. doi:10.1021/acs.energyfuels.8b00791

205. Yenumala SR, Maity SK, Shee D. Hydrodeoxygenation of karanja oil over supported nickel catalysts: influence of support and nickel loading. *Catal Sci Technol*. 2016;6(9):3156-3165. doi:10.1039/C5CY01470K

206. Alberton AL, Souza MMVM, Schmal M. Carbon formation and its influence on ethanol steam reforming over Ni/Al2O3catalysts. *Catal Today*. 2007;123(1-4):257-264. doi:10.1016/j.cattod.2007.01.062

# APPENDICES

# APPENDIX A

Supporting data for chapter 4

**Figure 38.** TEM images and elemental mapping of (a) Ni/γ-Al$_2$O$_3$, (b) Ni-Cu/γ-Al$_2$O$_3$, (c) Ni-Re/γ-Al$_2$O$_3$ and (d) Ni-Cu-Re/γ-Al$_2$O$_3$ catalysts.



(a) Ni/γ-Al$_2$O$_3$

(b) Ni-Cu/γ-Al$_2$O$_3$



(c) Ni-Re/γ-Al$_2$O$_3$
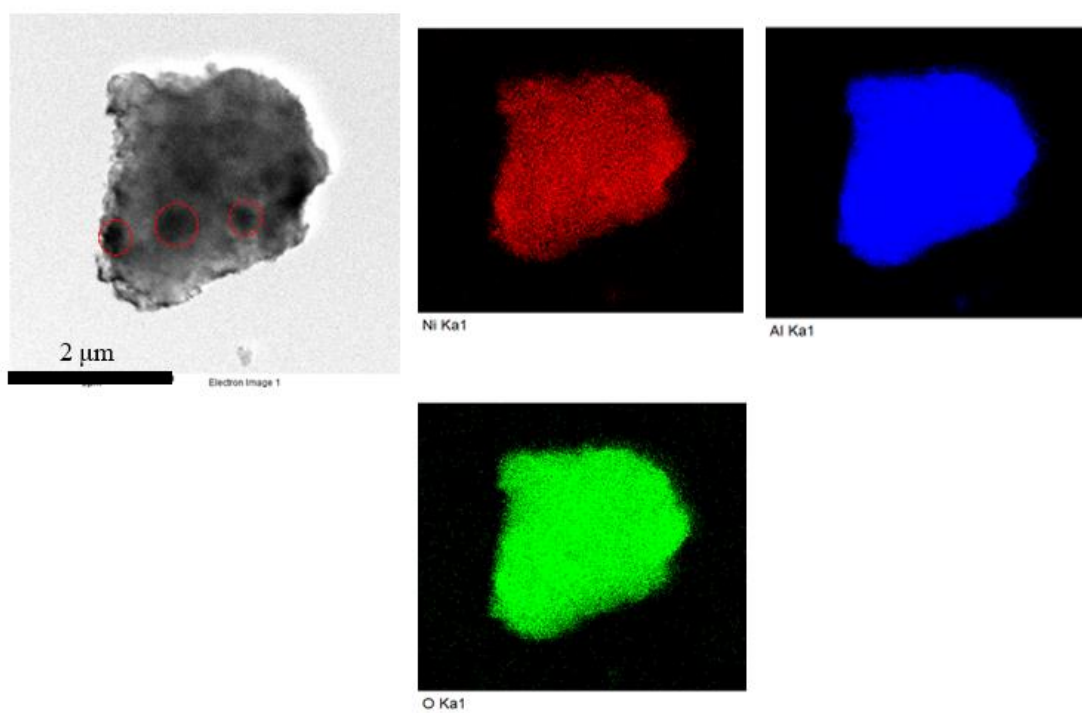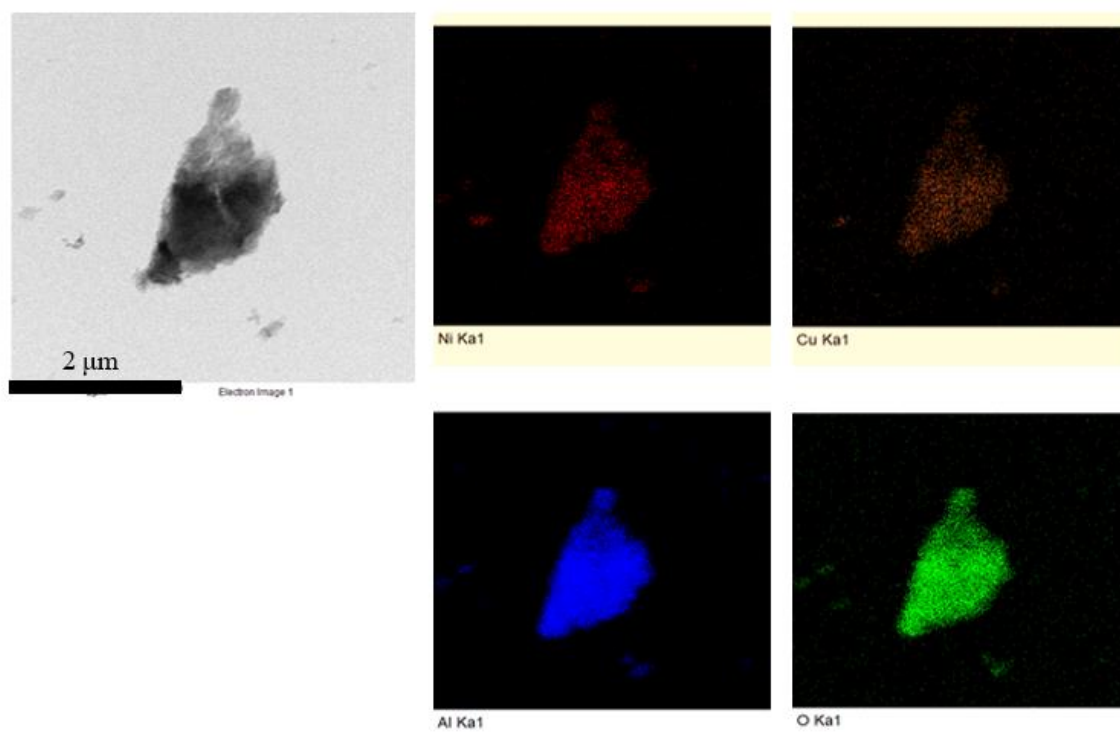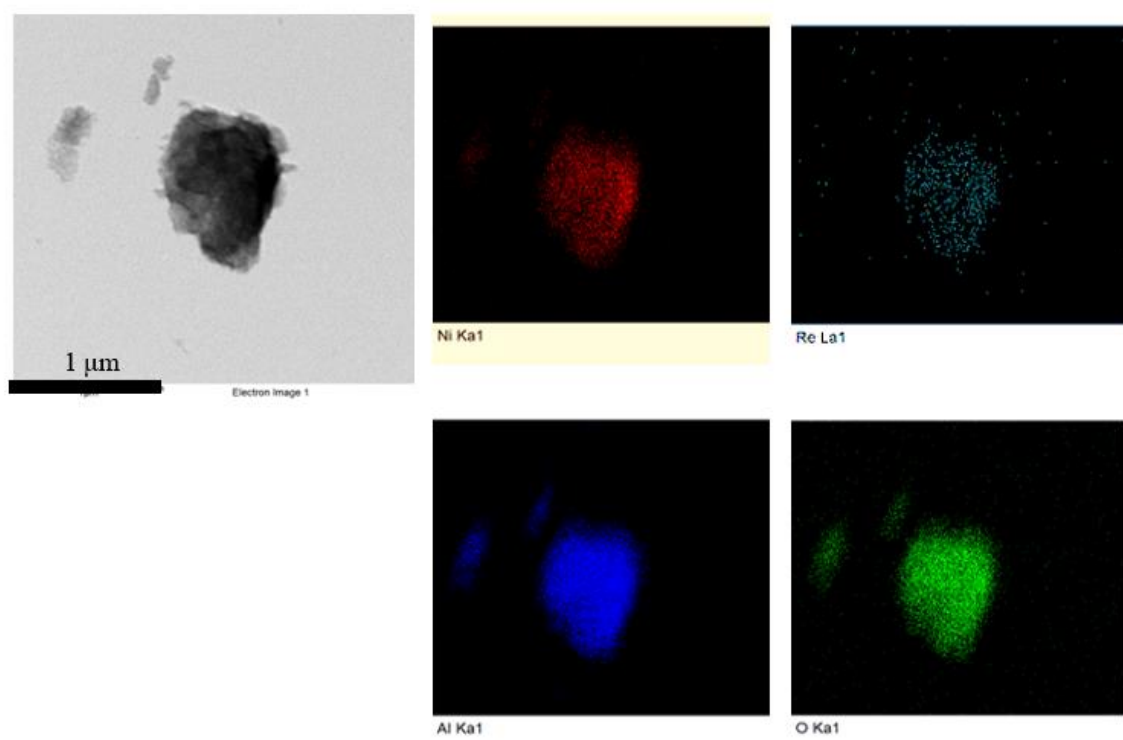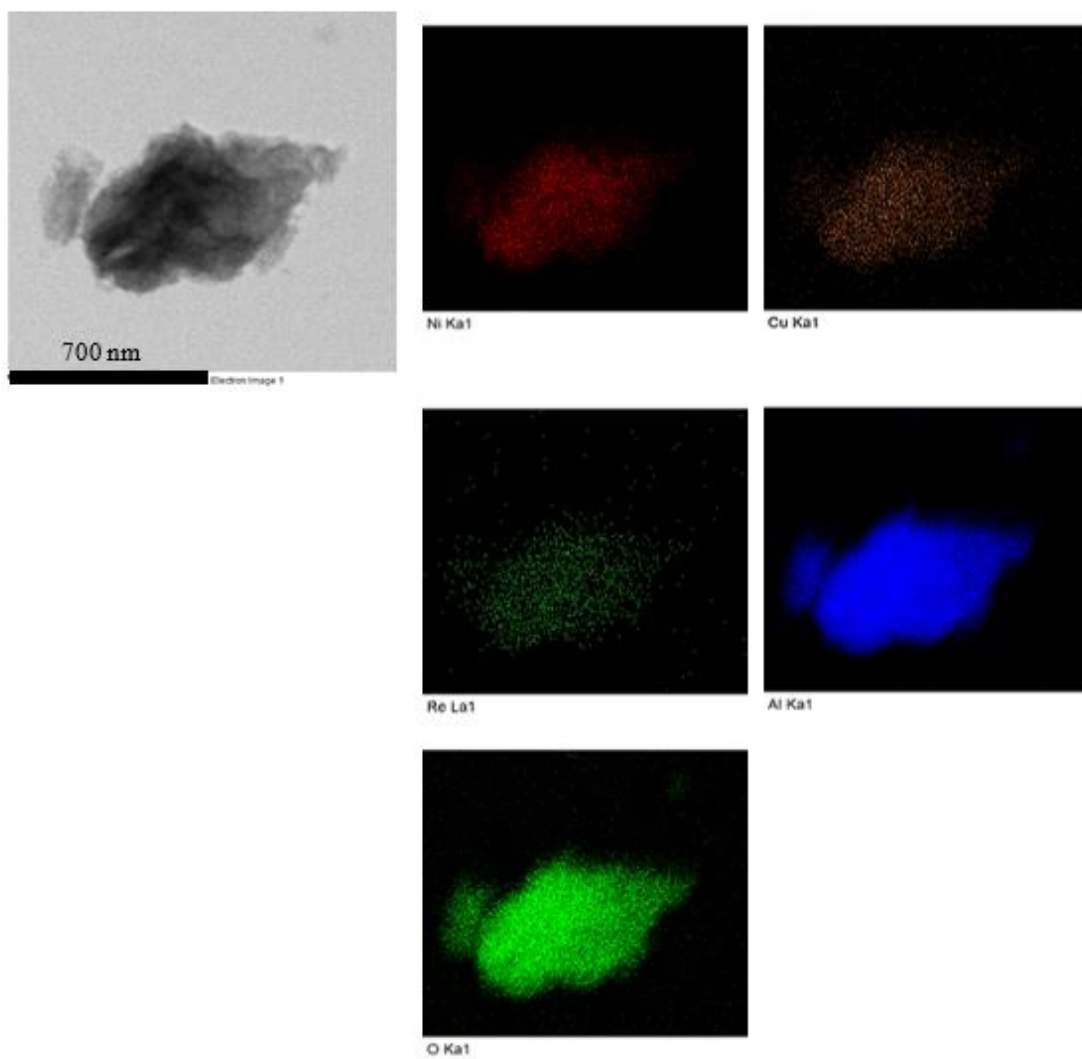
(d) Ni-Cu-Re/γ-Al₂O₃

**Figure 39.** GC-MS total ion chromatograms of (a) the algae bio-crude oil, the upgraded bio-oil over (b) non-catalytic, (c) Ni/$\gamma$-Al$_2$O$_3$, (d) Ni-Cu/$\gamma$-Al$_2$O$_3$, (e) Ni-Re/$\gamma$-Al$_2$O$_3$ and (f) Ni-Cu-Re/$\gamma$-Al$_2$O$_3$. All experiments were performed at 350 °C, initial hydrogen pressure of 75 bar and reaction time of 4 h.
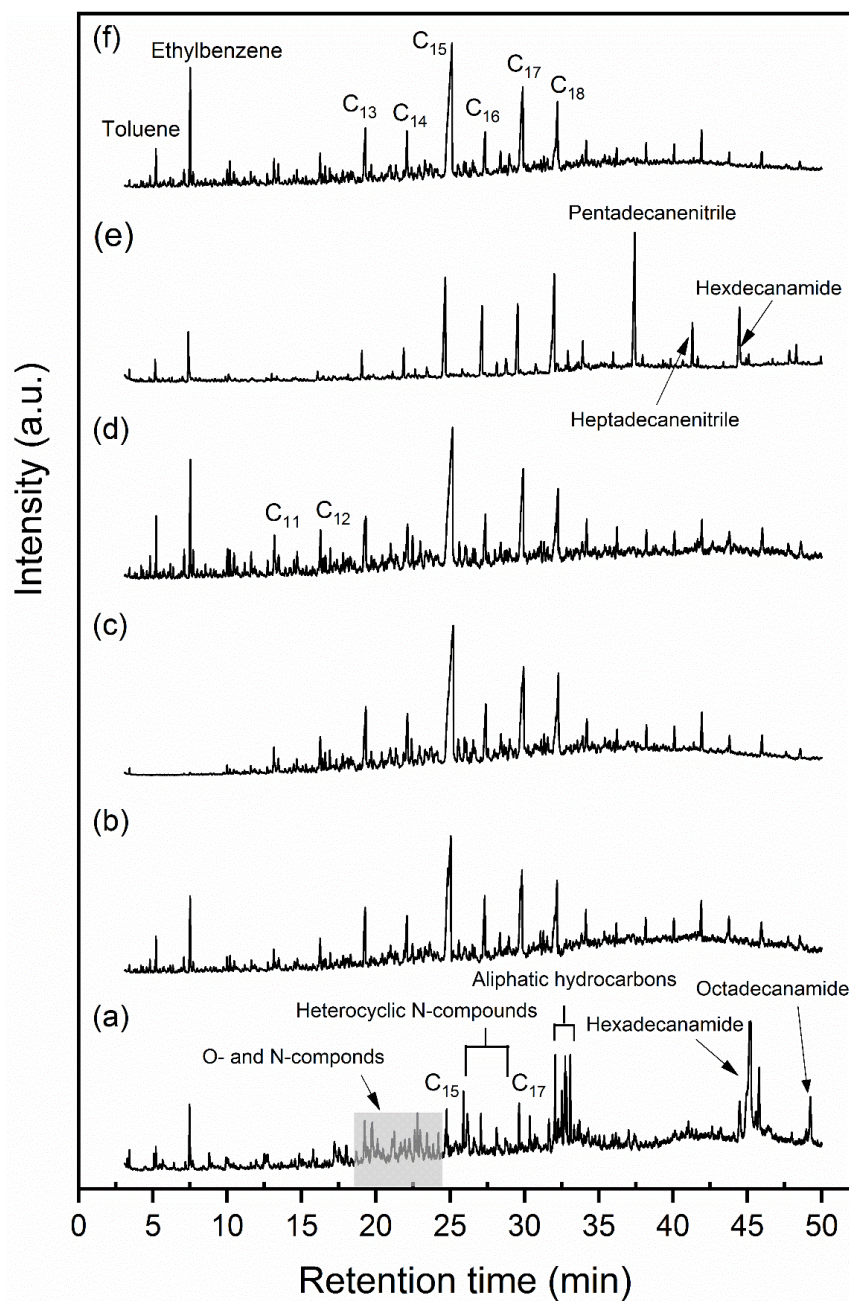
**Table 15.** FT-IR absorbance and relative functional groups of the algae bio-crude oil and upgraded bio-oils.

| Wavenumber range ($cm^{-1}$) | Wavenumber ($cm^{-1}$) | Assignments | Functional group |
|---|---|---|---|
| 3200-3650 | 3290 | O-H stretching/N-H stretching | Water, alcohols, phenols, amino group |
| 3000-3150 | 3016, 3053 | =C-H stretching | Alkenes |
| 2840-2970 | 2854, 2922, 2957 | $C-H_2$, $C-H_3$ stretching | Alkanes |
| 1690-1780 | 1701 | C=O stretching | Conjugated aldehyde, ketones, carboxylic acids |
| 1647-1655 | 1651 | C=O stretching | Amide I |
| 1525-1580 | 1551 | N-H bending, C-N stretching | Amide II |
| 1480-1525 | 1515 | $C=C_{Ar}$ stretching | Aromatics |
| 1350-1480 | 1377, 1402, 1454 | C-H deformation | Alkanes |
| 1000-1260 | 1026, 1060, 1094, 1169, 1260 | C-O stretching | Alcohols, esters, ethers |
| 700-820 | 700, 738, 800 | C-H deformation | Aromatics |

**Table 16.** Chemical composition of the algae bio-crude oil and upgraded bio-oils as determined by GC-MS.

| Compounds | Total area (%) | | | | | |
|---|---|---|---|---|---|---|
| | Algae bio-crude | No catalyst | Ni | Ni-Cu | Ni-Re | Ni-Cu-Re |
| **Open-chain hydrocarbons** | | | | | | |
| Heptane, 2,4-dimethyl- | | | | 0.37 | 0.13 | 0.30 |
| 2-Pentene, 3-ethyl-2-methyl- | | | | | | 0.19 |
| Octane, 4-methyl- | | | | 0.28 | 0.10 | 0.26 |
| Heptane, 3-ethyl-2-methyl- | | | | | | 0.24 |
| Nonane | | 0.31 | | 0.66 | 0.26 | 0.54 |
| Decane | | 0.33 | 0.28 | 0.78 | 0.23 | 0.61 |
| Undecane | | 0.50 | 0.89 | 1.37 | 0.32 | 0.98 |
| Undecane, 2-methyl- | | | 0.26 | | | |
| Dodecane | | 0.87 | 1.41 | 1.60 | 0.47 | 1.10 |
| Undecane, 2,6-dimethyl- | | | | | | 0.54 |
| Tridecane | | 2.19 | 3.68 | 3.65 | 1.57 | 3.02 |
| Dodecane, 2,6,10-trimethyl- | | 0.46 | 0.89 | 0.00 | 0.50 | 0.78 |
| Tetradecane | | 1.89 | 3.13 | 2.45 | 1.73 | 2.70 |
| Tetradecane, 4-methyl- | | | 0.88 | 0.96 | | 0.85 |
| Pentadecane | 1.09 | 11.93 | 21.31 | 17.15 | 8.26 | 18.36 |
| 1-Pentadecene | 1.49 | | | | | |
| Tetradecane, 3-methyl- | | | 0.63 | 0.37 | | |
| Hexadecane | 2.11 | 2.83 | 4.14 | 2.68 | 4.95 | 2.61 |
| 1-Hexadecene | | | | | 0.95 | |
| Pentadecane, 2,6,10-trimethyl- | | 1.28 | 1.99 | 1.40 | 1.48 | 1.72 |
| Heptadecane | | 6.33 | 9.94 | 7.91 | 5.22 | 8.67 |
| Octadecane | | 2.61 | 3.72 | 1.13 | 2.82 | 2.46 |
| Hexadecane, 2,6,10,14-tetramethyl- | 3.29 | 3.21 | 5.73 | 5.22 | 7.12 | 5.14 |
| 2-Hexadecene, 3,7,11,15-tetramethyl-, [R-[R*,R*-(E)]]- | 5.71 | | | | | |
| Octadecane, 3-methyl- | | 2.01 | | | 1.04 | 1.62 |
| Nonadecane | | 2.20 | 3.15 | 2.06 | 3.23 | 1.89 |
| Eicosane | | 1.42 | 2.27 | 1.76 | 1.98 | 1.38 |
| Heneicosane | | 1.42 | 2.30 | 1.33 | 1.41 | 2.75 |
| Docosane | | 2.01 | 1.76 | 1.56 | 1.69 | 1.40 |
| Tricosane | | 2.21 | 2.79 | 2.03 | 1.57 | 2.36 |
| Tetracosane | | 1.80 | 1.55 | 1.68 | 1.70 | 1.49 |
| Tricosane, 2-methyl- | | | | | 2.40 | |
| Pentacosane | | 1.81 | 1.67 | 2.34 | 1.95 | 1.47 |
| Hexacosane | | 1.73 | 0.91 | 1.29 | 3.11 | 0.52 |

**Cyclic hydrocarbons**

| | | | | | |
|---|---|---|---|---|---|
| Ethylidenecyclobutane | 0.35 | | 0.13 | | |
| Cyclohexane, 1,2,4-trimethyl- | | | | | 0.16 |
| Cyclohexane, (2-methylpropyl)- | | | | 0.18 | |
| Cycloheptane, methyl- | | | 0.23 | | 0.24 |
| Cyclohexene, 3-methylene-4-(1,2-propadienyl)- | | | | 0.19 | |
| Bicyclo[4.2.0]oct-1-ene, exo-7-(1-cyclohexen-1-yl)- | | | 0.29 | | |
| Cyclopentane, decyl- | | | 0.72 | 0.61 | |
| Azulene, 4,6,8-trimethyl- | | 0.52 | 1.21 | 0.75 | |
| Cyclohexadecane | 1.31 | 1.51 | 1.17 | 0.79 | 1.57 |
| Tricyclo[4.4.1.0(2,5)]undeca-1(10),3,6,8-tetraene, 11-(1-methylethylidene)- | | | 0.28 | | |
| Cyclohexadecane, 1,2-diethyl- | 1.95 | | | | |
| [14]Annulene, 1,6:8,13-bis(methano)-, syn | | | 1.09 | 0.00 | |
| | | | | | |
| **Aromatic hydrocarbons** | | | | | |
| Toluene | 0.58 | 0.58 | 1.05 | 0.77 | 0.96 |
| Ethylbenzene | 1.98 | 1.60 | 2.92 | 2.17 | 3.51 |
| o-Xylene | 0.35 | | 0.71 | | 0.55 |
| p-Xylene | | | 0.37 | | 0.27 |
| Styrene | 0.59 | | | | |
| Benzene, propyl- | | 0.35 | 0.63 | | 0.75 |
| Benzene, 1-ethyl-3-methyl- | | 0.36 | 0.80 | | 0.57 |
| Benzene, 1,2,3-trimethyl- | | 0.33 | 0.25 | 0.68 | 0.45 |
| Benzene, butyl- | | 0.59 | 0.76 | 0.46 | 0.74 |
| Benzene, 1-butenyl-, (E)- | 0.38 | 0.48 | 0.74 | 0.24 | 0.53 |
| Benzene, 2-ethenyl-1,4-dimethyl- | | 0.50 | 0.54 | | 0.31 |
| Benzene, 2-butenyl- | | | 0.75 | | |
| Benzene, (3-methyl-2-butenyl)- | | 0.34 | 0.30 | 0.34 | 0.26 |
| 1H-Indene, 2,3-dihydro-4,7-dimethyl- | | 0.49 | 0.75 | 0.78 | 0.45 |
| Benzene, (1-ethyl-1-propenyl)- | | 0.46 | 0.31 | 0.46 | |
| Benzene, (3-methyl-2-butenyl)- | | 0.58 | 0.49 | 0.46 | |
| Benzene, 2-ethenyl-1,3,5-trimethyl- | | 0.33 | 0.45 | | |
| Naphthalene, 1,2,3,4-tetrahydro-6-methyl- | | 0.56 | 0.92 | 0.79 | 0.51 |
| Benzene, (3-methylcyclopentyl)- | | 0.42 | 0.48 | 0.38 | |
| Benzene, 4-(2-butenyl)-1,2-dimethyl-, (E)- | | 0.49 | 0.84 | 0.75 | 0.52 |
| Naphthalene, 2-methyl- | | 1.01 | 1.56 | 1.56 | 0.72 |
| Naphthalene, 1,2,3,4-tetrahydro-1,6,8-trimethyl- | 1.53 | | | | |
| Naphthalene, 1,2,3,4-tetrahydro-1,1,6-trimethyl- | 0.63 | 0.46 | 0.55 | 0.62 | 0.47 |
| Naphthalene, 1-methyl- | | 1.09 | 1.03 | | 0.69 |
| Benzene, 1,2,3,4-tetramethyl-4-(1-methylethenyl)- | | | | 0.69 | |
| Benzene, 1-(2-butenyl)-2,3-dimethyl | | 0.79 | | 0.86 | 0.69 |

| Compound | | | | | | |
|---|---|---|---|---|---|---|
| Naphthalene, 2,6-dimethyl- | | 0.82 | 1.79 | 1.40 | | 0.61 |
| Naphthalene, 2,7-dimethyl- | | 1.08 | 1.03 | 0.98 | 1.17 | 0.88 |
| Tetralin, 1,4-diethyl- | | | | 0.79 | | 0.87 |
| Benzene, 2,5-cyclohexadien-1-yl- | | | 0.62 | 0.76 | | 0.49 |
| Naphthalene, 1,6,7-trimethyl- | | 0.65 | 1.07 | 0.67 | | 0.82 |
| 3-(2-Methyl-propenyl)-1H-indene | | 0.71 | 1.03 | 0.80 | 1.41 | 0.65 |
| Naphthalene, 2,3,6-trimethyl- | | 0.64 | | 0.36 | | |
| 1,1'-Biphenyl, 2-methyl- | | 0.40 | | 0.68 | | 0.69 |
| 1,1'-Biphenyl, 3,4'-dimethyl- | | | | 0.42 | | |
| 3,3'-Dimethylbiphenyl | | | | 0.25 | | 1.65 |
| Tricyclo[5.2.1.0(2,6)]decane, 3-methylene-4-phenyl- | | | | | | 1.01 |
| 1,7-Dimethyl-3-phenyltricyclo[4.1.0.0(2,7)]hept-3-ene | | | | | | 0.94 |
| Benzene, 1,1'-methylenebis[2-methyl- | | | | 0.34 | | 1.61 |
| Phenanthrene, 1,2,3,4,5,6,7,8-octahydro- | | | | | 1.42 | |
| Anthracene, 1,2,3,4,5,6,7,8-octahydro- | | | | | 0.65 | |
| 1,1'-Biphenyl, 3,4-diethyl- | | 1.01 | | | | |
| Phenanthrene, 1-methyl- | | | | 0.85 | 0.94 | 0.84 |
| trans-1,1'-Bibenzoindanylidene | | 1.25 | | | | |

**Oxygen compounds**

| Compound | | | | | | |
|---|---|---|---|---|---|---|
| 2(3H,4H)-Cyclopenta[b]furanone, 3a ,6a-dihydro- | 0.22 | | | | | |
| Benzenepropanal | | 0.45 | | | | |
| 2,4-Nonadienal, (E,E)- | 0.34 | | | | | |
| 2-Cyclopenten-1-one, 2,3-dimethyl- | 0.74 | | | | | |
| 1,3-Benzenedimethanol, 2-hydroxy-5-methyl- | | | | | | 0.58 |
| Benzyl alcohol | | 0.41 | | | | |
| Cyclopentane Carboxaldehyde, 2-methyl-3-methylene- | 0.50 | | | | | |
| Benzene, 1-ethoxy-4-methyl- | 0.43 | | | | | |
| Acetic acid, 2-methylphenyl ester | 0.39 | | | | | |
| 2-Propenal, 3-(4-methylphenyl)- | | | | 0.64 | | |
| Heptanoic acid, anhydride | 0.44 | | | | | |
| Ethanone, 1-[4-(1-methyl-2-propeny phenyl] | | 0.75 | | 1.06 | | 1.32 |
| 2-Cyclohexen-1-one, 4,4,5-trimethoxy- | 1.17 | | | | | |
| 4-Pentenoic acid, 5-phenyl- | | 0.38 | | | | |
| 1(2H)-Naphthalenone, 3,4,5,6,7,8-hexahydro | 0.70 | | | | | |
| 5-Methyl-2-phenyl-2-hexenal | | 0.76 | | | | |
| 12-Oxatetracyclo[4.3.1.1(2,5).1(4,10)]dodecane, 11-isopropylidene- | | | | 0.38 | | |
| 6-Hydroxy-3-methyl-9-oxabicyclo[3.3.1]nonan-2-one | | 0.49 | | | | |
| Heptanal, 2-(phenylmethylene)- | | 0.46 | | 0.31 | | |

| Compound | | | | | | |
|---|---|---|---|---|---|---|
| 2,6-Octadien-1-one, 3,7-dimethyl--phenyl-, (E)- | | 1.11 | | | | |
| Spiro[3.6]deca-5,7-dien-1-one,5,9 9-trimethyl | | 1.47 | | | | 1.48 |
| Phenol, 3,4,5-trimethoxy- | | 0.66 | | | | 0.73 |
| 1,2,3,4,5,6,7,8-Octahydrophenanthrene-7-ol | | 0.90 | | | | |
| Cis-1-(4-methylphenyl)-2-(2-furyl)cyclopropane | | 0.85 | | | | |
| 3-Cyclopentylpropionic acid, 3-methylbutyl ester | | 1.24 | | | | |
| Ethanol, 1-(2,2-dimethyl-1-phenyl ethynyl cyclopropyl)- | | 0.92 | | | | |
| Ethyl citrate | 1.70 | | | | | |
| 1,2,3,4-Tetrahydrophenanthren-9-ol | 2.31 | | | | | |
| 2-Phenyl-3-(3-methylphenyl)-oxiran | | 0.98 | | | | |
| [1,1'-Biphenyl]-4-carboxaldehyde | | | 1.72 | | | |
| Benzenemethanol, .alpha.,.alpha.-diphenyl- | | 1.10 | | | | |
| Benzaldehyde, 2,4,5-trimethoxy- | | 0.35 | | | | |
| 2-Phenyl-3-(4-methylphenyl)-oxiran | | 2.58 | | | | |
| 2-Hydroxy-3-methoxybenzyl alcohol | 0.11 | | | | | |
| Methanone, phenyl(5,6,7,8-tetrahydro-1-naphthalenyl)- | | 0.76 | | | | |
| Ethanol, 2,2'-[1,2-ethanediylbis(oxy)]bis-, diacetate | 4.82 | | | | | |
| 2(3H)-Furanone, dihydro-5-tetradecyl- | 0.97 | | | | | |
| Benzeneacetic acid, 3,4-bis(acetyloxy)-, methyl ester | | 0.91 | | | | |

**Phenol and alkyl phenols**

| Compound | | | | | | |
|---|---|---|---|---|---|---|
| Phenol | 1.51 | 0.38 | 0.51 | 0.43 | | 0.43 |
| Phenol, 2-methyl- | | 0.27 | | 0.47 | 0.10 | |
| Phenol, 4-methyl- | 2.50 | 0.28 | | | 0.29 | 0.54 |
| Phenol, 3-methyl- | 0.46 | | | | 0.11 | 0.67 |
| Phenol, 3-ethyl- | 0.47 | | | | | |
| Phenol, 4-ethyl- | 0.94 | | | | | |
| Phenol, 2,3-dimethyl- | 0.26 | | | | | |
| Phenol, 2,3,6-trimethyl- | | 0.72 | | 0.47 | | 0.53 |

**Nitrogen compounds**

| Compound | |
|---|---|
| Pyridine | 0.40 |
| Pyridine, 3-methyl- | 0.33 |
| Pyrazine, 2,6-dimethyl- | 0.38 |
| Pyrazine, ethyl- | 0.39 |
| Pyridine, 3-ethyl- | 0.33 |
| 1,3-Benzenediamine, 4-methyl- | 0.58 |
| Pyrazine, 2-ethyl-6-methyl- | 0.52 |
| 4-Pyridinamine, 2,6-dimethyl- | 0.39 |
| Pyrazine, 3-ethyl-2,5-dimethyl- | 0.46 |

| Compound | | | | |
|---|---|---|---|---|
| Benzenamine, 3,5-dimethyl- | 0.21 | | | 0.24 |
| Pyrazine, 3,5-diethyl-2-methyl- | 0.19 | | | |
| 1H-Pyrrole, 3-ethyl-2,4-dimethyl | 0.20 | | | |
| Pyridine, 3-ethyl-5-methyl- | | 0.35 | 0.36 | |
| 1H-Pyrrole, 2-ethyl-3,4,5-trimethyl- | 0.99 | | | |
| Aniline, N-methyl- | | 0.61 | | |
| 2-Pyrrolidinemethanamine, 1-ethyl- | 2.34 | | | |
| Quinoline, 4-methyl- | 0.71 | | | |
| Indolizine | 1.15 | | | |
| Indole | 1.17 | | | |
| 1H-Indole, 6-methyl- | 1.55 | | | |
| 1H-Indole, 2,3-dimethyl- | | | 1.41 | |
| 3-Methylbenzylamine, N,N-diheptyl- | | 2.07 | | |
| Benzeneethanamine, 3,4,5-trimethoxy- | | 1.89 | | |
| 1H-Indole, 2,3-dihydro-1,3,3-trimethyl-2-methylene- | 1.37 | | | |
| Isoquinoline, 3,4-dihydro-1,3,3-trimethyl- | | 0.32 | | |
| 1-Phenyl-3,4-dihydroisoquinoline | | | 0.36 | |
| Pyridine, 4-(2-phenylethenyl)- | | 1.53 | | |
| 3-Methylcarbazole | | | 0.65 | |
| Benzenamine, 3-(2-phenylethenyl)-, (E)- | | | 0.35 | |
| Uleine, N-demethyl-N-ethyl- | | 1.01 | | |
| 9H-Pyrido[3,4-b]indole, 1-methyl- | 0.59 | | | |
| Carbazole, 1,5,7-trimethyl- | | 0.55 | 2.09 | |
| 5H-Indeno[1,2-pyridin-4-amine, 5-benzylidene- | 0.40 | | | |

**Nitriles**

| Compound | | | | |
|---|---|---|---|---|
| Benzonitrile, 2,4,6-trimethyl- | 1.93 | | | |
| 3-Pyridinecarbonitrile, 1,4-dihydro-1-methyl- | | 0.58 | | |
| Tetradecanenitrile | | | 1.62 | |
| Pentadecanenitrile | | | 11.37 | |
| Hexadecanenitrile | | | 1.54 | |
| Heptadecanenitrile | | | 4.15 | |
| Tricyclo[3.2.2.0(2,4)]non-8-ene-endo-3,exo-6,exo-7-tricarbonitrile, exo-3-phenyl- | | 0.54 | | |
| Acetonitrile, 2-(4,6,8-trimethyl-1-azulenyl)- | | 0.55 | | |

**Amides**

| Compound | | | | |
|---|---|---|---|---|
| Pyrazinamide | 0.13 | | | |
| 2-Pyrrolidinone, 1-methyl- | 0.65 | | | |
| Acetamide, N-butyl- | 1.15 | | | |
| N-(3-Methylbutyl)acetamide | 1.23 | | | |
| Acetamide, N-(2-phenylethyl)- | 1.77 | | | |
| Tetradecanamide | 0.84 | | 1.88 | |

| | | | | |
|---|---|---|---|---|
| Hexadecanamide | 16.85 | 0.81 | | 7.25 |
| N-(4-Methoxyphenyl)-2-hydroxyimino-acetamide | | 0.66 | 1.00 | |
| Octadecanamide | 3.02 | | | |
| **Other N-O compounds** | | | | |
| 2-Pyridinecarboxylic acid, 6-methyl | 0.27 | | | |
| Quinuclidine-3-ol | 0.50 | | | |
| 2,5-Pyrrolidinedione, 1-ethyl- | 0.56 | | | |
| Phenol, 3-(ethylamino)-4-methyl- | 0.30 | 0.52 | | |
| Phenol, 4-amino-2-isopropyl-5-methyl- | 0.28 | 0.95 | | |
| Pyrrolidine, 1-(1-oxopropyl)- | 0.21 | | | |
| 2,5-Pyrrolidinedione, 1-butyl- | 1.46 | | | |
| 2,4-Dimethyl-6-methoxy-8-nitroquinoline | | 1.18 | | 0.74 |
| 2-(p-Nitrobenzyl)pyridine | | | 0.36 | |
| Ethyl 6-formamidohexanoate | | | 0.39 | |
| 1-Propanone, 1-(2,6-dimethylphenyl)-2-methyl-3-(1-piperidyl)- | | | | |
| Quinoxaline, 2-butyl-3-phenyl-, 1-oxide | 1.37 | 0.58 | | |
| 3-Acetamidocarbazole | 3.38 | | | |
| 4,6(1H,5H)-Pyrimidinedione, 2-methoxy-1-methyl-5,5-di-2-propenyl- | | | | 0.80 |
| 3-Diethylaminobutyranilide | 2.32 | | | |
| Decanone, 3-O-methyloxime | 0.80 | | | |
| Benzoic acid, 2-[(2,3-dimethylphenyl)amino]-, methyl ester | | 0.29 | | |
| 1,2,3,4-Tetrahydroisoquinolin, 2-acetyl-6,7-dimethoxy-1-phenmethylene | | 0.75 | | |

*These compound listed are identified by GC-MS with more than 70% of NIST mass spectral library match.

# APPENDIX B

The catalysts were prepared using impregnation method: the 10%Ni, 2%Cu, and 2%Re were loaded into $\gamma$-Al$_2$O$_3$ (sieve size 1-0.25 mm). The catalysts was used to perform the experiment in chapter 5, and The H$_2$-TPR result is discussed below.

Monometallic Ni/$\gamma$-Al$_2$O$_3$ displayed a major broad peak at 560 °C attributed to the reduction of strongly interaction of NiO and support, or small particles located inside the pore, and small shoulder peak at 266 °C belongs to bulk NiO, which have weaker interaction with the support. Furthermore, a shoulder peak at 745 °C corresponding to the hardly reducible species as NiAl$_2$O$_4$ [205,206]. For the Cu containing catalysts, TPR profile shows the lower reduction temperature compared to monometallic Ni catalyst at 250-287 °C which can be attributed to the reduction of bulk CuO to Cu [79,179]; the peak at around 295 °C could be assigned to the NiO-CuO ensemble. In addition, the reduction peak of NiO and NiAl$_2$O$_4$ were shifted to lower temperature, indicating that the introduction of Cu can enhance the reducibility of Ni species. The result is consistent with the previous studies by Zhang et al [187] and Loe et al [175]. The reduction peak profile of Ni-Cu-Re/$\gamma$-Al$_2$O$_3$ is rather similar to that of Ni-Cu/$\gamma$-Al$_2$O$_3$; however, for Re-containing catalyst the small peak at 378 °C was observed, which could be ascribed to the reduction of Ni-Re oxide species [126]. Besides, the reduction intensity of NiCuRe/$\gamma$-Al$_2$O$_3$ significantly increased, and no NiAl$_2$O$_4$ was observed, implying that the addition of Re can promote the degree of reduction by hydrogen spillover [118,119,131], and also inhibit the NiAl$_2$O$_4$ formation by preventing Ni$^{2+}$ diffusion into Al$_2$O$_3$ lattice [126].

**Figure 40.** H₂-TPR profile of Ni/γ-Al₂O₃, Ni-Cu/γ-Al₂O₃, Ni-Re/γ-Al₂O₃, and Ni-Cu-Re/γ-Al₂O₃ catalysts.
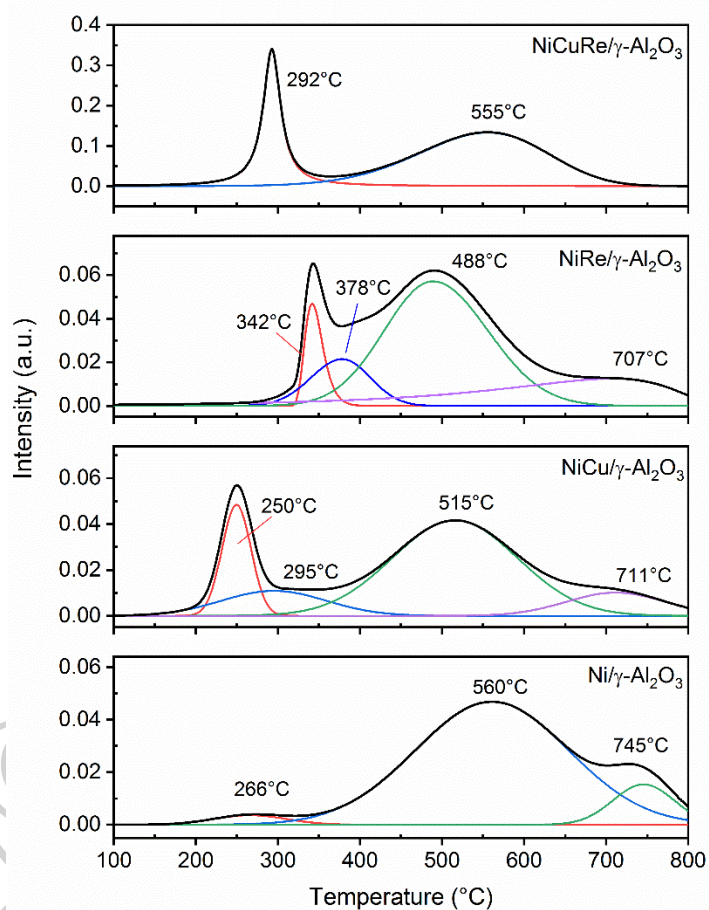
# VITA

**NAME**                           KANOKTHIP PONGSIRIYAKUL

**DATE OF BIRTH**        10 February 1989

**PLACE OF BIRTH**     Saraburi, Thailand

**INSTITUTIONS ATTENDED**  Department of Chemical Engineering, Silpakorn University, B. Eng.

**PUBLICATION**     K. Pongsiriyakul, W. Kiatkittipong, K. Kiatkittipong, N. Laosiripojana, K. Faungnawakij, S. Adhikari, S. Assabumrungrat, Alternative Hydrocarbon Biofuel Production via Hydrotreating under a Synthesis Gas Atmosphere, Energy & Fuels. (2017). https://doi.org/10.1021/acs.energyfuels.7b02207.